Design and Implementation of a Non-contact Microwave Level Measurement Instrument

Jonathan Michael Ward

A dissertation submitted to the Department of Electrical Engineering,
University of Cape Town, in fulfilment of the requirements
for the degree of Master of Science in Engineering.

Cape Town, November 2010

Declaration

I know the meaning of plagiarism and declare that all the work in this dissertation, save for that which is properly acknowledged, is my own. This dissertation is being submitted for the degree of Master of Science in Engineering in the University of Cape Town. It has not been submitted before for any degree or examination in any other university.

Signature of Author .....

Cape Town

30 November 2010

Abstract

This dissertation describes the design and implementation of a microwave level measurement instrument for sensing the level of a substance inside a tank up to 10 m in height. A radar transceiver had to be designed to replace an acoustic sensor on an existing 4-20 mA loop powered ultrasonic instrument and had to be compatible with its on-board acoustic signal processing hardware. Specifications are developed for a pulsed radar architecture operating at 5.8 GHz with a bandwidth around 1 GHz and at a repetition frequency of 3.58 MHz. A Venier time stretching technique is used to perform the distance measurements by cross-correlating the transmit pulse train with a separate but similar reference pulse train operating at a slightly lower repetition frequency, setting up an output range profile with ultrasonic time interval measurement parameters. Demonstration hardware operating at 580 MHz with 100 MHz bandwidth and at a repetition frequency of 3.58 MHz is designed and built. Short pulses (< 1 ns) with rise-times in the order of hundreds of picoseconds are generated and shaped into 12 ns RF pulses using bandpass filtering. Tests are performed to measure the time interval between the transmitted pulse and echo at several ranges, which show an overall accuracy of less than the required 2 cm can be achieved using the proposed system.

Acknowledgements

Firstly, I would like to thank our industry partner and sponsor, Kevin Barnfather at KAB Instruments for giving me the opportunity and the financial assistance to carry out the work for this dissertation.

I would like to thank my supervisor, Professor Inggs, for all his input, assistance and patience while I have worked on this dissertation. I would also like to acknowledge the suggestions of Dr Alabaster.

I would like to thank all the members of the Radar and Remote Sensing Group with whom I have had the opportunity of working over the past three years.

I would also like to thank the following people who provided me with assistance during my project:

- Stephen Schrire, for all your help with my circuit designs. Your insight has always been invaluable.
- Samuel Ginsberg, for all the time that you spent making my printed circuit boards.

Contents

List of Figures

List of Tables

List of Symbols

A complete list of symbols for the readers convenience.

$\%BW$	—	percent fractional bandwidth
A_e	—	effective aperture area
B	—	RF bandwidth
c	—	speed of propagation
c_0	—	speed of light in a vacuum
D_a	—	diameter of the antenna aperture
e_{ap}	—	aperture efficiency
F_b	—	diameter of the footprint of the antenna beam
F_p	—	diameter of the pulse footprint
f_{prf}	—	pulse repetition frequency
$f_{s,eff}$	—	effective sampling rate
G	—	gain
H	—	height above the target surface
P	—	process pressure in bar absolute
P_N	—	pressure under normal conditions (1 bar)
P_r	—	received power
P_t	—	transmitted power
R_{max}	—	maximum unambiguous range
SNR	—	Signal-to-noise Ratio
T_e	—	equivalent system noise temperature
T_n	—	pulse repetition interval
T_{rep}	—	time expanded repetition interval
t_{ds}	—	time expanded delay / interval
t_d	—	time delay / time interval
t_r	—	pulse rise-time
TSF	—	time stretching factor

$\delta\,()$	—	Dirac delta function
ε_r	—	relative permittivity
ε_{rr}		relative permittivity of DR
ε_{rN}	—	dielectric constant under normal conditions (1)
θ	—	process temperature in Kelvin
θ_N	—	temperature under normal conditions (273K)
λ	—	wavelength
σ	—	standard deviation
τ	—	pulse width
ω_n	—	angular frequency
Γ	—	return loss

Nomenclature

Beamwidth—The angular width of a slice through the main lobe of the radiation pattern of an antenna in the horizontal, vertical or other plane.

BJT—Bipolar Junction Transistor.

CAD—Computer Aided Design.

COTS—Commercial Off The Shelf.

DPO—Digital Phosphor Oscilloscope.

Dielectric Constant—The ratio of the permittivity of the material to the permittivity of free space.

DR—Dielectic Resonator.

Echo—A portion of the energy of the transmitted signal that is reflected of the target.

EIRP—Effective Isostropic Radiated Power.

ESR—Equivalent Series Resistance.

FFT—Fast Fourier Transform.

FT—Fourier Transform.

FM-CW—Frequency-Modulated Continuous-Wave.

FWHM—Full Width Half Maximum.

ITU—International Telecommunications Union. It is the leading United Nations agency for information and communication technologies. The ITU-R fulfils the role of standardising the international RF spectrum.

ISM Band —Industrial, Scientific and Medical radio bands defined by the ITU-R. Reserved internationally for the use of RF electromagnetic fields for industrial, scientific and medical purposes other than communications. Communication equipment operating in the ISM bands must be tolerant of interference from other ISM equipment.

Microstrip–A type of electrical transmission line which can be fabricated on a printed circuit board. It consists of a conducting strip separated from a ground plane by a dielectric layer known as the substrate.

Modulation—The process of varying the amplitude, frequency, or phase of an RF carrier wave.

PCB—Printed Circuit Board.

PRF—Pulse repetition frequency.

PRI—Pulse repetition interval.

Radar—A method of estimating the distance of an object by bouncing high frequency signals off the object and measuring the reflected signal. RADAR = Radio Detection And Ranging.

Range—The distance from a radar to a target.

Resolution—The degree of detail. The smallest amount that can be measured.

Sampling—The process of encoding an analog signal in digital form by reading (sampling) its level at precisely spaced intervals of time.

SMPS—Switch-mode Power supply.

SRD—Step-Recovery Diode.

TI—Time interval.

TIM—Time-interval-measurement.

TSF—Time stretching factor

TOF—Time-of-flight.

VCO—Voltage Controlled Oscillator.

VNA—Vector Network Analyser.

Chapter 1

Introduction

1.1 Project Background

This dissertation describes the design, implementation and testing of a microwave level measurement instrument for sensing the level of a substance inside a tank of defined size. Many applications in industry require the use of large tanks for storage, which can include the chemical, food, oil, mining, water supply and beverage industries. Accurate level data of the contents of every tank is vital where inventories, batching and process efficiency are critical measurements. Due to the large surface areas of these industrial storage tanks, a small change in level can correspond to a large change in volume. Most *contact* (mechanical) level measurement devices are not very accurate and are often prone to problems due to the hazardous internal environment of the tanks. They are particularly susceptible to corrosion and parallax errors.

KAB Instruments in Johannesburg, the sponsor for this project, manufacture ultrasonic level measurement instruments. As shown in Figure 1.1, these instruments are placed atop a large industrial storage tank and monitor the level of the inventory inside the tank. This can be very important in an industry where an inventory level has to be tightly controlled or monitored and requires, in certain cases, a very high accuracy height measurement .

Ultrasonic level measurement is a well established technology and is used widely across the aforementioned industries. But there are certain limitations to it in terms of accuracy. For example, the speed of sound in air can vary by more than 10% in environments with changing temperature [see section 2.4.1]. Harsher environments, in which there is dust, vapour or foam, also inhibit the functionality of ultrasonic devices. They are also more prone to noise from external acoustic sources. The low cost, however, has made it a very popular choice. Some of the benefits that radar has over competing non-contact technologies, amongst which include ultrasonic as well as capacitive, hydrostatic pressure and radiometric sensors, to name but a few, are [48, 25, 17, Chp7]:

- Higher accuracy

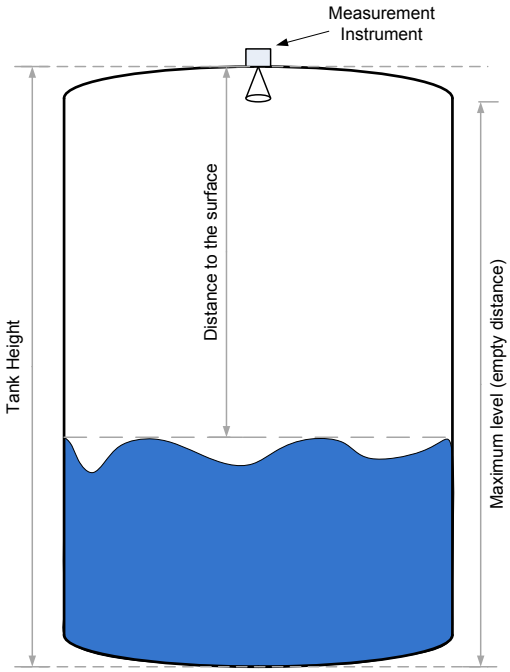

Figure 1.1: A diagram of a typical industrial storage tank. By determining the range (H) to the surface by the pulsed time-of-flight of sound, the level (L) can be calculated by subtracting this distance from the known full-scale distance (E). Therefore L = (E - H).

- No moving parts
- Unaffected by powders, heavy vapours, turbulence and foam
- Operation largely unaffected by wide temperature and pressure ranges
- Low power
- Low maintenance
- Low operating costs

These benefits have led to radar-based sensors gaining a large market share at the expense of these competing technologies and has also led to significant investments by commercial manufactures into proprietary radar-based level sensor technology [28]. Since KAB Instruments have all of their expertise in ultrasonic systems, they have had to procure radar instruments for their clients from overseas competitors at great cost. They suggested a collaboration between KAB and UCT to develop an entry level radar-based sensor that they could use to replace their ultrasonic transceiver. They also wished for the radar technology to co-exist with their timing and power management hardware while being small enough to fit in the same enclosure.

The most important specification of both the existing ultrasonic sensor and the desired radar sensor is that the instrument be compatible with the industry standard two-wire 4-20 mA current loop [4, 13]. This standard allows the sensors to both run and

communicate over two wires. The measurement data is represented on the loop as a linear analogue current between 4 mA and 20 mA. Multiple devices using this same standard, even different sensor types, can therefore be gathered to operate on a bus with a single data acquisition point as shown in Figure 1.2. As long as the operator knows what type of sensor the data is coming from, it can be displayed correctly using a 4-20 mA indicator. Instructions can also be modulated and sent over the loop to the instrument using special communications protocols. One popular analogue example of this is called HART[1]. The disadvantage of this configuration is that two-wire sensors have to draw all their supply current from the loop, which means that only the first 4 mA is available for use by the instrument itself. Instruments that require more than 4 mA of current require an additional pair of wires for power and are called four-wire sensors.

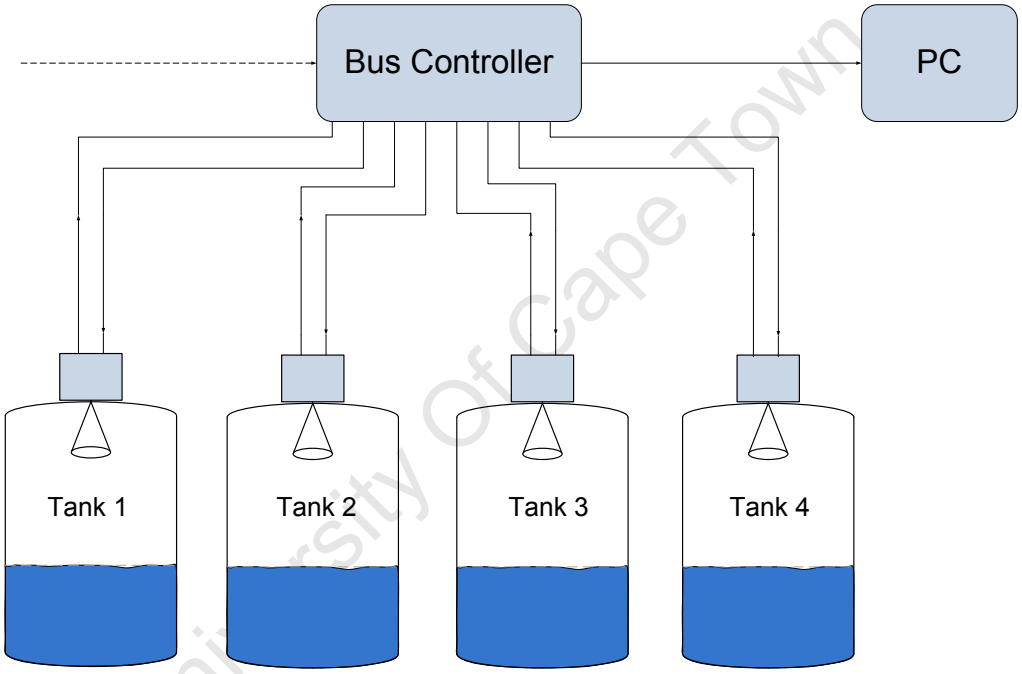

Figure 1.2: A diagram of several level sensors connected to a bus using the 4-20 mA standard. The current on each loop is monitored by the bus controller and sent to a remote terminal for display. 4 mA would represent an empty level and 20 mA a maximum level. All other levels would be scaled linearly to a current in between these values.

1.2 User Requirements

The project is heavily constrained by the user requirements of the sponsor:

- A measurement range of up to 10 m.
- A measurement accuracy of 2 cm.

[1] http://www.hartcomm.org/protocol/about/aboutprotocol_what.html

- A measurement display resolution of 2 cm.
- A measurement update rate of 1 Hz.
- Operate from a 24 V DC 4-20 mA two-wire loop power supply (instrument supply current less than 4 mA).
- Operate over a wide range of temperature (-40 C to +80 C) and pressure (-100 kPa to 300kP).
- Compact design.
- Comparable in cost to an ultrasonic level measurement instrument.
- Frequency of operation must be within an unlicensed band (5.8 GHz or 24 GHz) and emissions must be within the standard guidelines of the regulator.
- Output range profile signal should be compatible with the existing on-board ultrasonic signal processor.

Additional optional user requirements include:

- Variable gain and variable output power (if necessary)
- A changeable sampling time

1.3 Requirements Analysis and Review

The following conclusions were drawn based on the user requirements and in consultation with KAB Instruments:

- *The range of the measurement must be up to 10 metres:* This means that the maximum empty distance of the vessel will be 10 m. The signal will have to travel a maximum return distance of 20 m. This parameter would effect the maximum unambiguous range of the instrument. For example, in pulsed radar waveforms, the pulse repetition frequency would have to be below 15 MHz, in order for an echo to return to the receiver from the full scale distance before the next pulse is transmitted. In the same way, this would effect the sweep time or dwell time for any frequency domain methods.

  This maximum range parameter is also important in determining the lowest received signal strength and hence the required minimum signal-to-noise ratio (SNR). The received echo signal power of the level measurement instrument cannot be calculated by the conventional radar equation. With a few assumptions the inverse-square law for received power can be ignored, since all of the transmitted power is going hit the target surface. This theory is used in airborne and space-borne altimeters [18, 19, 71].

- *A measurement accuracy of 2 cm:* By definition, the accuracy requirement of a measurement instrument is the maximum deviation of a sequence of measured values from the known reference values *over the entire measuring range*. In simpler terms, this means that the measured value should not be more than 2 cm from the true value for any range. The accuracy is specified after any averaging and calibration has been performed. Accuracy in a radar level measurement system can be affected by a number of factors, which could include the interaction of the microwaves with the tank itself.

- *A measurement display resolution of 2 cm*[2]*:* This is the smallest change in the measured value that the instrument will display. This requirement is separate from the accuracy requirement because it only refers to the current that is to be set on the loop and displayed. The level, which is calculated to the required accuracy, is brought to the nearest 2 cm and the corresponding loop current between 4 mA and 20 mA is then set. Any further change smaller than 2 cm in level will not update the loop current or the display. This means that there will be 500 possible readings on the display. The loop current will change in steps of $32\mu\mathrm{A}$. This is a function of the current loop controller and measurement processor, which is already present on the existing ultrasonic sensor.

- *A measurement update rate of 1 Hz:* This requirement means that the instrument should output a level measurement every second. This would include the time taken to acquire the measurement and any calculation or processing time. In the case of a pulse-echo radar, at distances of less than 10 m, the time for a single pulse-echo is in the order of several nanoseconds, which indicates that there is sufficient time for many pulse-echo measurements to be taken between update periods. This means that several pulse-echoes could be integrated together to form a single level measurement and would also result in an improvement to accuracy and an increased signal-to-noise ratio. A lower transmit power could then be used while maintaining the accuracy requirement. In the same way, this fairly long update interval can be exploited in the FFT process by frequency domain methods.

- *Operate from a 24 V DC 4-20 mA two-wire loop power supply:* This is the most crucial limitation and has been previously introduced. The sensor has only the first 4 mA to power all its circuitry. This means that low-power design is critical in the project as there can be no additional source of power. This requirement places restrictions on the complexity of the technology used in the instrument as power-hungry components will have to be kept to a minimum. This requirement alone

[2]This should not be confused with the range resolution requirement which is found in many conventional radars. In this application, only the level of the closest target surface is important. This would only be applicable if there were two liquids floating on one another and one wished to differentiate between the two layers.

greatly steers the design towards a pulse radar architecture, since frequency domain architectures would require frequency domain processors to perform FFT calculations which will draw several mini-amperes more supply current. The 4-20 mA circuitry in the existing ultrasonic instrument should be reused for this purpose.

- *Operate over a wide range of temperature and pressure:* This means that the effects of varying the temperature and pressure need to be taken into account. As already mentioned, electromagnetic signals are relatively immune to changes in temperature and pressure, but the effect on propagation velocity should nevertheless be considered. The electronic components used in the design must be tolerable to these ranges as well. This is not to say that the instrument should be able to tolerate drastically changing temperatures. It is more application specific. Careful mounting and heat-sinking methods could be applied in applications which require very high temperatures or the device could be mounted externally and transmit through a window in the vessel if the pressure is too high. The temperature can affect the stable operation of the microwave circuits and could lead to drift in the oscillators or shifts in centre frequency of the distributed microwave circuits. The design should incorporate some tuning options to account for this.

- *The instrument should have a compact design:* While not a critical requirement for prototyping, this means the design should be kept as compact as possible so that it can go into the existing enclosure of an ultrasonic instrument. Careful, professional, multilayer PCB layout could reduce the size of any prototype hardware that is too large to fit into the enclosure. After discussion with KAB it was decided that the radar transceiver should ideally occupy around 5 cm x 6 cm of PCB real-estate.

- *Comparable in cost to an ultrasonic level measurement instrument:* This means that careful consideration should be given to cost during the design of the instrument. Once again this requirement may place an additional constraint on the technology used in the instrument as the number of components and the complexity of the circuit layout will push the cost of the device higher. Prohibitively expensive off-the-shelf components and manufacturing techniques should be avoided. After discussion with the sponsor it was decided that the cost per sensor should be less than R1000 in addition to any existing ultrasonic hardware.

- *Frequency of operation must be within an unlicensed band (5.8 GHz or 24 GHz) and emissions must be within the standard guidelines of the regulator:* This requirement is pretty straight forward. It means that the device must not operate at frequencies that are reserved for other applications and the emissions must be at a level that is compliant with those set by regulatory bodies. After discussion with the sponsor, it was decided that the instrument should use either 5.8 GHz or

24 GHz, which lie in unlicensed ISM bands. These bands are mostly unlicensed worldwide so it makes sense to stick within these bands so that sales could be made to many countries without having to apply and pay for licensing.

- *Output range profile signal should be compatible with the existing on-board ultrasonic signal processor:* This means that the signal processing hardware on the ultrasonic instrument must be reused. This requirement, once again, steers the architecture towards a time domain process. The obvious drawback in this requirement is that radar signals propagate nearly six orders of magnitude faster than acoustic signals, which means that direct time-interval-measurement (TIM) will not be possible without first modifying the signal.

1.4 Project Outline

To avoid confusion on the reader's part, the terms *microwave* and *radar,* which will be used throughout this dissertation, are defined as follows. The term *microwave* refers to electromagnetic waves, the signal, in a specific part of the frequency spectrum (usually around 300 MHz to 30 GHz) but this often varies from reference to reference. A more general way of describing the term *microwave* is when the length of the transmission lines of the circuitry become comparable to the wavelength of the signals in that circuit and special design and layout techniques should be employed to ensure maximum power is transferred between nodes in the circuit. The term *radar* refers to the actual device that use the microwaves to perform various detection and ranging functions. During the dissertation the two terms are often used interchangeably.

This dissertation is structured around the four project objectives laid out by the sponsor, namely:

- **Investigate a suitable radar technology to use in the instrument and ensure that it can be adapted for use with some of the existing ultrasonic hardware**
  - Chapter 2 begins with a more detailed description of how level sensors function. Both time and frequency domain methods are discussed as possible candidates for the radar technology but pulsed radar is highly favoured because of its compatibility with the time domain ultrasonic system and the fact that it is likely to draw less supply current.
  - The architecture of the ultrasonic instrument is then examined in Section 2.2. The sub-systems which will need to be modified for radar operation are then highlighted.
  - The important physical properties which effect the electromagnetic signals of these systems are then discussed in Section 2.4.

  - The power supply constraints are then discussed in more detail in Section 2.3. The operation and the components that make up the 4-20 mA loop are then described and reasons behind the use of the standard are highlighted.
  - Some of the more notable manufacturers of radar level measurement instruments are then introduced in Section 2.6.

- **A suitable operating frequency within an unlicensed band should be selected.**

  - Sections 2.5.1-2.5.3 discuss the important considerations for the antenna of the instrument such as centre frequency selection, RF emission regulations as well as cost of implementation. An operating frequency is finally chosen in Section 3.5, which also discusses the types of antennas that are well suited for level sensing as well as specifications for the antenna beamwidth. A description of a 5.8 GHz horn antenna that was provided by the sponsor is also given.

- **Calculations should be done to determine whether the approach is able to meet the user requirements, particularly in terms of accuracy, cost and power consumption. An instrument architecture with desired specifications should be presented.**

  - Chapter 3 begins with the selection of pulse radar technology for the instrument. Calculations are then performed in Sections 3.2-3.6 in order to derive specifications for the SNR, pulse rise-time and pulse-width.
  - The timing constraints are then examined in Sections 3.7-3.10 and a technique for time interval measurement by Vernier time-stretching will be proposed. The radar transceiver output will then be compatible with the existing ultrasonic instrument's timing hardware and produce a time expanded range profile. Simulations in both Matlab and SystemView are presented to illustrate the concept.
  - The specifications for the instrument, including the time expansion, are then summarised in Section 3.11.

- **Suitable demonstration hardware should be designed, constructed and tested.**

  - Chapter 4 describes the architecture of the instrument and identifies the sub-systems. The individual requirements for each of the sub-systems is then addressed and hardware options for meeting these requirements are

presented. Where appropriate, real components are selected and their properties simulated using programmes which include *SystemView*, *Matlab*, *LTSpice/SwitcherCAD* and *Genesys*. In some cases simple prototypes are constructed. Each hardware option is then carefully considered and accepted or rejected.

- Chapter 5 then focuses on improving and implementing the hardware that met the acceptance criteria in Chapter 4. Layout issues and component choices are discussed in more detail as well as the choice of substrate. The generation of the short pulses is a crucial step in the design and this chapter presents two candidate methods, namely the MIR pulse driver and the avalanche pulse driver. All of the sub-systems are individually tested to ensure that they meet the desired specifications.
- Chapter 6 then discusses the integration and testing of the complete system. Firstly, tests are carried out on the complete transmitter using both the avalanche and MIR pulse driver circuitry. The final pulse driver technique is then chosen, after which the proposed time interval measurement technique using time stretching is demonstrated. The compliance of the system to the set of desired specifications is then reviewed.
- Chapter 7 ultimately summarises the important results and findings of this project. Some future work is then recommended.

1.5 Project Scope

This dissertation describes the design and implementation of a microwave level measurement instrument. Only microwave techniques have been investigated. All the other numerous level measurement techniques are beyond the scope of the project. The objective is to only demonstrate the technology and provide an output measurement signal that is compatible with the time domain processor of an ultrasonic instrument, so it is beyond the scope of this project to produce a working, commercially viable device. The aim is to set up a platform for further development. Measurement software, casing/packaging and antenna design is also beyond the scope of the project. Due to time constraints it was assumed that the instrument would be operating at room temperature and nominal atmospheric pressure. The target surface is also assumed to be flat and the level to be static during all measurements.

1.6 Summary

In this chapter the plan of development for this project was laid out and the user requirements for the instrument were specified. Power consumption, accuracy and cost

were identified in an initial requirements analysis as being critical parameters. Due to the limited supply current and the fact that the research is aimed at replacing the transceiver for a pulsed ultrasonic instrument, it heavily suggests that a pulsed radar architecture would be the most likely candidate to pursue.

Chapter 2

Background

This chapter begins with a brief introduction of radar level sensors. Radar architectures operating in both the time and frequency domain are then discussed as possible candidates and some examples from industry are presented. The architectures are not only compared to each other in terms of their ability to meet the stringent user requirements but also for compatibility with any of the existing ultrasonic hardware. The architecture of an ultrasonic level measurement instrument is then introduced and the sub-systems that will be replaced or augmented with microwave technology will be highlighted. The important physical properties of the environment and its effects on the electromagnetic signals of the instrument will then be discussed. The two wire 4-20 mA loop power supply will then be described in some detail. The frequency of operation of the instrument is then discussed based on the emission regulations as well as the cost of implementation.

2.1 Introduction to Radar Level Measurement

Radar level measurement instruments work in a similar way to the ultrasonic level sensors which were introduced in Chapter 1. They are usually located at the top of a vessel containing the substance that the user wishes to monitor. High frequency electromagnetic waves are transmitted down toward the surface of the material. Some of the energy that is transmitted is reflected off the target surface and received by the instrument. Since electromagnetic waves travel at the speed of light, the time-of-flight (TOF) of the transmitted and reflected signal can be used to determine the range of the target surface from the radar. The level is then found by subtracting this range from the known full-scale height of the tank.

As mentioned in Chapter 1, radar technology allows for the creation of an extremely reliable measurement device and lists several advantages over other competing technologies[25, 48, 17]. Radar level measurement can be executed in a wide variety of techniques, however, the sponsor decided that the research should focus only on the two most widely

used techniques, *pulsed radar* and *FMCW radar*. The operation of both these techniques is covered very thoroughly in the literature [78, Chps 12,14][74, pg 195]. The pulse radar is the more similar of the two to an ultrasonic instrument because they both determine the level using *pulse-delay ranging*, in which the time delay between a transmitted pulse and a received echo is measured and used to calculate the distance to the target surface by using the propagation speed of the signal. FMCW radars use a waveform that is swept in frequency at a fixed rate. The frequency of the reflected signal is compared to that of the signal being transmitted. The result of this process is called the *beat frequency,* which is directly proportional to the distance that the signal has travelled [37].

While both techniques have similar requirements for bandwidth and SNR to meet a required accuracy, the pulsed radar has the advantage in that it has lower power supply requirements and its architecture is much simpler. Unlike the FMCW radar, the pulse radar does not transmit continuously, which means that energy can be stored up in between pulses. This makes it an ideal choice for two-wire loop operation. The pulsed radar also does not require any power hungry frequency domain signal processors and does not suffer as much from processing delays. For example, a good commercial off the shelf (COTS), low power, FMCW transceiver operating at 5 GHz requires approximately 100 mA of supply current [73]. In applications like level sensing, where space requirements make it necessary to use a single antenna for transmitting and receiving, pulsed radar has another benefit in that it transmits and receives at different times and there is no interference between the two circuits. In FMCW systems isolation would have to be provided, since the transmitter is is always on [78]. It is also unlikely that any frequency domain technique could compete cost-wise to a pulsed system as FMCW systems have at least 30% more components [33].

2.2 Existing Ultrasonic Instrument Specifications

Figure 2.1 shows a block diagram of a typical ultrasonic level measurement instrument. The loop-power supply provides the instrument with power as well as controlling the current flowing to represent the measurement level; a microprocessor calculates the time interval between each transmitted pulse and its corresponding echo and calculates the level measurement; software can be used to train the instrument to reject false echoes caused by reflections from the tank walls; the transmitter is responsible for generating an electrical pulse when triggered; a transducer converts the electrical energy from the transmitter into acoustic energy and back into electrical energy for the receiver; the receiver is responsible for the detection of the reflected echos. The goal for this project is that the transmitter, transducer and receiver (bounded in the red box) be replaced by electromagnetic equivalents in order that microwaves can be used in the place of sound waves but that the remaining timing microprocessor and power supplies

remain the same.

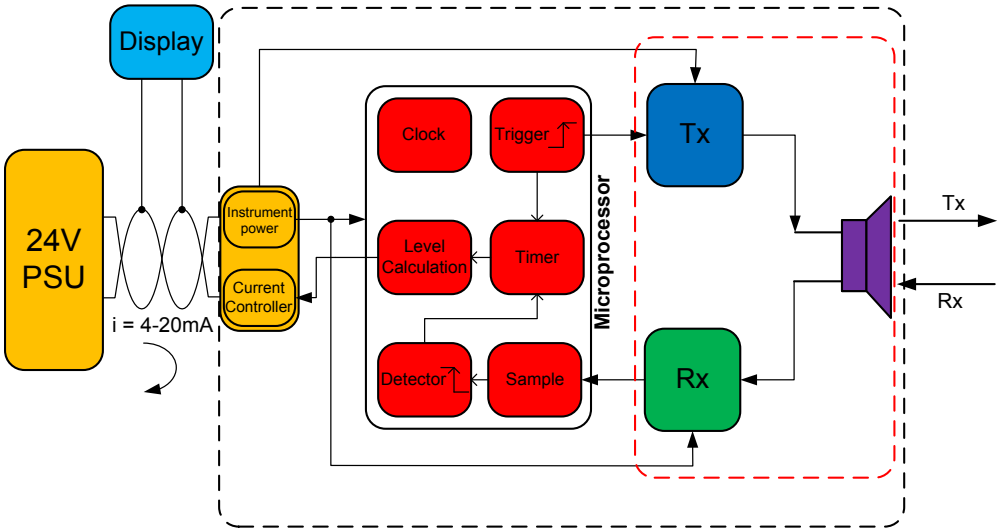

Figure 2.1: Simplified block diagram showing how the sub-systems of an ultrasonic instrument are interconnected.

2.3 4-20 mA Loop Power Supplies

A 24 V supply is used because it is the most common supply voltage for sensing instruments. The use of the 4-20 mA standard helps to satisfy the requirements to make the instrument intrinsically safe, a necessity in many process applications [3]. Intrinsically safe means that the instrument is incapable of causing explosions with the heat or spark energy inside it. This means that the instrument can be opened while it is operating on site if necessary.

The operation of the current loop is very straightforward and is described in detail in the literature [4, 13, 14, 40]. Figures 2.2 and 2.3 illustrate the operation of a typical 4-20 mA sensor. In the case of a level measurement instrument, the detected level is converted to a proportional current, with 4 mA representing the zero or lowest-level output and 20 mA representing the full-scale output. This current is maintained in the loop where a receiver at a remote end can convert the 4-20 mA current into a voltage that can then be processed and displayed by a computer. This method is particularly useful when level measurement information has to be transmitted over a long distance. The advantage of using current to convey this information is that voltages tend to become attenuated due to the long resistive pathway between the instrument and the remote monitor. Signal carrying conductors are also susceptible to noise pickup from other conductors. Sending a current over long distances produces voltage losses proportional to the length of the wiring. But these voltage losses do not reduce the 4-20 mA current as long as the transmitter and loop supply can compensate for these drops.

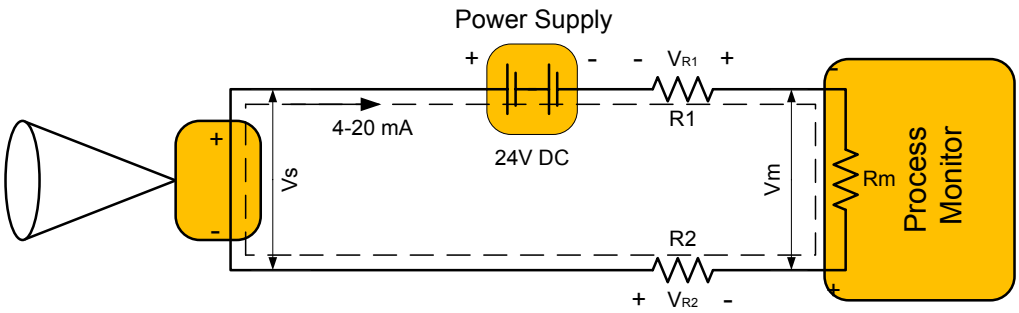

Figure 2.2: Components in a loop power system. The sensor, voltage to current converter, the loop power supply and the process monitor are all connected in a closed series loop configuration. The sum of the voltages around the loop must also not exceed the total supply voltage when the current in the loop is at its maximum. V_s- the minimum operating voltage of the instrument, V_m - the voltage drop due to the burden of the resistance of the process monitor and V_{R2} and V_{R1} - the voltage drop due to the resistance of the wires.

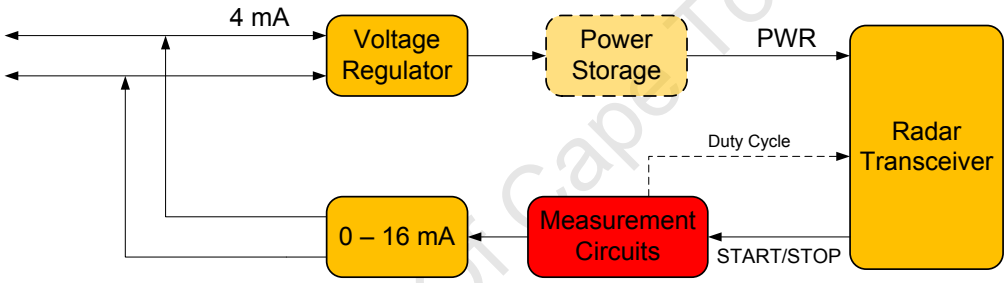

Figure 2.3: Block diagram showing the flow of current in the sensor. The voltage regulator ensures that exactly 4 mA of current is drawn to power the radar and provides the appropriate supply voltages. An optional storage element could be added to provide temporary storage and then supply higher current surges to power the instrument on a reduced duty cycle such that the average current remains 4 mA at the regulator. An analogue current proportional to the measured level is adjusted to modify the total current flowing in the loop to between 4 mA and 20 mA.

2.4 Important Properties of Microwave Signals

This section describes important physical properties that affect microwave systems. The properties of the environment in which the instrument is placed, as well as the properties of the medium, can affect the level measurement results. Although it was mentioned earlier that microwave techniques were relatively immune to most conditions, this section describes in more detail the effects of temperature, pressure and dielectric constant on the measurement result.

2.4.1 Effects on Propagation Speed

The electromagnetic waves from a radar propagate at close to the speed of light by the well-known equation:

$$c = \frac{c_0}{\sqrt{\mu_r \varepsilon_r}} \tag{2.1}$$

Where μ_r and ε_r are the relative permeability and the relative permitivity of the medium respectively. Although the frequency is not influenced by changes in the propagation medium, the wavelength (λ) and the velocity of propagation (c) can be slightly affected in certain level applications. Temperature, pressure and composition of the air inside the vessel have an effect on the dielectric constant of the propagation medium. Free space (air) has a dielectric constant close to one. A slight variation in the dielectric constant will affect the propagation speed of the wave and therefore the distance calculation. The dielectric constant of the propagation medium can be calculated from [17, Page 18]:

$$\varepsilon_r = 1 + (\varepsilon_{rN} - 1)\left(\frac{\theta_N P}{\theta P_N}\right) \tag{2.2}$$

Table 2.1: Variables for Equation 2.2

Variable	Description
ε_r	- calculated dielectric constant
ε_{rN}	- dielectric constant under normal conditions (1)
θ_N	- temperature under normal conditions (273K)
P_N	- pressure under normal conditions (1 bar)
θ	- process temperature in Kelvin
P	- process pressure in bar absolute

The error caused by variations in temperature, pressure and dielectric constant can be calculated by using equation 2.1 and equation 2.2. Figures 2.4 and 2.5 show the percentage error against temperature and pressure[1] respectively. Note that the error in propagation velocity for the microwaves is very small over the entire range of operating temperatures specified by the user requirements. On the other hand the acoustic waveform propagation error is very large by comparison. The pressure has a more significant effect on the microwave signals, however, it is still extremely small over the entire operating range. Acoustic signals in air at a constant temperature are not affected by changes in the pressure. The maximum overall error that can occur, based on both graphs, is 0.134%.

[1]Note: to convert Bar into Pa multiply by 1×10^5

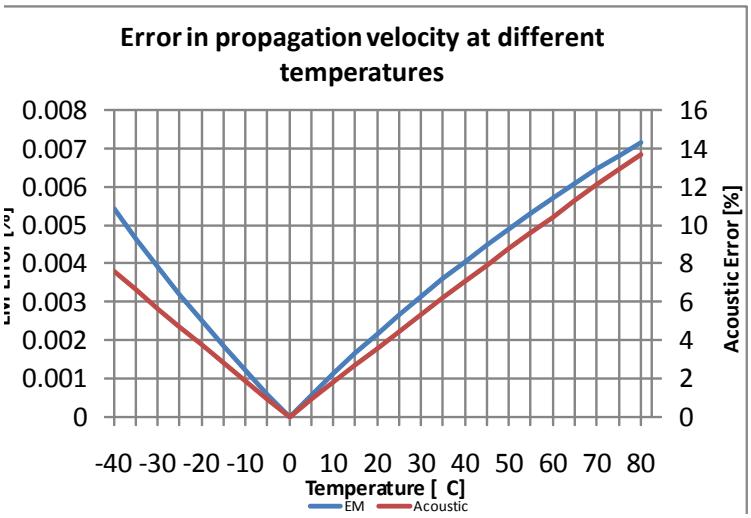

Figure 2.4: The graph shows the effects of temperature on the propagation velocity. The error in the electromagnetic propagation velocity is shown by the red curve while the error in acoustic propagation velocity is shown in blue for comparison. The pressure is held constant at 1 Bar.

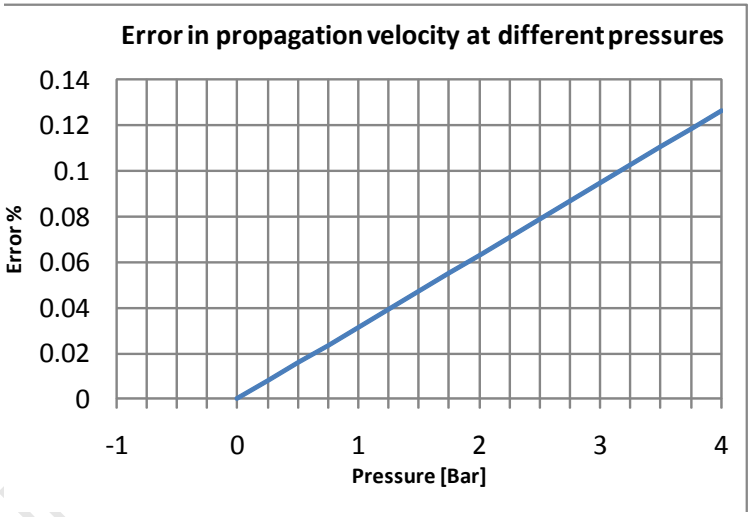

Figure 2.5: The graph shows the effects of pressure on the EM propagation velocity. The temperature is held constant at 273 K.

2.4.2 Reflection from the Surface Medium

When the instrument transmits a wave, a portion of the energy must be reflected back off the surface of the target medium for the instrument to calculate the level. This reflected wave is referred to as the echo. If the surface is conductive, the wave will readily reflect and produce a large echo. If the surface is a dielectric, then the amount of reflected energy depends on the contrast between its dielectric constant and that of the propagation medium, which for all cases will be assumed to be air.

It must be noted that a dielectric material is characterised by both its permittivity, ε, and conductivity, σ. It is a complex quantity as shown in Equation 2.3[39]:

$$\varepsilon_c = \frac{\sigma + j\omega\varepsilon}{j\omega} = \varepsilon' + j\varepsilon'' \tag{2.3}$$

In a loss-less dielectric $\sigma = 0$. In this case ε_c is real and equal to $\varepsilon' = \varepsilon'_r\varepsilon_0$. Here, ε'_r is described as the relative real permittivity. The imaginary part, ε'', of the complex permittivity is associated with losses. In the case of a lossy dielectric, the real and imaginary parts are generally measurable and the ratio between them is called the loss tangent as seen in,

$$\tan\theta_{loss} = \frac{\varepsilon''}{\varepsilon'} = \frac{\sigma}{\omega\varepsilon'} \tag{2.4}$$

where $\epsilon'' = \sigma/\omega$. This leads to a relationship between relative imaginary permittivity (or relative loss factor ε''_r), also dimensionless, and conductivity as given by,

$$\varepsilon''_r = \frac{\sigma}{\omega\varepsilon_0} \tag{2.5}$$

A low-loss dielectric material is defined as a material that has small loss tangent, namely $\sigma/\omega\varepsilon \ll 1$. Or, equivalently, the imaginary part of the complex permittivity (2.3) is small compared to the real part.

Equation 2.6 [17, page 23] below describes the relationship between the percentage reflected power and the dielectric constant of the surface, assuming loss-less dielectrics. Figure 2.6 shows this relationship graphically.

$$\Gamma = 1 - 4\frac{\sqrt{\varepsilon_r}}{(1+\sqrt{\varepsilon_r})^2} \tag{2.6}$$

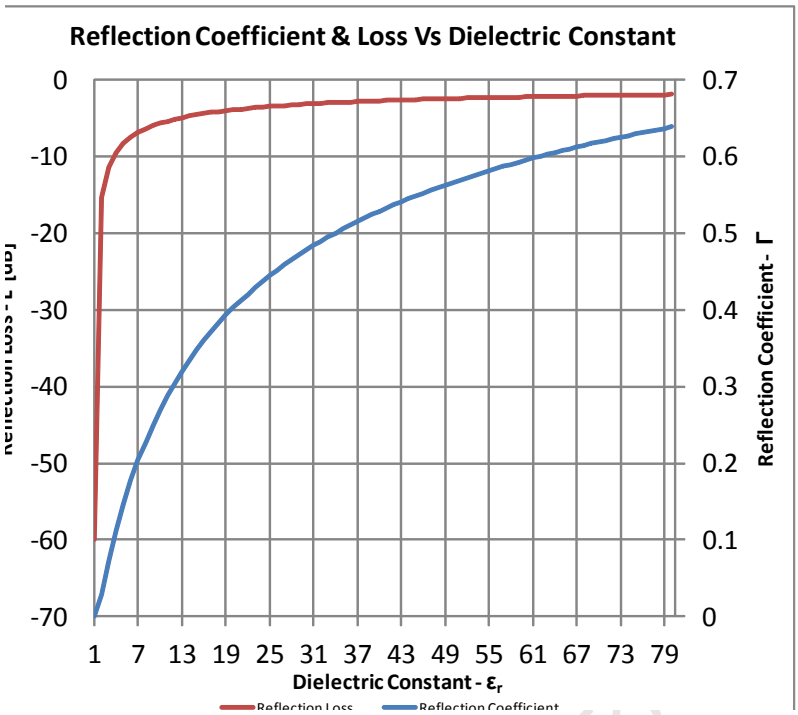

Figure 2.6: The graph shows the reflection coefficient and the reflection loss from lossless materials with different dielectric constants.

To put these figures into perspective, water has a high dielectric constant at approximately 80, while liquid butane at the other end of the scale has a low dielectric constant of approximately 1.4. As can be seen, the larger the contrast, the larger the amount of reflected power. At dielectric constants of less than 5, the amount of reflected power is critically small.

2.5 Operating Frequency

The choice of operating frequency must be made from licensing considerations, cost and availability of microwave components and the technical advantages brought about by the wavelength of signal. Level measurement instruments typically operate at microwave frequencies between 5 GHz and 26 GHz, but there is no single frequency that is ideally suited for every application [17, Pages 62-67]. As was mentioned earlier in Section 1.3, due to licensing constraints, most radar level manufacturers are forced to use frequencies in the unlicensed ISM bands. 5.8 GHz and 24 GHz are the most common centre frequencies. The sponsor of the project insisted that the instrument use one of these frequencies. This section begins by describing some of the advantages or disadvantages offered by both high and low frequency radar. The cost of implementation is then addressed and regulation guidelines are further discussed.

2.5.1 Advantages and Disadvantages of High and Low Frequency Operation

Higher frequencies, which have shorter wavelengths, will reflect off small objects or scatter off agitated surfaces, which have areas comparable to these wavelengths. These reflections can cause false echos. Larger wavelengths simply ignore these small objects or surface disturbances.

In terms of the antenna, gain is inversly proportional to λ^2 and directly proportional to aperture area. Although gain also depends on the aperture efficiency, the highter the frequency of the radar, the higher the gain, all other factors being equal. Another attractive feature of an operating frequency of 24 GHz is that the wavelength is of the same order of magnitude as that of an ultrasonic signal, which means that the acoustic transducer and the microwave antenna can be comparable in size. This is illustrated in Figure 2.7.

Higher frequency radar suffers more signal attenuation caused by condensation and material buildup as well as by steam and dust. This results in the receiver having to be able to cope with smaller echo signals. Lower frequencies perform better than higher frequencies when there is foam present. Although, it also depends on the type of foam and how dense it is. Higher frequencies also tend to have a shorter minimum distance because the rise times are shorter.

Figure 2.7: Photo showing (from left to right) a 5.8 GHz horn antenna (Tokimec MRG-10), an ultrasonic transducer (KAB SHORTI LP) and a 24 GHz antenna (Vegapuls 61) connected to their respective sensors. The size of the ultrasonic transducer is comparable to the 24 GHz antenna, while the 5.8 GHz antenna is much larger.

2.5.2 Cost of Implementation

Unfortunately it is difficult to implement 24 GHz in low cost surface mount technology. A quarter wavelength at 24 GHz is roughly 3 mm, which is of the same order of magnitude as the dimensions of many surface mount components. This means that wavelength effects will be a severe limitation and special design care and complex layout and assembly techniques will have to be employed on expensive substrates. This increases the cost of manufacturing considerably.

To counter the effect of diminishing wavelength, the component size can be reduced by designing with a monolithic technology such as MMIC's (monolithic microwave integrated circuits). But this would also put up the cost of the instrument so that it is no longer competitive with an ultrasonic instrument, which could be manufactured on silicon chips. Clearly a 5.8 GHz system would be much cheaper to implement and will not suffer too much from wavelength effects when implemented in surface mount technology. The downside is that the antenna would have to be much larger.

2.5.3 Regulations

In Chapter 3, it will be shown that radars that have a high accuracy requirement need a large signal bandwidth. If the fractional bandwidth is greater than 20% of the centre frequency, the instrument is classified as Ultra-wideband (UWB). The fractional bandwidth or percentage bandwidth is defined in equation 2.7 from [80, pg 12], where f_H and f_L are the upper and lower band edges of the signal. Since UWB transmissions can extend over a very large band of frequencies, this band may include frequencies on which other types of services are running and may interfere with their operation.

$$\%BW = \frac{2\,(f_H - f_L)}{f_H + f_L} \times 100 \tag{2.7}$$

The International Telecommunications Union (ITU) is responsible for establishing an international standard to regulate the emissions of devices incorporating UWB technology. In 2006 the ITU published a recommended framework for the regulation of UWB devices based on the regulations imposed by the FCC (United States), CEPT (Europe) and Japan [41]. As of 2007 the ITU-R has been in the process of establishing standard emission masks for UWB devices but have not yet come to a final resolution.

UWB systems are classified according to application. Radar level measurement instruments are classified as short-range indoor devices, as long as they are pointing towards the ground. Different emission limits exist for different classifications, which include Ground Penetrating Radar (GPR), imaging systems, surveillance systems, medical imaging systems, vehicular radar systems as well as indoor and outdoor communications systems. Currently, the ITU-R has assigned frequency bands at 5.725–5.875 GHz (centre frequency 5.8 GHz) and at 24–24.25 GHz (centre frequency 24.125 GHz),

for industrial use. Centre frequencies of 5.8 GHz and 24 GHz fall within these emission guidelines as long as the maximum EIRP is -41 dBm/MHz.

2.6 Existing Radar Level Measurement Technology and Intellectual Property

As mentioned earlier, there are several commercial manufacturers that have radar level measurement instruments on the market. In this section some of the more notable manufacturers will be introduced and some of the pioneers of intellectual property and proprietary technology in the field will be presented.

2.6.1 VEGA Controls Ltd.

VEGA[2] are a well established manufacturer of a wide variety of instrumentation for level measurement and are considered to be market leader in the field of radar level measurement. In 1975 VEGA produced their first ultrasonic level measurement instrument for measuring solid and liquid levels. Beginning in 1989 they started experimenting in radar level measurement and decided to concentrate on the development of pulse radars because of their low power consumption and reduced reliance on processing power and frequency domain hardware. In 1991 they produced their first pulse radar product but it was not until 1997 that they completed their first two-wire, loop powered, 4-20mA sensor, the VEGAPULS 50 [17, pg 263]. VEGA currently hold over 50 patents for proprietary technology developed in the field of radar level sensors in the United States alone.

2.6.2 Other Manufacturers

In addition to Vega, the other noteworthy manufacturers of level measurement equipment are:

- Siemens
- Endress & Hauser
- Omega

2.6.3 McEwan Technologies

McEwan Technologies[3] is a company that was founded in 1996 by Tom McEwan. The company does not sell any instruments but licenses patents for the manufacturing

[2] http://www.vega.com/
[3] http://www.getradar.com/

and sale of radar based sensors. Tom McEwan is most well-known for inventing the Micropower Impulse Radar (MIR) [82], while he was working for Lawrence Livermore National Laboratories. McEwan now boasts the worlds largest radar sensor patent portfolio with over 50 patents in the United States alone.

2.7 Summary

2.7.1 Introduction to Radar Level Measurement

Radar technology allows for the creation of an extremely reliable measurement device. Commercially the two most popular techniques for level measurement are pulsed radar and FM-CW radar. The pulsed radar is the more similar of the two to an ultrasonic instrument because they both determine the level using pulse-delay ranging. In addition, the pulsed radar has the advantage of lower power operation, a lower component cost and less prone to interference between the transmitter and receiver circuitry.

2.7.2 Existing Ultrasonic Instrument Specifications

A block diagram of the existing ultrasonic instrument architecture has been described. In order to incorporate the existing hardware into the radar instrument, it was shown that the acoustic transceiver sub-systems would have to be replaced with microwave equivalents.

2.7.3 Power Supply

It was noted that 4-20 mA loop power supplies are the standard for process monitoring applications. The configuration requires that only two wires need to be connected to the instrument. Care must be taken in the design process to ensure that the instrument draws less than 4 mA of continuous current but the 4-20 mA current controller and voltage regulators from the existing ultrasonic instrument can be reused.

2.7.4 Physical Properties

It was shown that temperature and pressure could have an effect on the propagation velocity of the signal, degrading instrument accuracy. But these errors have been shown to be sufficiently small for microwaves over the temperature and pressure ranges required. It was also shown that the temperature greatly affected the propagation of acoustic waveforms, highlighting one of the advantages of changing to electromagnetics. If the temperature and pressure are known to the user, the instrument could be calibrated for the new velocity of propagation. If the temperature and pressure are

varying substantially with time, a temperature or pressure sensor should be included for real time adjustments.

It was also noted that the dielectric constant of non-conductive surface mediums affected the amount of energy that is reflected toward the instrument. This is an important property to bear in mind when considering potential applications. Level measurements at dielectric constants less than 5 are not recommended since the amount of reflected power is critically small [17, pg 24].

2.7.5 Operating Frequency

Frequency selection is usually based purely on application, but both high and low frequencies seem to have individual advantages. High frequency transmitters tend to have more focused beams at smaller aperture dimensions, but the reflected power can be lower because of scattering. 24 GHz has the advantage of reduced antenna size but the circuit design and layout is far more complex and expensive.

2.7.6 Existing Technology

Vega is the leading manufacturer in field of radar based level sensors but there are also several other competitors in the market. Vega and McEwan Technologies hold the most patents in the field of radar sensors.

Chapter 3

Technology Selection & Instrument Specifications

This chapter begins with the final choice of radar technology for the instrument as well as the operating frequency. Calculations are then performed in order to derive the important instrument specifications. The timing constraints are then examined and a technique for time interval measurement is introduced that will enable the radar transceiver output to be compatible with the existing ultrasonic instrument's timing hardware.

3.1 Instrument Architecture Selection

After comparing time domain and frequency domain techniques in Section 2.1, there was no candidate that offered a clear advantage in terms of accuracy. Any technology would indeed be capable of meeting this requirement given sufficient bandwidth. However, when comparing them on the basis of cost, complexity and power consumption, the conclusion was that a pulsed radar would be a better candidate to meet these requirements. In addition it made more sense to focus on a time domain system since the existing acoustic sensor already operated using time domain analysis and it would be a much simpler task to integrate a new pulsed radar transceiver in the place of the existing pulsed acoustic transceiver.

3.2 Theory of Operation

The sensor functions like a short-range altimeter, the details of which can be found in the literature [19, 18, 71]. The sensor is situated at a height, H, above the target surface. A short pulse is transmitted towards the surface at time, t_1. The pulse propagates at close to the speed of light, c and is reflected by the surface. The *leading edge* of the echo, which corresponds to the surface nearest to the sensor is received at time, t_2. The

primary variable of interest in a pulse radar level sensor is, therefore, the time delay $t_d = t_2 - t_1$. The height can then be calculated by:

$$H = \frac{ct_d}{2} \tag{3.1}$$

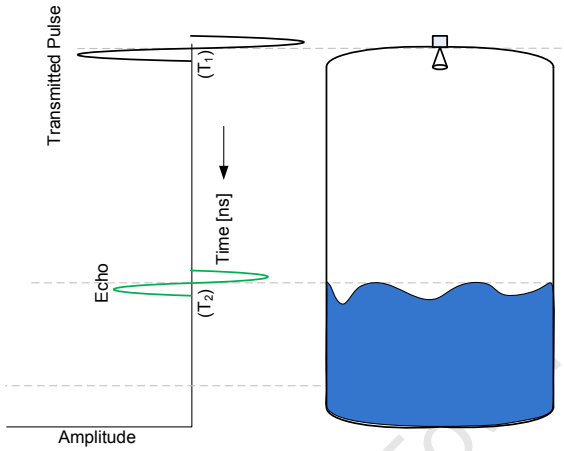

Figure 3.1: Diagram of pulse radar for level measurement

3.3 Pulse Specifications

The range measurement accuracy of the instrument is related to the time delay measurement accuracy, δt_d. The timing accuracy in an ideal system is proportional to the "sharpness" of the pulse [79, Page 394], therefore, a faster rise-time, t_r, would mean a better timing accuracy. However, in the presence of additive white Gaussian noise (AWGN) and when the signal-to-noise ratio (SNR) is relatively good, it is more appropriate to write the timing accuracy in the form [74, page 319]:

$$\delta t_d = \frac{t_r}{\sqrt{2SNR}} \tag{3.2}$$

From equation 3.1, the range measurement accuracy is then:

$$\delta H = \frac{ct_r}{2\sqrt{2SNR}} \tag{3.3}$$

Sources of error include: [71, 33, 19, Page 177]

- Pulse dispersion as it is scattered from a rough surface
- Clock accuracy & period jitter
- Speed of propagation to the target surface
- Multi-path

As can be seen in table 3.1, a fast rise-time and a high SNR are necessary to achieve the time interval measurement accuracy. A rise-time $t_r < 1\text{ns}$ and $SNR > 13\text{dB}$ are good target specifications. The minimum distance is also effected by the pulse-width. Narrower pulses give the radar a better ability to detect close targets since echoes cannot be received while the instrument is transmitting. So in addition to a fast rise-time, the pulse should be as short as possible, $\approx 1\text{ns}$

Table 3.1: A table showing the single-shot range measurement accuracy [cm] at different rise-times [ps] and SNR [dB]. Faster rise-times and higher SNR result in better range accuracy.

SNR	$t_r = 500\text{ps}$	$t_r = 800\text{ps}$	$t_r = 1000\text{ps}$	$t_r = 1500\text{ps}$
10	1.68	2.68	3.35	5.03
11	1.49	2.39	2.99	4.48
12	1.33	2.13	2.66	4.00
13	1.19	1.90	2.37	3.56
14	1.06	1.69	2.12	3.17
15	0.94	1.51	1.89	2.83
16	0.84	1.34	1.68	2.52
17	0.75	1.20	1.50	2.25
18	0.67	1.07	1.34	2.00
19	0.60	0.95	1.19	1.79
20	0.53	0.85	1.06	1.59

3.4 Dispersion

Dispersion is a phenomenon, in which the group velocity of a signal is dependent on frequency as it propagates through a medium. Dispersion is, therefore, a problem for multi-band and wide-band systems because the different frequency components of the signal propagate at different speeds through the dispersive medium, which can result in a large change between the input and output as the different components arrive at the output at different times. This can lead to a variety of effects, which include distortion, broadening of the pulse and chirping [1], all of which can limit the spectral content of the signal.

One of the causes of dispersion in this type of system is likely to be the transmission line media. Another source of dispersion will be the antenna, although its design is not considered in this study. The group delay of any microwave components, such as transmission lines, filters, couplers and antennas should be carefully analysed to avoid large dispersive effects.

3.5 Choice of Operating Frequency and Antenna

The choice of operating frequency can be based on the findings of section 2.5. Having weighed the advantages and disadvantages of using an operating frequency of 5.8 GHz or 24 GHz, it was decided that 5.8 GHz would be more suitable for this project as it would be easier and less expensive to implement prototype hardware at the lower frequency. Although there are some nice advantages of the 24 GHz frequency, it was decided that that should be the focus of future work.

3.5.1 Antenna Specifications

Horn antennas and dielectric rod antennas are the best suited for level measurement applications [17, Page 77]. Since the function of the antenna is to direct the maximum amount of energy towards the target surface, it makes sense that very directive antennas such as these are used as it is inefficient and undesirable for any energy to be radiated in any direction other than downwards. Antennas such as parabolic dishes and planar arrays are less common because, although they can be very directive, they are rather bulky and expensive.

The leading edge of the echo signal corresponds to the surface nearest to the sensor. This may not necessarily be directly below. Since it is not possible to unambiguously determine the exact location of the reflecting area within the illuminated footprint of the antenna beam, it is desirable to have as narrow a beam-pattern as possible. The illumination footprint of the antenna must also be considered. Since the instrument is a pulsed radar, there are two situations which can occur. The illumination footprint of the antenna beam, F_b, could be smaller than the illumination footprint of the pulse, F_p, in which case the antenna is called *beam-limited*. If the situation is reversed then the antenna is called *pulse-limited* [19]. In this situation we would like all of the transmitted power to be contained in the antenna beam so a beam-limited setup would be the most appropriate. Care must therefore be taken when choosing the operating frequency and the antenna dimension.

The 5.8 GHz horn, which is shown in Figure 2.7, was provided by KAB Instruments as a possible antenna. Table 3.2 shows whether the antenna is beam-limited when the pulse length, τ, is 1 ns. As can be seen, the horn provided will not result in a beam-limited footprint over the entire measurement range. It was calculated that a minimum antenna aperture of 15 cm or a beam angle of 20° at 5.8 GHz is needed to meet this requirement.

Table 3.2: 3.2a shows that the antenna is only beam-limited for the first 3 m of range for the provided 5.8 GHz horn. 3.2b shows that, if the aperture, D_a , is increased to 15 cm, the antenna is beam-limited for the entire range.

(a) Footprint diameter [m] for $D_a = 0.09\text{m}$, $\tau = 1\text{ns}$

Range	$\mathrm{F_b} \approx \frac{\lambda \mathrm{H}}{\mathrm{D_a}}$	$\mathrm{F_p} \approx 2\sqrt{\mathrm{c}\tau\mathrm{H}}$	$\mathrm{F_b} \leq \mathrm{F_p}$
1	0.57	1.10	√
2	1.15	1.55	√
3	1.72	1.90	√
4	2.30	2.19	x
5	2.87	2.45	x
6	3.45	2.68	x
7	4.02	2.90	x
8	4.60	3.10	x
9	5.17	3.29	x
10	5.75	3.46	x

(b) Footprint diameter [m] for $D_a = 0.15\text{m}$, $\tau = 1\text{ns}$

Range	$F_b \approx \frac{\lambda H}{D_a}$	$F_p \approx 2\sqrt{\mathrm{c}\tau H}$	$F_b \leq F_p$
1	0.34	1.10	√
2	0.69	1.55	√
3	1.03	1.90	√
4	1.38	2.19	√
5	1.72	2.45	√
6	2.07	2.68	√
7	2.41	2.90	√
8	2.76	3.10	√
9	3.10	3.29	√
10	3.45	3.46	√

3.6 SNR and Transmitted Power Specifications

As was mentioned earlier, altimeters have a different derivation for the received SNR than conventional radars, since all of the transmitted power is contained within the illumination footprint and hits the target surface. The total reflected power is, therefore, the transmitted power less the reflection loss of Figure 2.6. Assuming that the target surface is flat and that the energy is re-radiated with a spherical expansion, the received SNR can be written as [19, Page 180]:

$$SNR = \frac{\Gamma P_t A_e}{4\pi H^2 k T_e B} \tag{3.4}$$

To illustrate, if we take the SNR from Section 3.3 as 13 dB, a bandwidth of $B = \frac{1}{\tau} = 1\,\text{GHz}$, an effective aperture area of $A_e = e_{ap}\left[\pi\left(\frac{D_a}{2}\right)^2\right]$,where antenna diameter $D_a = 0.15\,\text{m}$ and aperture efficiency $e_{ap} = 0.6$, with a return loss $\Gamma = 0.2$. And we assume an equivalent noise temperature $T_e = 1000\,\text{K}$ and height $H = 10\,\text{m}$. Then the peak transmitted power, P_t, requirement can be calculated as $163\,\mu\text{W}$.

3.7 Initial Simulation

Figure 3.2 shows the result of a *SystemView* simulation of a transmitted pulse and its corresponding echo. The pulse is assumed to have a Gaussian shape because the rise and fall times are comparable to the pulse width. The time delay between the transmitted signal and the echo can be observed to be in the order of several nanoseconds. The maximum round trip time delay for 10 m can be calculated using equation 3.1 at approximately 67 ns. This is nearly six orders of magnitude faster than an acoustic

pulse, which would take approximately 58 ms[1] to cover 10 m and back. The time interval measurement capabilities of the existing ultrasonic instrument will therefore be insufficient and will not be able to measure such short delays. Clearly an alternative approach is required in order to meet the accuracy requirement.

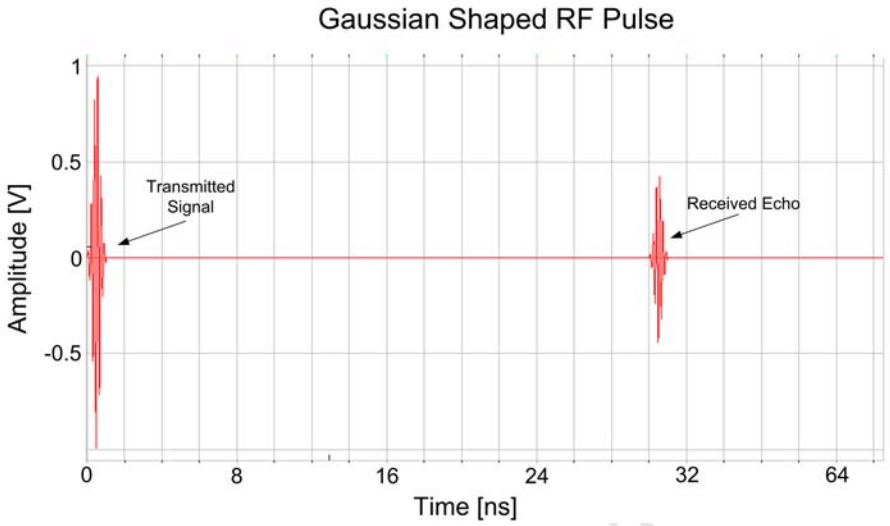

Figure 3.2: Plot of the transmitted signal and the received echo at 5.8 GHz. The pulse width is approximately 1 ns.

3.8 Time Interval Measurement

The requirements for the pulse waveform have already been discussed in Sections 3.2-3.6 and specifications have been suggested. The need for a fast and accurate time interval measurement (TIM) procedure now becomes the important requirement. Clearly there is a practical problem with sampling a short pulse at 5.8 GHz. The sample interval would have to be a few picoseconds to obtain the required accuracy and a large amount of memory would be required. But since we are only interested in the leading edge of the received echo, this can be used to trigger an event timer.

There are several techniques described in the literature that could be used to measure the time interval with sub-nanosecond accuracy between a start and a stop trigger. Kalisz provides a good review of analogue as well as digital methods in his 2004 paper [43]. In addition, TIM could be performed by using a COTS device called a time-to-digital conversion (TDC) chip [2]. Examples are shown in Table 3.3. These chips directly convert a measured time interval between a start and stop trigger into a digital value, which can be processed on a microcontroller. The chips can also be operated on a duty cycle to reduce the average current consumption and boast impressive timing accuracy and resolution. The implementation of such chips can, however, be very complex, require several additional components, professional multi-layered PCB design and drastically increase the cost of the instrument. The disadvantage of these methods is that

[1] with the speed of sound being 343m/s at room temperature

substantial modification of the existing ultrasonic timing hardware will be required to implement TIM with sub-nanosecond accuracy.

Table 3.3: Table of available TDC chips

Part no.	Resolution [ps]	Supply Current
TDC-GP1	125	20 mA /s
TDC-GP2	50	15 mA / s
TDC-GPX	10 (M-mode)	45 mA / s

3.9 A Vernier Time Stretching Approach

The user requirements stipulate that a distance measurement has only got to be computed every second. Since a single pulse-echo run-time is in the order of nanoseconds, the remaining time can be used to incorporate more pulse-echoes into a single distance measurement.

The pulse radar has a regularly repeating signal and if the PRF is high enough there can be thousands of pulses produced every second. This regularity can be exploited and used in a sequential sampling scheme. When using sequential sampling, the range profile is built up over a longer time period or "expanded time". Instead of taking a sample twice per period, as required by the Nyquist theorem, the sampling period is made longer. Since the period of the signal and sample are not the same, each successive pulse is sampled at a slightly different point and over a long enough time period the entire signal can reproduced on a time expanded axis. The relationship between the expanded and original time scale, therefore, depends on the difference in the two time periods. A common example of this principal is a stroboscope used to slow down fast periodic movements of machinery [17, Page 55]. The term stroboscopic sampling is derived from this. This approach was first noticed in the literature for TIM in some digital circuits [5].

A slightly different approach is taken in [17, Page 58], in which a sequential sampling scheme is combined with a cross-correlation procedure (matched filter). Instead of using a rapid sampler, an exact copy $v_r(t)$ of the original transmitted pulse train $v_t(t)$ is made but it is given a slightly longer time period between the pulses. So instead of taking a short voltage sample, the cross-correlation procedure multiplies a point of the transmitted pulse or echo by the corresponding point on the sampling or reference pulse. This corresponding "multiplication" pulse is then integrated to form a point on a time expanded curve which corresponds to the position of the transmit pulse relative to the reference pulse. After many pulses have been multiplied these points form the time expanded pulse. This process is illustrated by the block diagram of Figure 3.3 with the corresponding waveforms in Figure 3.4.

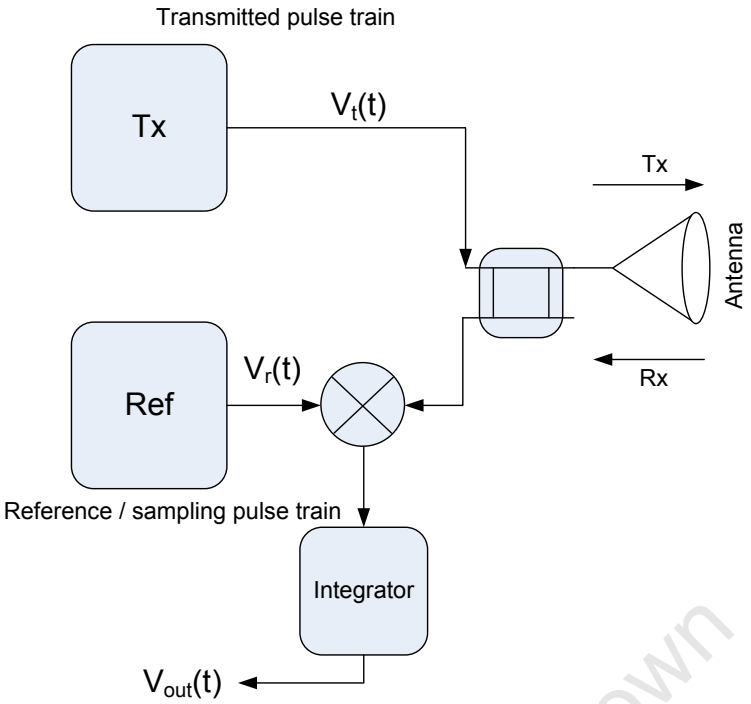

Figure 3.3: Block diagram of time expansion implementation. The envelope of the transmitted pulse train $v_t(t)$ and the envelope of the reference pulse train $v_r(t)$ are identical except that the pulse repetition intervals (PRI's) T_1 and T_2 differ slightly.

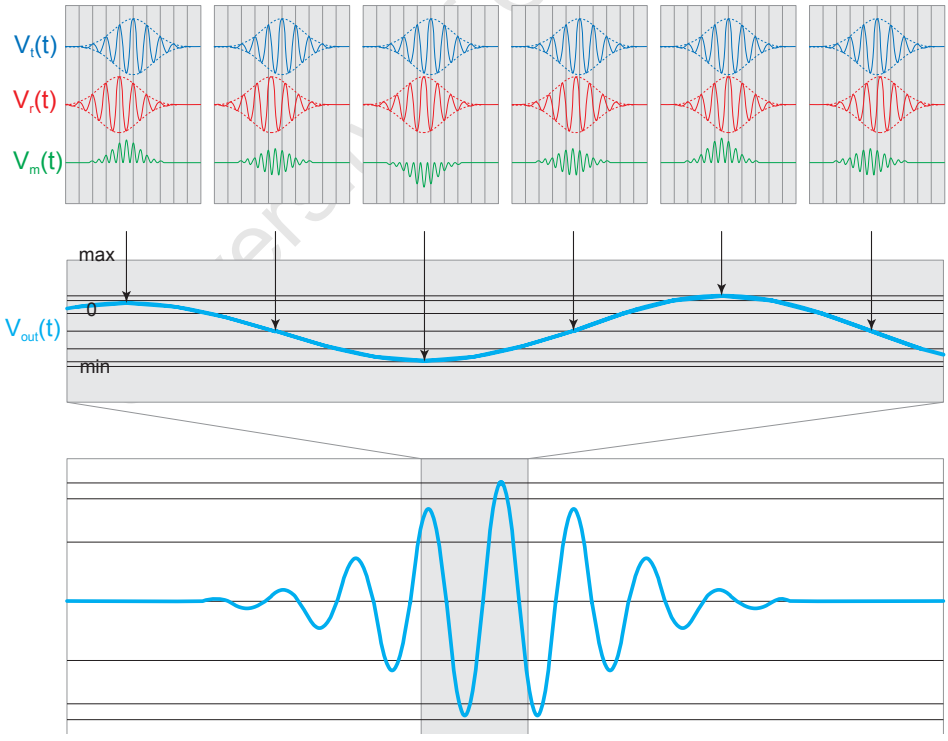

Figure 3.4: Cross correlation of the transmitted/received signal $v_t(t)$ and the reference $v_r(t)$. The product $[v_t(t)v_r(t)]$ is then integrated to produce the expanded time curve $v_{out}(n)$. The technique builds a complete picture of the echo curve [17].

3.9.1 Mathematical Analysis

It must be noted that the PRI T_1 can refer to the transmitted pulses or the received echoes. Assuming that the pulses are Gaussian in shape, we can write the transmitted and reference pulse trains as:

$$v_t(t) = \sum_{n=-\infty}^{\infty} \exp\left[\frac{-(t-nT_1)^2}{2\sigma^2}\right] \tag{3.5}$$

$$v_r(t) = \sum_{n=-\infty}^{\infty} \exp\left[\frac{-(t-nT_2)^2}{2\sigma^2}\right] \tag{3.6}$$

It can be shown that the output voltage for the n^{th} pulse , $n = 0, 1, 2, ...\text{positive interger}$, is:

$$v_{out}(n) = \sum_{n=-\infty}^{\infty} \sqrt{\pi}\sigma \exp\left[\frac{-\mathrm{n}^2(\mathrm{T}_2-\mathrm{T}_1)^2}{4\sigma^2}\right] \tag{3.7}$$

It can also be shown that the Fourier transform of v_{out} can be written as equation 3.8, where ω_1 and ω_2 are the angular frequencies of the transmit and reference frequencies and δ is the Dirac delta function:

$$V_{out}(\omega) = \frac{\omega_1\omega_2}{2\pi} \sum_{n=-\infty}^{\infty} V_t(n\omega_1)\, V_r(n\omega_2)\, \delta(\omega - n[\omega_2 - \omega_1]) \tag{3.8}$$

In the frequency domain we note that the spectral content is now spaced at the difference of the two PRF's. In the time domain, the time expanded pulse repetition interval becomes:

$$T_{rep} = \frac{T_1T_2}{T_2 - T_1}\ [\mathrm{s}] \tag{3.9}$$

This is when the rising edge of the transmitted pulse train and the reference pulse train once again coincide. This corresponds to the time stretching factor, shown in equation 3.10 and the equivalent sampling rate shown in equation 3.11.

$$TSF = \frac{T_1}{T_2 - T_1} \tag{3.10}$$

$$\mathrm{f}_{\mathrm{s,eff}} = \frac{1}{\mathrm{T}_2 - \mathrm{T}_1} \tag{3.11}$$

This concept might seem very complicated mathematically but it is relatively simple to achieve in analogue circuitry. Referring back to Figure 3.3, it is shown that the

multiplication is achieved using a mixer while the integration can be performed using a capacitor.

Another advantage of this TIM scheme is that since many pulses are integrated to form the range profile, the SNR of the time expanded signal can be orders of magnitude better than that of a single pulse. The time expansion factor can also be chosen such that the output waveform is comparable to the range profile of an acoustic waveform, which means that the timing circuitry on the existing acoustic instrument can remain unmodified. To illustrate, an ultrasonic transducer transmits at a frequency of about 70 kHz. In order to expand a 5.8 GHz frequency to 70 kHz, a time expansion factor of approximately 82000 is required. This can be achieved by taking:

$$T_1 = \frac{1}{3.58\,\mathrm{MHz}} = 279.32961\,\mathrm{ns}$$

$$T_2 = \frac{1}{3.58\,\mathrm{MHz} - 43.7\,\mathrm{Hz}} = 279.33302\,\mathrm{ns}$$

$$TSF = 81920$$

$$f_{s,eff} = 293.25\,\mathrm{GSa/s}$$

3.9.2 PRI Jitter and TSF Stability

As can be seen from the mathematical analysis above, the TSF relies on the stability of the PRI's of the transmit and reference pulse trains. Consequently To ensure good TSF stability, the PRI's must also be stable. Referring back to Figure 3.4, it can be seen that the multiplication pulse amplitude relies on the relative positioning of the transmitted pulse and the reference pulse in time. If the transmitted signal is not correctly aligned to the reference signal due to PRI jitter at a particular point in time, an error is introduced into the amplitude of the resulting multiplication pulse. Fortunately, the output waveform is the result of integrating a very large number of these pulses so any errors to due this jitter will average out over the duration of the expanded pulse. According to McEwan [57], preventing distortion of the time stretched waveform requires that the period jitter must be kept below one-quarter of the RF carrier cycle (43 ps or less for 5.8 GHz).

The difference between the PRI's in the time stretching procedure needs to be accurately maintained to achieve a stable TSF. This means that the two timing sources should be phase-locked to this fixed offset. The effects of the PRI jitter should average to zero during the integration stage, which means that the TSF stability relies solely on the quality of the phase-locking mechanism. If the timing sources are not locked they will

drift slowly apart and the TSF will change. The required tolerance of the TSF depends on the range that is being measured. This is illustrated in Figure 3.5, which shows that a tolerance of 0.2% or better is required in order to maintain the accuracy requirement over the entire measurement range.

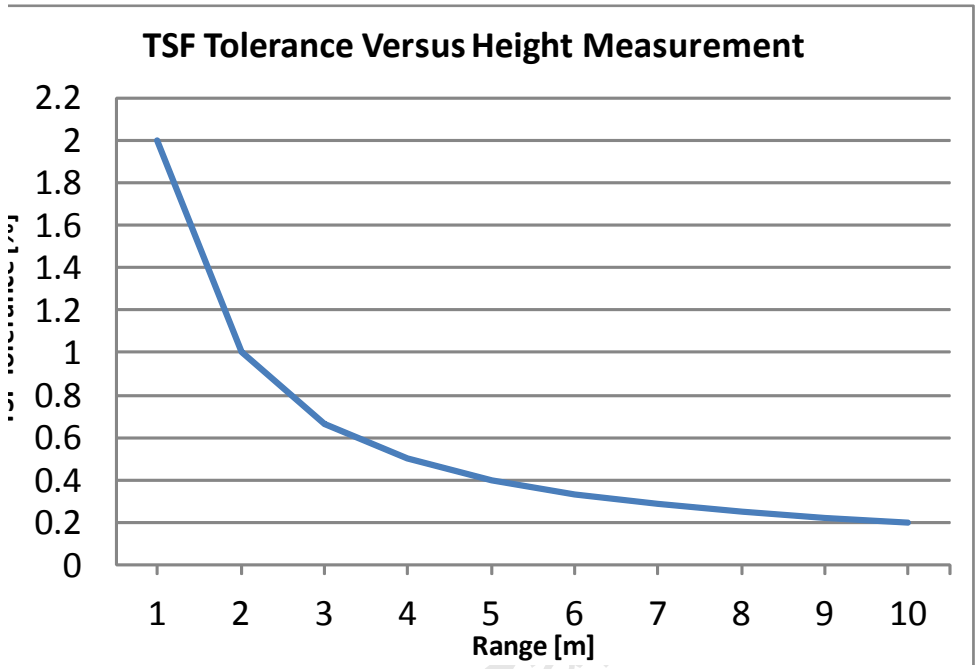

Figure 3.5: The required tolerance of the TSF changes depending on the range being measured. Long range requires a better tolerance.

3.10 Time Stretching Simulation and Timing Strategy

Figures 3.6-3.8 illustrate the concept of time stretching in Matlab and SystemView using the parameters in the example above. The first step in the height measurement is to determine the time stretching factor from the PRI's of the transmit and reference signals. This can be achieved by calculation or by measurement/calibration, since the clock frequency is unlikely to be exactly the intended value due to manufacturing tolerance.

Once this has been determined the system can be left to run. The TIM, t_{ds}, is performed using a simple, low frequency sampler on the time stretched output signal, shown in Figure 3.7, between the leading edges of the transmitted pulse and the received echo. In the example in Section 3.9.2, the centre frequency of the time expanded output would be 70 kHz with a bandwidth of about 12 kHz. The sampling frequency of the ultrasonic instrument well exceeds the required Nquist sampling rate of 152 kHz for this signal.

The time expanded time interval is then divided by the known TSF to determine the real-time interval and the true height measurement, as shown in Equation 3.12. Height accuracy is, therefore, determined by the accuracy of the time interval measu-

rement, δt_{ds}, and the TSF. The specifications in Section 3.11 should be used to achieve the required height accuracy.

$$H = \frac{c\,(T_2 - T_1)\,t_{ds}}{2T_1} \tag{3.12}$$

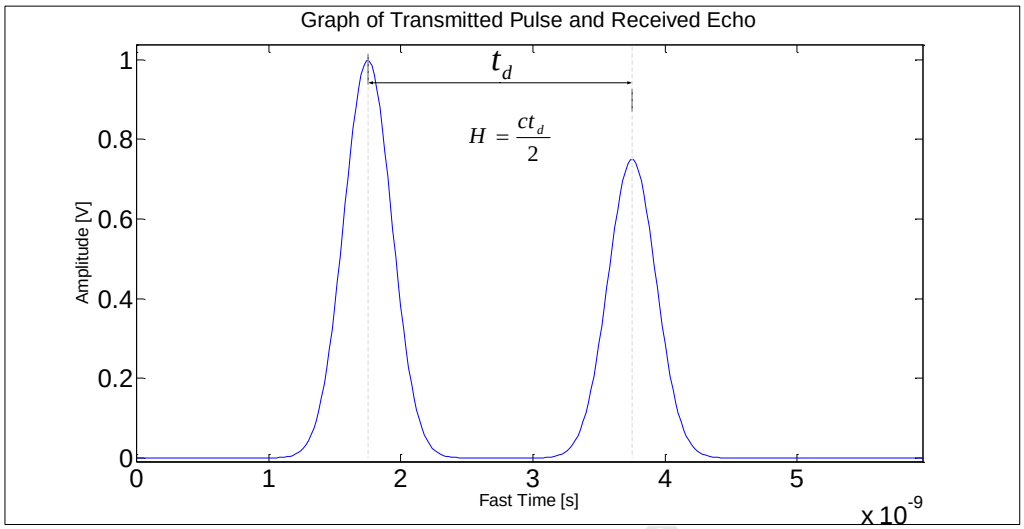

Figure 3.6: The transmitted signal and a corresponding echo is generated from equation 3.5. The distance, H, from the transmitter to the target interface can be calculated by measuring the time interval. $\tau = 1\,\mathrm{ns}$.

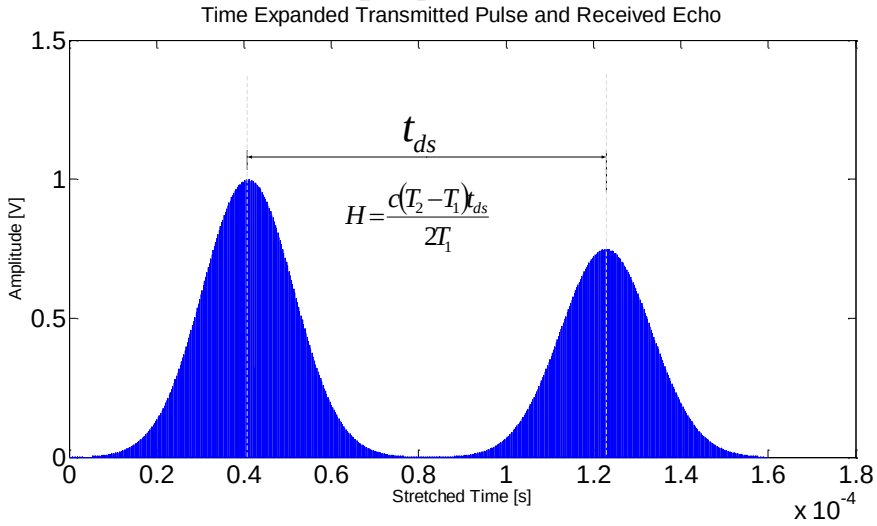

Figure 3.7: The transmitted pulse train with echo is then multiplied with a reference pulse train containing the same waveform but having a slightly different PRF. The result of the multiplication shows two distinct pulses on a time expanded axis. The true time interval is found by dividing the measured time expanded interval by the time expansion factor.

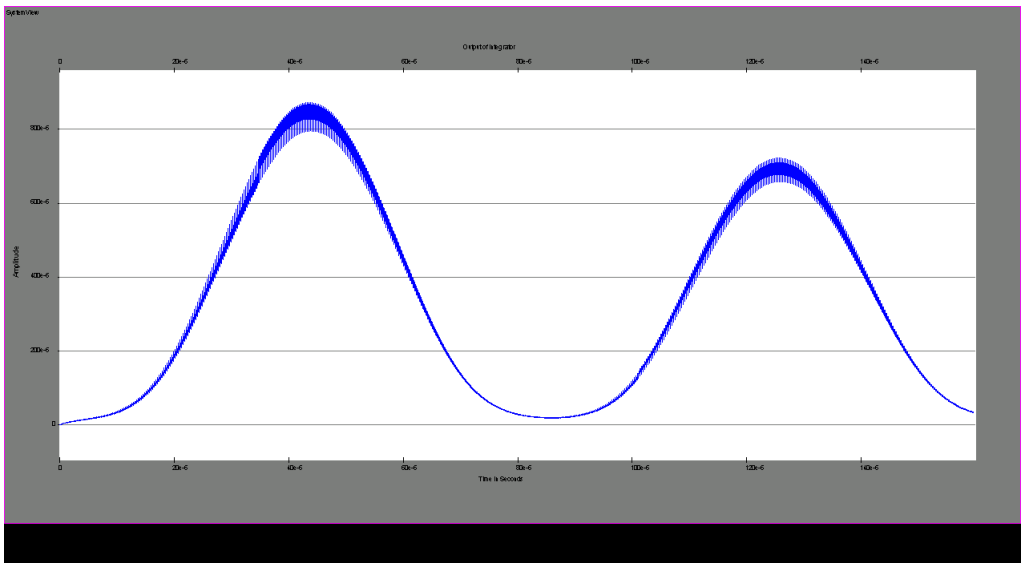

Figure 3.8: A graph showing the output of the integrator in SystemView.

3.11 Instrument Specifications

Based on the findings of this chapter, the hardware should be designed to meet the specifications summarised in Table 3.4 to fulfil the user requirements.

Table 3.4: Instrument specifications

Specification	Value
Type	Pulsed radar
Operating frequency	5.8 GHz
SNR	$\geq 13\,\mathrm{dB}$
P_t	$\geq 165\mu\mathrm{W}$
T_e	$\leq 1000\,\mathrm{K}$
Rise-time	$\leq 800\,\mathrm{ps}$
Bandwidth	$\geq 1\,\mathrm{GHz}$
Pulse width	$\leq 1\,\mathrm{ns}$
PRF Tx	3.58 MHz
PRF ref	3.58 MHz - 43.7 Hz
PRF jitter	$\leq 43\,\mathrm{ps}$
TSF	$82000 \pm 0.2\%$
Antenna	Beam-limited
Antenna Beam-width	$\leq 20°$
Power supply	24 V @ < 4 mA

3.12 Summary

A pulse radar architecture was chosen for the instrument due to its compatibility with the existing ultrasonic hardware and its low cost and low power consumption when compared to frequency domain techniques. An operating frequency of 5.8 GHz was

chosen because it would be easier and cheaper to implement in the demonstration hardware.

The TIM between the leading edges of the transmitted pulse and the received echo was then identified as the next crucial stage. Although the literature points to several techniques, which are capable of accurate TIM, few of the techniques researched could be used without modifying the existing timing hardware of the ultrasonic instrument. A time expansion technique, which is based on a Vernier principal, was then introduced and it was shown that if the time stretching factor is adjusted correctly, an output profile can be produced that is both comparable to an acoustic range profile and also compatible with the existing timing hardware of the instrument.

Specifications for the SNR, pulse rise-time, pulse-width and antenna beam-width were then estimated or calculated from the relevant theory. It was shown that, along with these waveform and antenna specifications, a time expansion factor of approximately 82000 would be required.

Chapter 4

Hardware Analysis & Review Options

This chapter and the subsequent chapters focus on the design and implementation of the demonstration hardware of the radar transceiver. As discussed in section 2.2, the goal is to replace the existing acoustic transceiver with an equivalent radar transceiver, which can produce an output range profile that be can processed by the original timing hardware of the instrument. In chapter 3, the issue of TIM was addressed and it was decided that Vernier time-stretching would be the best technique to utilise. Modifications to the timing hardware, which is incompatible with the fast propagation speed of radar, could then be avoided.

Firstly, the architecture of the instrument and its sub-systems is described. The requirements for each individual sub-system are then generated. Suitable candidate hardware options are then proposed and discussed. Where appropriate, some quick prototypes are shown and simulations are performed with the aid of CAD software, which includes *LTSpice*, a SPICE-based simulator; *Ansoft Designer,* a simulator for microwave circuits and *Genesys,* an EM analysis and optimisation tool.

4.1 Sub-system Analysis

Figure 4.1 illustrates the proposed architecture of the radar transceiver for the level measurement instrument in block diagram form. Note that the original power supplies, microprocessor and timing hardware are not shown because they will not be modified. The components of the pulse train generator, specifically the PRF generator, the pulse driver and the pulse shaper will be discussed separately in the subsequent sections followed by the description of the directional coupler, cross-correlator and amplifier.

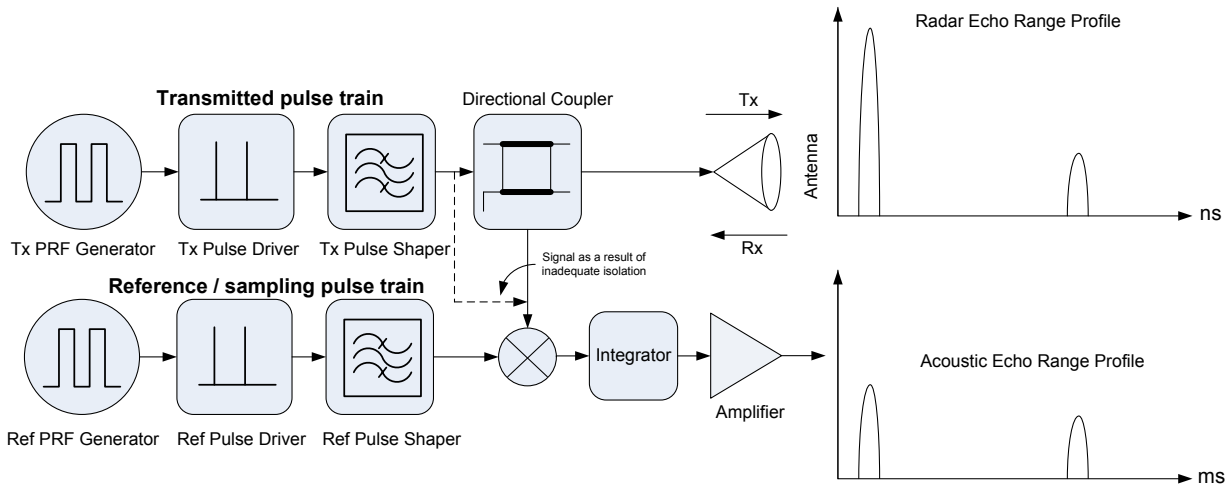

Figure 4.1: The architecture of the radar transceiver requires two pulse train generators, a mixer (multiplication) and an integrator (integration) for cross-correlation and an amplifier. This architecture allows for the transmitted signal to resemble the profile of a radar signal, while the output after time-stretching resembles that of an acoustic profile. The TSF is set by controlling the difference in PRF between the transmit and reference pulse trains.

4.2 PRF Generator

The PRF generator sets the pulse repetition frequency for the system. The waveform required is a simple square-wave clock signal. A fast rise-time is favoured to provide a rapid trigger for the pulse driver. Since the architecture of the instrument implements Vernier time-stretching, the PRF generators will also set the time expansion factor by equation 3.10. High TSF linearity is needed in order to meet the measurement accuracy requirement. This means that both PRF generators have to be stable so that the frequency difference is constant during a measurement. The PRF generators will also have to be tunable so that the frequency can be adjusted either manually or via a feedback circuit to compensate for any medium or long term drift. Unfortunately, due to time constraints, it was decided that a phase-locking mechanism for the PRF generators would be part of a future study.

Simple relaxation oscillators and timer IC's are a poor choice for this application. Since they rely on charging a capacitor through a resistor and then discharging it rapidly when the voltage reaches a certain threshold, the values of the components become critically small when one approaches the required 3.58 MHz. Component tolerances also affect the predicted frequency and fine tuning is almost always necessary. Adding tunable elements also adds circuit noise and short term instability [38, pg 285]. Some more noteworthy techniques of generating the required waveform are mentioned below.

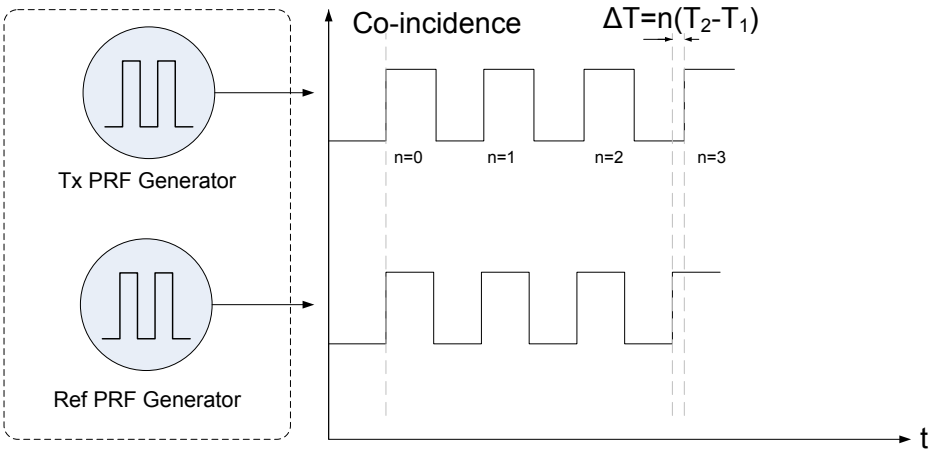

Figure 4.2: Theoretical signals from the PRF generator.

4.2.1 Crystal Oscillator

Crystal oscillators are very good when it comes to stability. Crystals can be combined with low-power CMOS to create a very stable, low power, square-wave oscillator as shown in Figure 4.3 [38, pg 302]. The down-side is that they have very little tuneability. During prototyping one would have to replace the crystal to get a different clock frequency. Another disadvantage for prototyping is that there are only a few values of COTS crystals available. Although one can order a crystal for a certain frequency, they are not available in small quantities. This would make a crystal oscillator ideal for a final product but prototyping would be rather tedious.

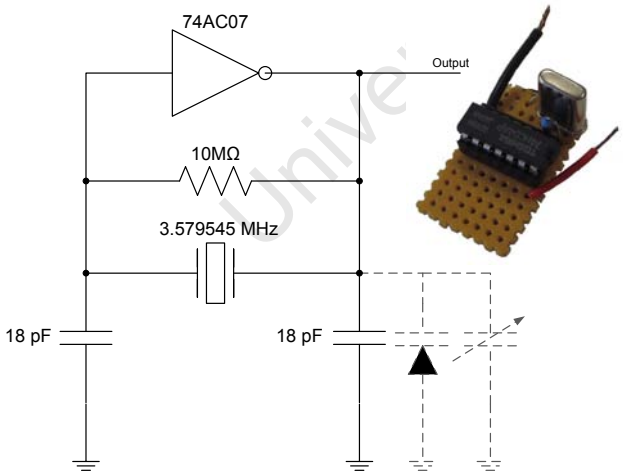

(a) Circuit diagram and photo of a simple, low power crystal oscillator.

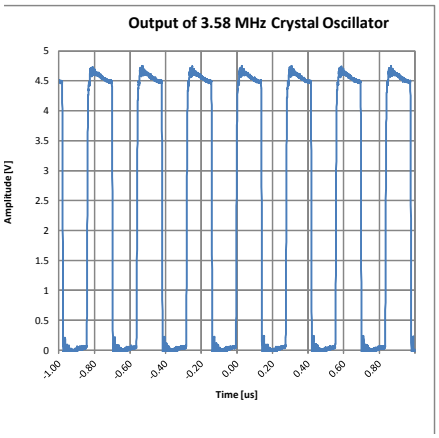

(b) Output waveform of circuit 4.3a.

Figure 4.3: A test circuit to illustrate how a simple crystal oscillator was constructed with low power CMOS. A trimmable capacitor or a varicap diode can be added but can only provide a small amount of tuning capability to this circuit. The crystal is stable in frequency to around 50 ppm but more expensive crystals could provide even better short term stability.

■ 150Ω CMOS Output Driver
■ Low Profile (1mm) SOT-23 (ThinSOT™) Package

APPLICATIONS

■ Low Cost Precision Programmable Oscillator
■ Rugged, Compact Micropower Replacement for Crystal and Ceramic Oscillators
■ High Shock and Vibration Environments
■ Portable and Battery-Powered Equipment
■ PDAs and Cellular Phones

LT, LTC and LTM are registered trademarks of Linear Technology Corporation.
ThinSOT is a trademark of Linear Technology Corporation.
All other trademarks are the property of their respective owners.

TYPICAL APPLICATION

Micropower Clock Generator

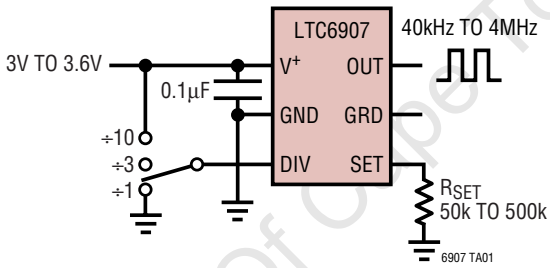

Typical Sup

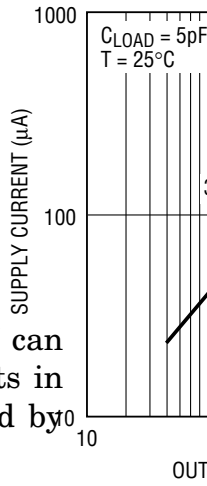

Figure 4.4: Circuit diagram for the recommended connection of the LTC6907. N can be set to 10, 3 or 1 so that the highest value resistor can be used, which results in the smallest current being drawn. The desired frequency can easily be changed by re-soldering one resistor [84, pg 1].

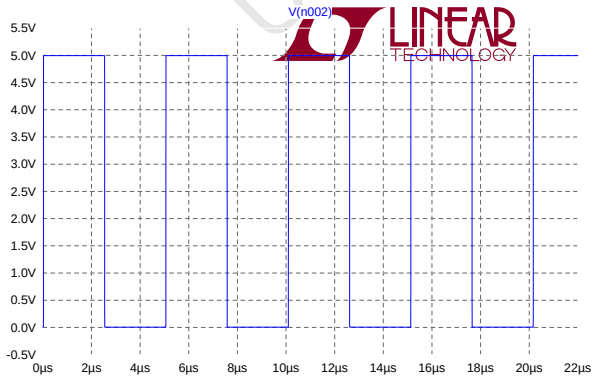

(a) $R_{SET} = 1\,\mathrm{M\Omega}$, $f_{out} = 200\,\mathrm{kHz}$.

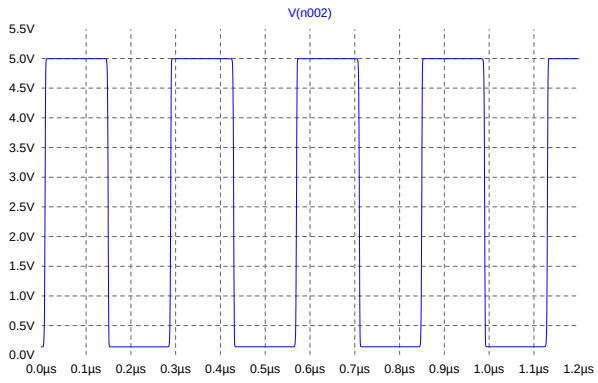

(b) $R_{SET} = 55.8\,\mathrm{k\Omega}$, $f_{out} = 3.58\,\mathrm{MHz}$.

Figure 4.5: Spice simulations of the LTC6907 silicon oscillator.

4.2.2 Silicon Oscillator

Silicon oscillators offer a good compromise between stability and flexibility for prototyping. The LTC6907 silicon oscillator from *Linear Technology* is a good example of a low power, tunable square-wave oscillator. It is programmed by selecting a single resistor and has an initial accuracy better than 0.5%. While its stability is not as good as a crystal, it can span a frequency range between 4 kHz and 4 MHz while consuming less than 300 uA [84]. Figure 4.5 illustrates the operation of this device with a Spice simulation. Unfortunately the short term stability or period jitter could not be quantified by a simple simulation.

The chip is programmed by the following formula [84, pg 7]:

$$f_{OUT} = \frac{4\mathrm{MHz}}{N}\left(\frac{50\mathrm{k\Omega}}{R_{SET}}\right) \tag{4.1}$$

output frequency can
100:1 total frequency

The LTC6907 is easil
simple formula:

$$f_{OUT} = \frac{4\mathrm{MHz}}{N} \bullet \left(\frac{50}{R_S} \right.$$

The LTC6907 is availab
package.
Contact LTC Marketin
shutdown feature or lo

4.3 Pulse Driver

The pulse driver is responsible for generating short pulses. It is triggered by the leading edge of the output waveform of the PRF generator. According to the specifications in Section 3.11, the pulses should be around 1 ns in width with rise-times less than 800ps to achieve the accuracy requirement. The generation of these pulses usually requires complex techniques and often expensive equipment and components are utilised. In order to achieve the user requirement of low cost, the search was limited to include only techniques that could be implemented with readily available components. Some of these techniques are discussed further below.

4.3.1 Step-Recovery Diodes

A step-recovery diode (SRD), or snap-off diode is a type of diode that has the ability to generate very short pulses. When the diode switches from forward bias to reverse bias, only the charge which is stored in the junction still flows. When all this charge is removed the diode switches very abruptly, typically in the order of hundreds of picoseconds, from a low impedance to a high impedance. This characteristic has been exploited in the literature to generate pulse trains [42, 31, 72] and to improve the rise-time of existing pulses [36, 70].

It follows that the operating frequency of such a diode is determined by the amount of charge that is stored in the junction. The stored charge, in turn, is proportional to the *minority carrier lifetime,* τ, of the diode and the charging current. Typical values of τ range from 10 ns - 1 us in silicon. In order to produce efficient, high amplitude pulses, the minority carrier lifetime has to be sufficiently long so that there is no recombination before the diode snaps. Therefore, the parameter τ should be chosen to be at least 10x the period of the input signal [36, Section 3d]. This means that the PRF of SRD pulses is typically 10 MHz to 1000 MHz in silicon [46, Chp 5]. Unfortunately the desired PRF of 3.58 MHz is well outside the lower frequency limit.

4.3.2 Fast Transistor Switch (MIR)

Transistors can be used to generate the short UWB pulses. This is done by rapidly switching the transistor from an “off” state to an “on” state and discharging a stored charge through a load. A good example of this is the impulse generator from the Micro-Impulse Radar (MIR) [57]. This is illustrated in Figure 4.6, which shows a MIR impulse generator that has been slightly modified [77, 8] and uses low cost components. The input square-wave clock signal from the PRF generators goes through a pulse shortening stage, consisting of 74HC04 inverters, to produce a 20 ns pulse to trigger the BRF91A transistor base on the rising edge. When the transistor switches, the charge in capaci-

tor C4 discharges and produces a negative pulse at the output, as shown in Figure 4.7. The BAT81 diode, D1, prevents the capacitor from re-charging from the output.

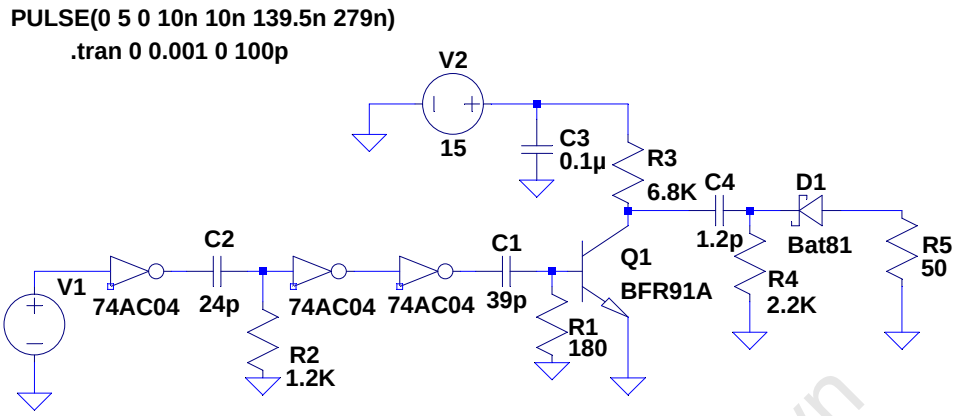

Figure 4.6: Circuit diagram of the impulse generator from the MIR.

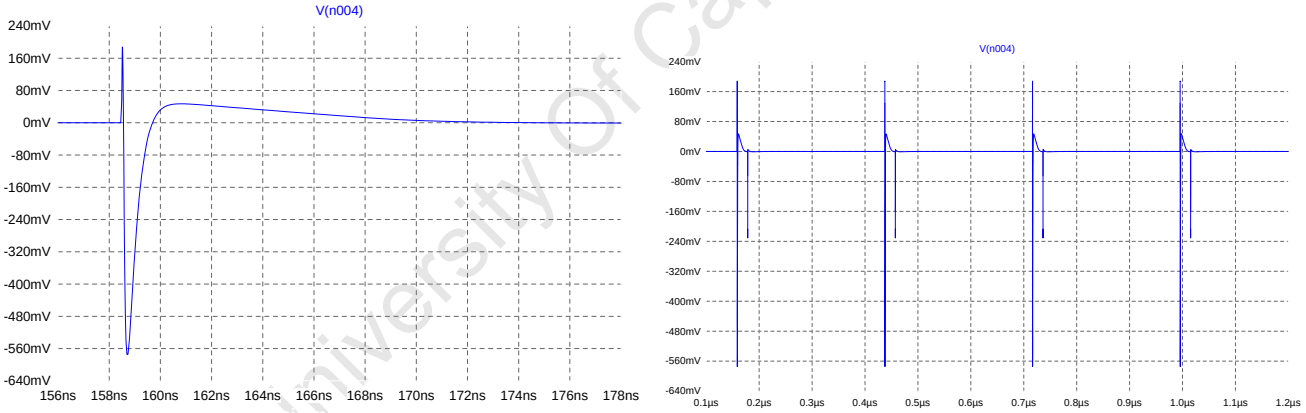

(a) Simulated pulse into 50Ω.

(b) Simulated pulse train into 50Ω.

Figure 4.7: A Spice simulation showing that a short, negative pulse of approximately 1 ns can be generated. The circuit is also able to achieve the required PRF of 3.58 MHz, however, the amplitude of the pulses is less than 1 V.

4.3.3 Avalanche Breakdown

An abnormal mode of transistor operation called *avalanche breakdown* can be a very useful and simple technique for achieving this requirement. The concept, which is well covered in greater detail in the literature [35, 34, 30, 51], will be described in this section.

During avalanche breakdown the collector voltage of a BJT is made high enough so that electrons in the heavily reverse biased collector-base junction gain sufficient energy to

rip apart and form mobile hole-electron pairs. Electrons accelerate towards the collector and the holes accelerate towards the base. While these charge carriers accelerate they bash into other atoms and may generate additional pairs. This process is called *avalanche multiplication*. Once avalanche breakdown occurs, the collector current increases rapidly. This is caused by the electron multiplication in the collector as well as the increased base current produced by the holes. The increase in base current causes an increase in collector current by normal transistor action. An impedance is used to bias the base and raise the base voltage as the current following through it increases. This causes the resistance between the collector and the emitter to rapidly go very low. The transistor remains in this state until collector current drops sufficiently to cut off conduction.

Figure 4.8 shows a simple pulse generator which exploits the transistor's avalanche behaviour. The pulse shape and width is determined by the storage element and the characteristics of the transistor. More specifically, the leading edge of the pulse is effected by the trigger pulse and the trailing edge is determined by the discharge time of the storage element. [51, 35, 24].

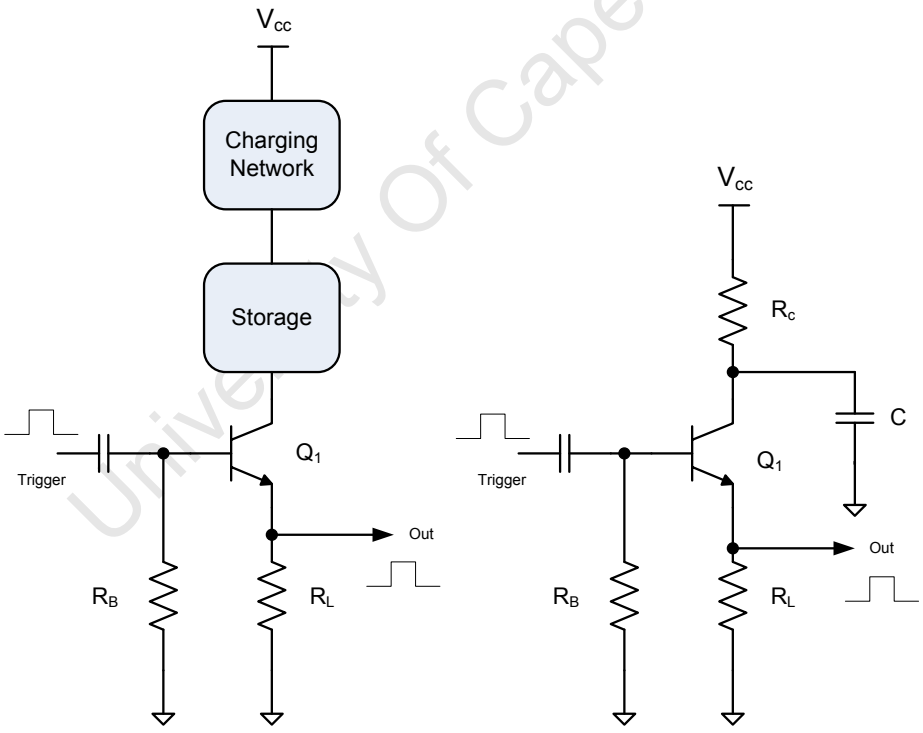

Figure 4.8: Schematic and design of basic avalanche pulse generator. The storage element is charged via the charging network between pulses to a critical level just before breakdown occurs. When a short triggering pulse is applied to the base through a small capacitor, the transistor is pushed over the edge, avalanche breakdown is initiated, and the storage element discharges through the load, R_L. Following turn-off renewed charging of the storage element through R_c takes place before the arrival of the next triggering pulse.

The advantages of avalanche circuitry include [34]:

- Economy of circuit components
- Minimum temperature sensitivity
- Extremely fast action time
- Short propagation delay

Disadvantages include:

- Limited repetition rate or low duty cycle
- Large ratio of recovery time to action time
- Propagation delay is dependent upon the input trigger
- Possibility of failure of the transistor

Understanding the effects of stray reactance in avalanche transistor circuits is critical to achieving good operation. Figure 4.9 shows a spice model of an avalanche pulser based on that shown by Kilpela [45]. It is illustrated in figure 4.10 that the stray inductance should be kept to a minimum in order to obtain a higher amplitude pulse. Additionally the stray capacitance should be kept low as any additional capacitance other than the storage element itself will result in a broader pulse.

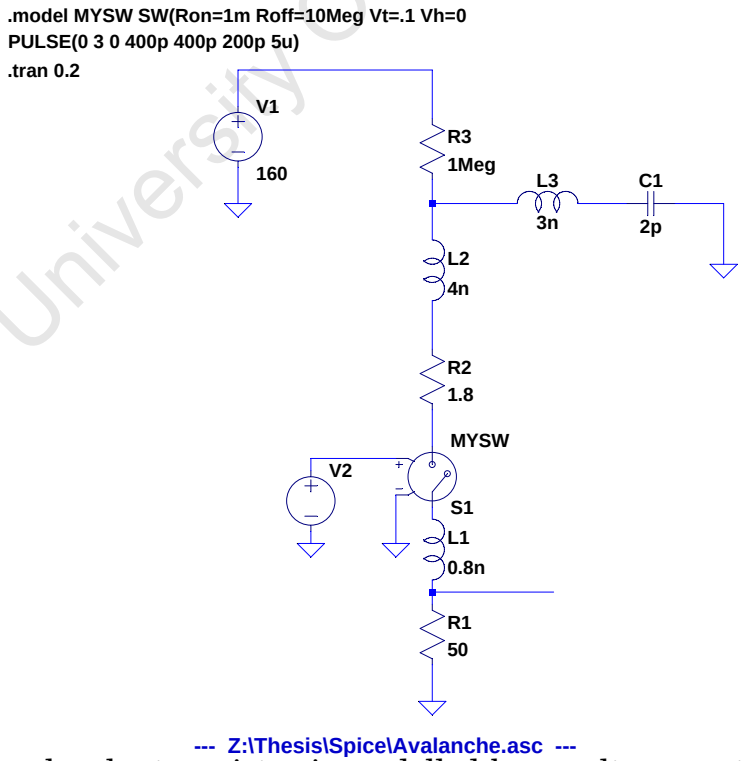

Figure 4.9: The avalanche transistor is modelled by a voltage controlled switch with an *off* resistance of $10\,\mathrm{M\Omega}$ and an *on* resistance of $10\,\mathrm{m\Omega}$ in series with resistor R2. The switch is controlled by an ideal pulse generator. L1 represents the stray inductance of the leads, L2 represents the inductance of the transistor's package and L3 represents the inductance of the PCB.

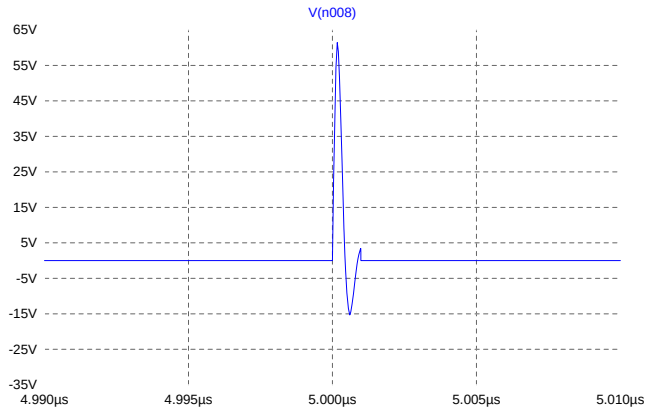

(a) Output measured across R1. L1 = 0.8nH.

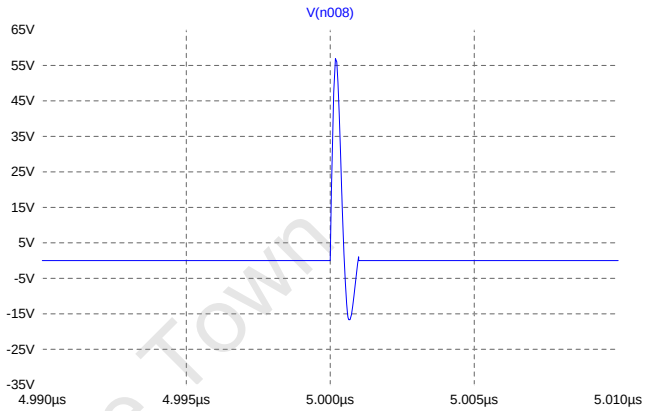

(b) Output measured across R1. L1 = 3nH.

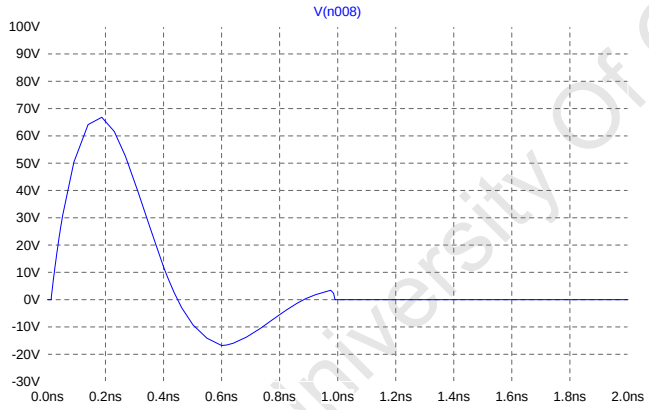

(c) Output measured across R1. C1 = 2pF.

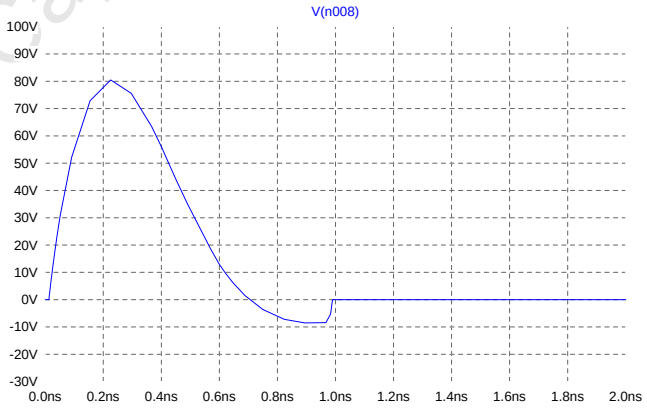

(d) Output measured across R1. C1 = 4pF.

Figure 4.10: 4.10a-4.10d show the effects of stray inductance and capacitance in this circuit, which are caused by poor circuit construction. 4.10a and 4.10b show that if the length of the leads of the transistor package are too long, pulse amplitude is sacrificed. Almost a 5 V drop for an increase of 2.2 NH. Similarly, 4.10c and 4.10d show that an undesired increase in the storage capacitance C1, causes the pulse width to increase.

The disadvantage of slow recovery time in this circuit is primarily due to the charging time associated with the storage capacitor C1. The charge time to 60% of maximum is given by the product of R3 and C1. In order to allow the storage element to fully recharge, the maximum PRF has to be well below 250 kHz. In order to meet to desired specification of a 3.58 MHz PRF, this obstacle has to be overcome. A special charging network can be added to circuit to achieve this. This is illustrated Figure 4.11, which shows the output of the pulse generator with different PRF settings.

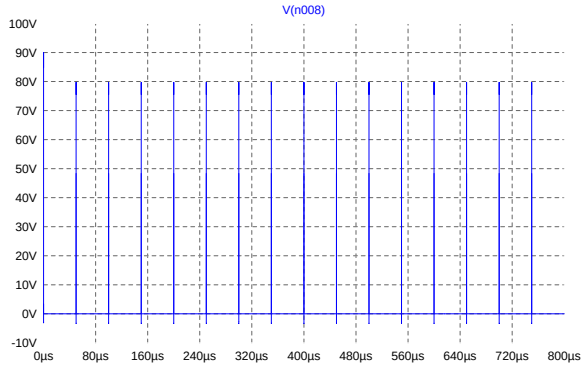

(a) Output of the pulse generator with PRF=20 kHz.

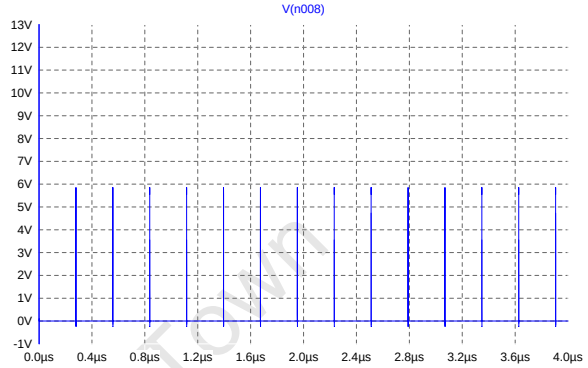

(b) Output of the pulse generator with PRF = 3.5 MHz.

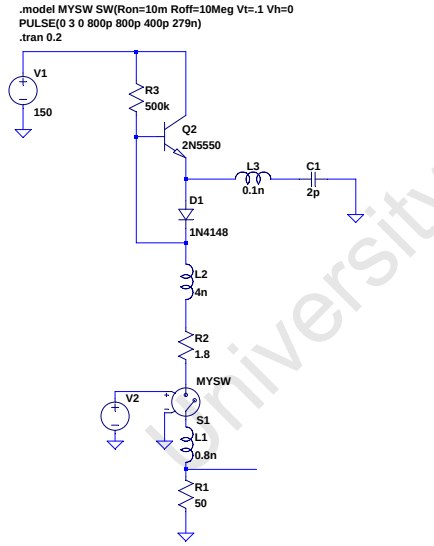

(c) Spice model of the avalanche pulse generator with a charging network.

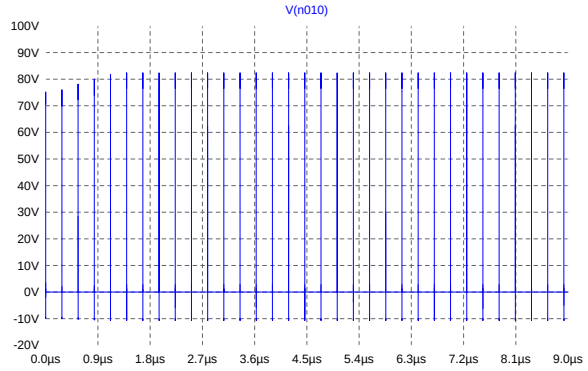

(d) Output of pulse generator with charging network with PRF=3.5MHz.

Figure 4.11: 4.11a and 4.11b illustrate the loss of pulse amplitude as the PRF is increased. A charging circuit to increase the PRF by bypassing R3 and allow C1 to charge through a smaller resistance is shown in 4.11c [35]. When S1 is off, C1 charges through R4. When S1 avalanches, the transistor Q1 turns off due to the voltage drop across D1 and the collector of S1 connects to the supply via R3. 4.11d shows the output of 4.11c at 3.58 MHz. Note the pulse amplitude has been restored.

The selection of D1 in figure 4.11c is critical. It needs to be able to switch very fast but it also needs to be able to handle a large amount of current. Assuming that the resistance of the output load and the internal resistance of the transistor when on is

$R_L + R_R \approx 50\,\Omega$, then the peak current through D1 can reach nearly 2.5 A. Although it is only for a very short duration, care must be taken to ensure that the diode is capable of dissipating the heat. A PIN diode is a good choice because of its fast switching time, low capacitance, high breakdown voltage and robustness towards large peak currents.

4.4 Pulse Shaper

The pulse shaper is required to take in the baseband pulses from the output of the pulse driver and modulate them into short RF pulses at 5.8 GHz. The duration of the RF pulses should be comparable to the duration of the baseband pulses. Conventional switched CW microwave oscillators are a poor choice as they consume a comparatively large amount of current and are not suited to the generation coherent pulse trains [22]. Each RF pulse must start with the same initial phase. Since these oscillators generally have a large Q factor, the start up and settling time of the oscillations is also generally very long. Consequently, the methods examined in this section focus on utilising the very broad spectrum of the baseband pulse and filtering out the desired frequencies.

4.4.1 Dielectric Resonator Filter

Dielectric Resonators (DR) coupled to microstrip lines, as shown in figure 4.13a, are widely used as microwave filters because of the low loss, temperature stable properties of the materials, small size and low cost [68, 29]. Figures 4.13 and 4.14 illustrate the implementation of a simple, low cost DR filter on microstrip [68]. 4.14b shows the S-parameters of the filter. The initial observation is that the bandwidth of the filter is very narrow due to the very high Q-factor of the resonator. The insertion loss is also relatively high. However, it was seen that decreasing the gap between the transmission lines and having the resonator sitting on top of the transmission lines increased the bandwidth and improved the insertion loss, which warranted further investigation.

4.4.2 Transmission Line Filter

It is also possible, with the help of CAD filter software, to synthesise planar microstrip filters at the required frequency and bandwidth. The theory behind these microwave filters is well understood but can be mathematically and computationally intensive, which makes the CAD software a very attractive option to speed up the design process. Planar microstrip filters also have the benefit of small size and a low fabrication cost.

The design of a hairpin filter, as illustrated in figure 4.15, is accomplished using *Genesys* to achieve a centre frequency of 5.6 GHz and a bandwidth of 2 GHz. After synthesis, a linear optimiser is run on the filter parameters so that the result matches the desired

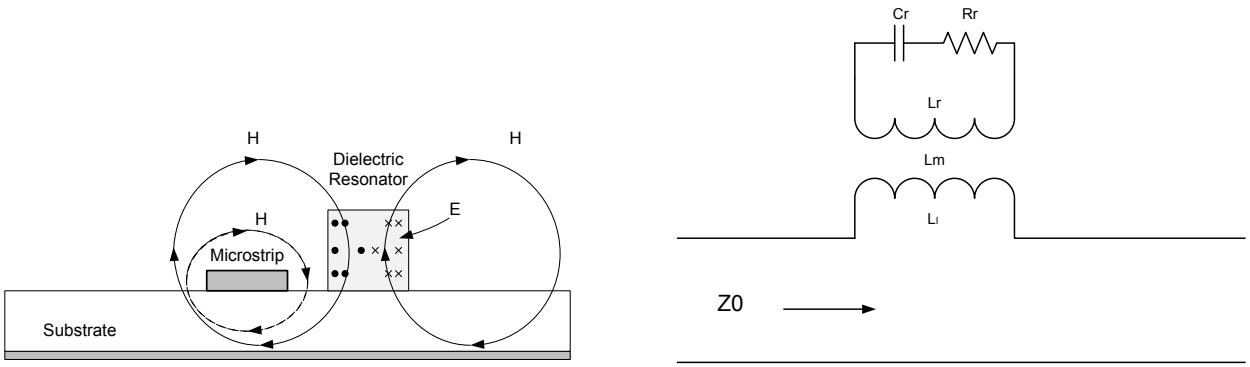

(a) Coupling on microstrip.

(b) Equivalent circuit.

Figure 4.12: 4.12a shows the coupling between a DR and a microstrip line [15]. The DR resonates at a certain frequency determined by its relative permittivity ε_{rr}, diameter and height.4.12b shows the equivalent circuit [29, 47].

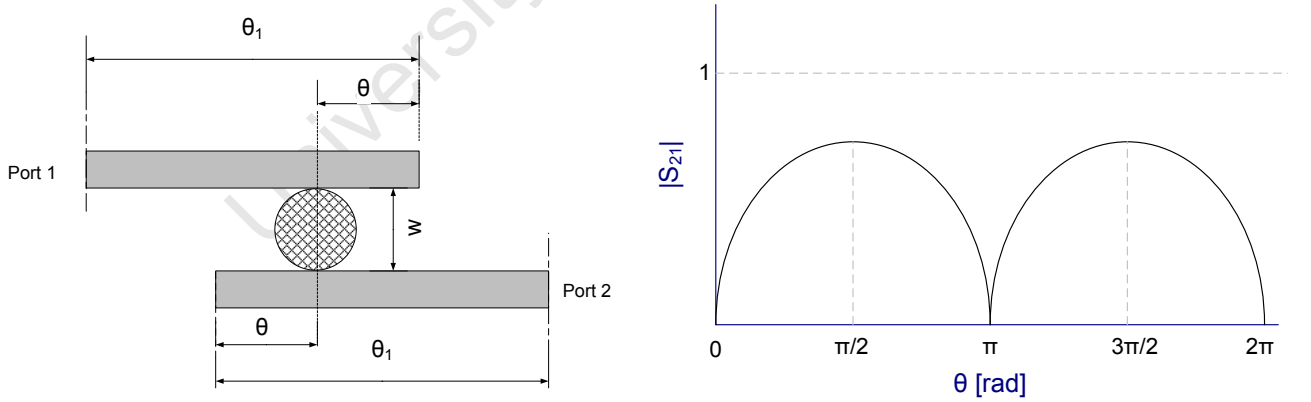

(a) Configuration for the dielectric resonator filter.

(b) Transmission coefficient magnitude as a function of DR position θ.[68]

Figure 4.13: The value of θ is chosen so that the transmission coefficient magnitude between the two transmission lines is maximum. As can be seen from the plot in Figure 4.13b, the best transmission occurs when $\theta = \frac{\pi}{2}\,\mathrm{rad}$ or quarter of a wavelength. The maximum value depends on the coupling factor between the resonator and the transmission lines which is related to its proximity to the lines.

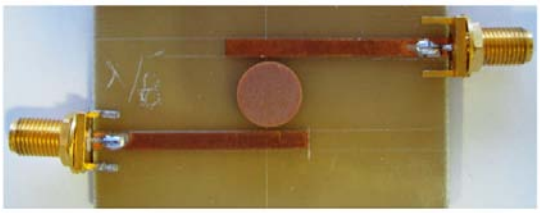

(a) Photo of the first dielectric resonator filter.

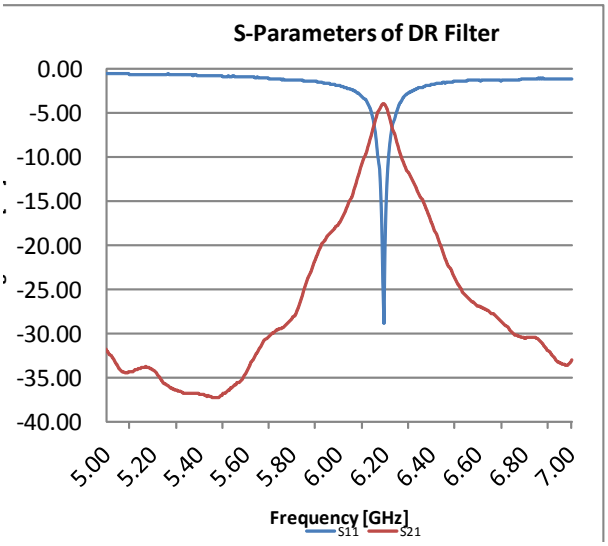

(b) Plot of the S-parameters of the first dielectric resonator filter.

Figure 4.14: 4.14a shows a photo of a prototype filter at 5.8 GHz. Transmission lines initially made of adhesive copper foil tape were stuck onto FR4 substrate to produce the filter. Corrections to the dielectric resonator placement could then be done relatively easily by removing the foil tape and sticking down a replacement.

response. The hairpin filter topology was chosen because it was able to realise the desired frequency and bandwidth with practically realisable microstrip dimensions [51, pg 838].

4.5 Directional Coupler

This component must allow the instrument to operate with a single antenna. It must operate over a relatively wide bandwidth and have low loss for the signal passing through it. Passive, planar microstrip circuits are favoured as they are relatively cheap to construct and can provide the necessary bandwidth.

4.5.1 Circulators

Circulators are passive three or four port ferrite devices. The ports are non-reciprocal, which means that energy only travels in one direction and enters and exists the ports in a predictable pattern. They are, therefore, a good way for interfacing a transmitter and receiver with a single antenna. The advantage of circulators is that they can have very low loss between the ports and can handle very high powers (not applicable this application). The disadvantage is that they are expensive and relatively difficult to design, layout and fabricate [6, 21, 86]. The best option would be to procure a drop-in circulator from a reputable circulator manufacturer. This expense is, however, only

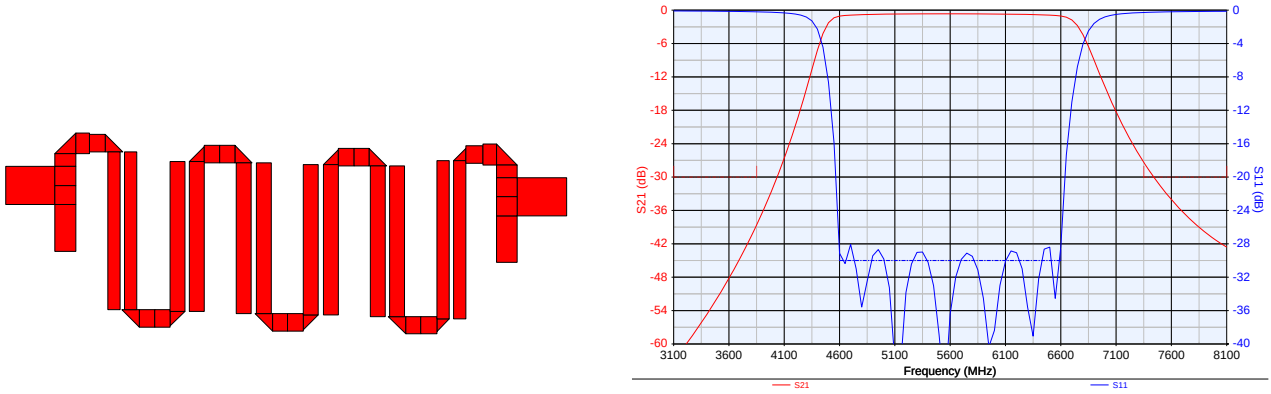

(a) Synthesised Layout.

(b) optimised linear response.

Figure 4.15: 4.15a and 4.15b show the layout and result of a linear synthesis and optimisation. In practise, the filter should not perform as well as the ideal linear design suggests, which is why the filter parameters have been over designed. This is because linear synthesis models do not take the effects of the material, discontinuities and coupling between non-adjacent lines into account. The results of this simulation, however, indicate that a practical filter is realisable in this way with some careful analysis and adjustments.

recommended if other design options prove fruitless and will not be considered further here.

4.5.2 Branch-line Coupler

A branch-line coupler, also know as a quadrature hybrid [51, pg 196], is shown in Figure 4.16. It is four port device with each side of the central box being $\frac{\lambda}{4}$ in length. The impedance of the branches can be chosen to specify the desired ratio of powers to be delivered to the two output ports, while having decent isolation to the remaining port. This imperfect isolation can be exploited in this case to allow a portion of the transmitted pulse to enter the receiver and undergo time stretching to provide a reference of the transmitted pulse in the output. There are other planar structures, which are suitable for directional couplers, such as the parallel-coupled line coupler and the rat-race hybrid, but the parallel-coupled line coupler has the disadvantage in that the gaps between the microstrips become too narrow for tight coupling and the rat-race hybrid has the disadvantage in that its ports are not adjacent and cross-over connections are often required [64]. This makes the branch-line coupler the most suitable choice.

Ansoft Designer was used to simulate a branch-line coupler at 5.8 GHz. Figure 4.17 shows the theoretical S-parameters in which port 1 has been used as the input port. As can be seen, the signal is equally split between ports 3 and 4 at the centre frequency, while port 2 remains well isolated from port 1. Since the circuit is symmetrical we can expect the same behaviour if the input is from any of the other three ports.

The main disadvantage of this circuit is the large 6 dB loss between the transmitted

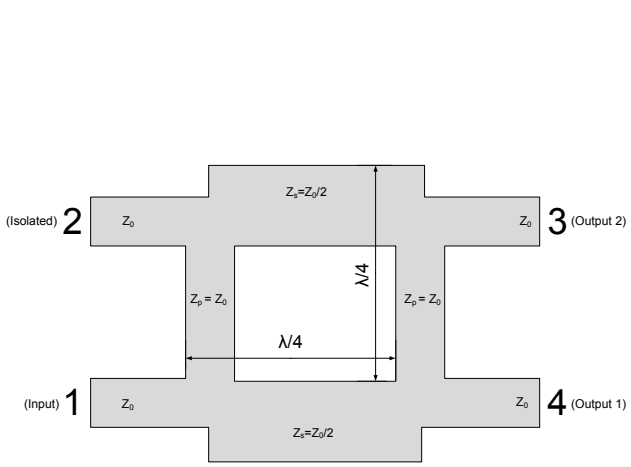

(a) Planar layout

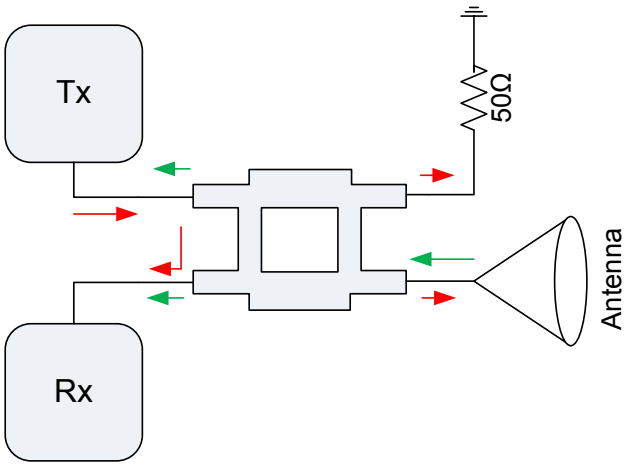

(b) Connections between the coupler, transmitter, receiver and antenna.

Figure 4.16: 4.16a shows a 3 dB branch-line coupler layout [51, pg 199]. 4.16b shows the path of the signal from the transmitter as it is split between the antenna and its adjacent port, which is terminated. The received signal splits again but the signal of interest is at the receiver. The signal at the transmitter will terminate into its $50\,\Omega$ load. Due to the imperfect isolation a small portion of the transmitted pulse is able to leak through to the receiver to provide the reference.

and received signal in the coupler itself. It must also be noted that due to the wavelength criteria of the design, it is not useful for signals which have fractional bandwidths higher than 15% [51]. A method of increasing the bandwidth of this circuit is needed if it is to meet the acceptance criteria.

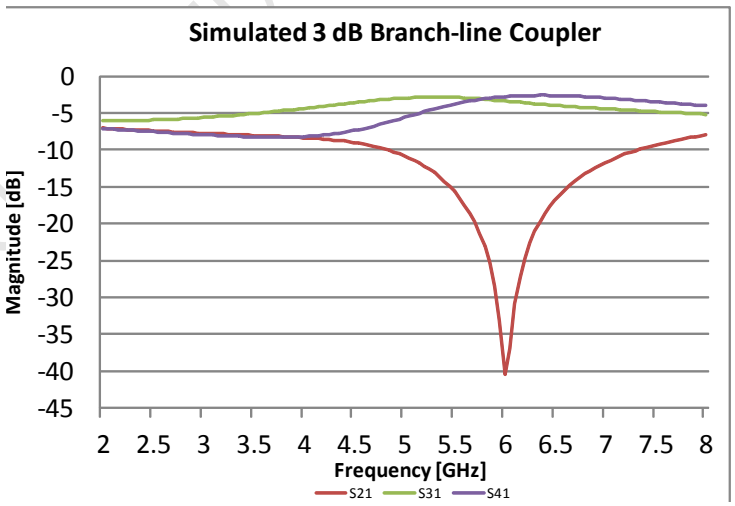

Figure 4.17: Simulated S-parameters of a 3 dB branch-line coupler.

4.6 Cross-correlator

The mixer and the integrator make up the components for the receiver of the instrument. A diode-mixer would be suitable for the multiplication. The integration can be

performed by a resistor and capacitor with an integration time long enough to produce a smooth output curve.

4.6.1 Integrator Circuit

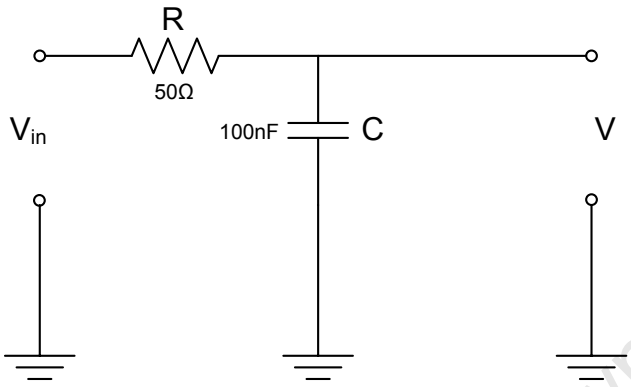

Figure 4.18: RC Integrator circuit [38, pg 26].

Figure 4.18 shows a circuit that performs integration over time of an input signal. The voltage across the resistance, R, is $V_{in} - V$. Therefore, the current is:

$$I = \frac{V_{in} - V}{R} = C\frac{dV}{dt}$$

If $V \ll V_{in}$, then

$$C\frac{dV}{dt} \approx \frac{V_{in}}{R} \text{ or } V(t) = \frac{1}{RC}\int^{t} V_{in}(t)\,dt + C$$

In order to keep $V \ll V_{in}$, the integration time (here $RC = 5\,\mu$s) must be kept long. This restriction means that the amplitude of the output signal is small and requires amplification.

4.6.2 Amplifier

The requirements for the receiver amplifier are good gain, high stability and linearity as well as a low noise figure. Voltage amplification can be performed with an operational amplifier but these components can have high noise and high cost. The gain-bandwidth product can also be very low, which would require some sort of cascade arrangement. This would impact negatively on the power budget for the instrument.

A simple common-emitter amplifier can be designed that would have high gain and low noise figure, while requiring a very low supply current. This is illustrated in Figure 4.19 [38, pg 76]. A Spice simulation of this amplifier is shown in Figure 4.20. Multiple stages can be cascaded together to increase the overall gain.

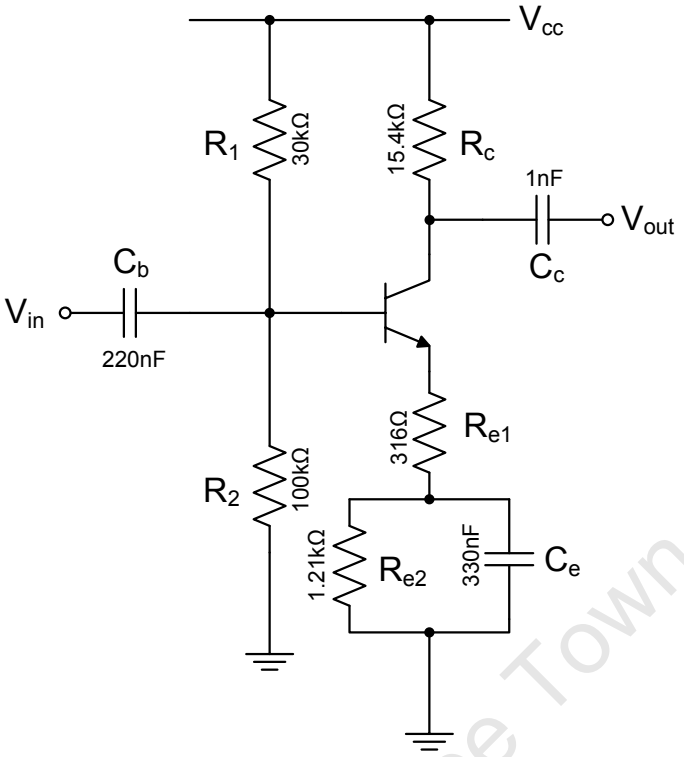

Figure 4.19: An AC common-emitter voltage amplifier with high stability, linearity and gain. The capacitors C_b and C_c pass AC signals and block any DC signal at the input and output. The quiescent current of the amplifier is set by the base bias (R1, R2) and emitter resistor R_e. The DC emitter resistance ($R_{e1} + R_{e2}$) can be set to $0.1R_c$ for ease of biasing. The value of C_e should be set so that its impedance at the frequency of operation is very low. The AC signal will then bypass R_{e2}. The gain for the AC signal can then be set by R_{e1}, which can be made a small value.

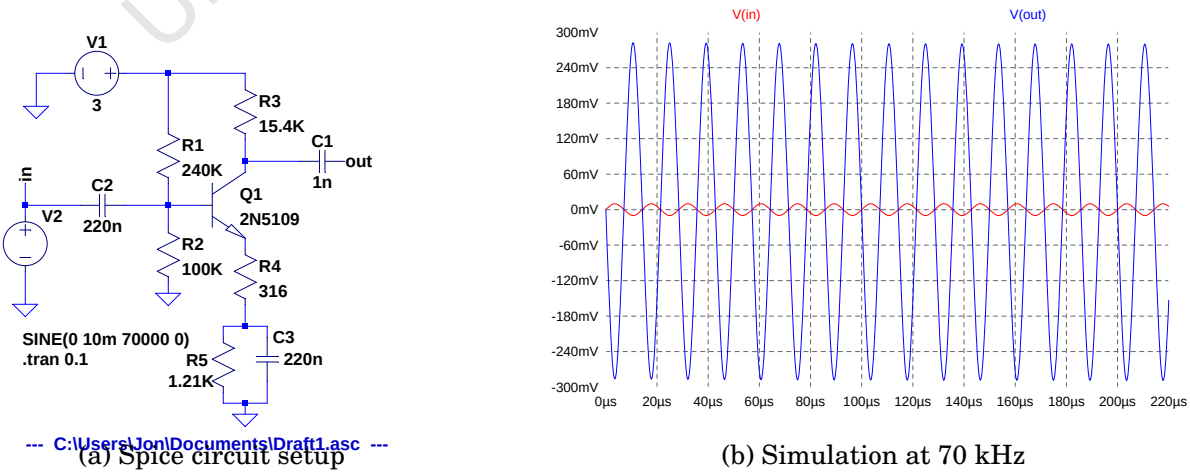

(a) Spice circuit setup

(b) Simulation at 70 kHz

Figure 4.20: A Spice simulation of a common-emitter voltage amplifier. The gain is approximately 28 at 70 kHz. The quiescent current is less than 100 uA.

4.7 Additional Power Supplies

The circuitry may require additional power supplies to those already available on the instrument. The instrument can only provide regulated voltages at $\pm 9\text{V}$ and $\pm 5\text{V}$. The avalanche pulse driver, for example, would require the voltage to be stepped-up to approximately 150V to operate. Some circuitry such as the silicon oscillator and amplifier may require a lower voltage at approximately 3V.

The LT1073 is a good choice as it can be made into both a step-up or step-down converter and requires only a few external components. The switching current can also be controlled by a resistor. This is illustrated in figure 4.21. The output voltage is set according to the following formula [83]:

$$V_{OUT} = (212\text{mV})\left(\frac{R2}{R1} + 1\right) \tag{4.2}$$

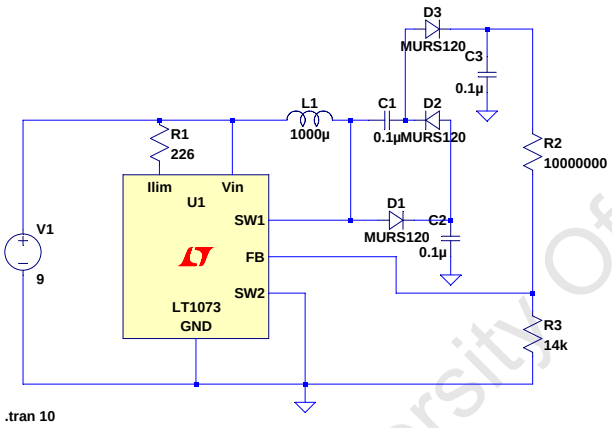

(a) 9 V to 150 V converter.

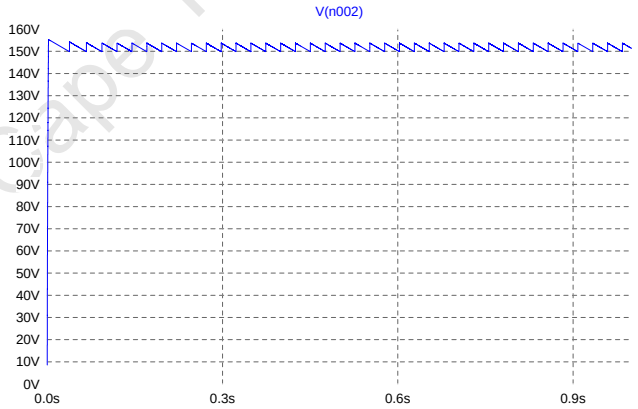

(b) Simulated output of the 9 V to 150 V converter.

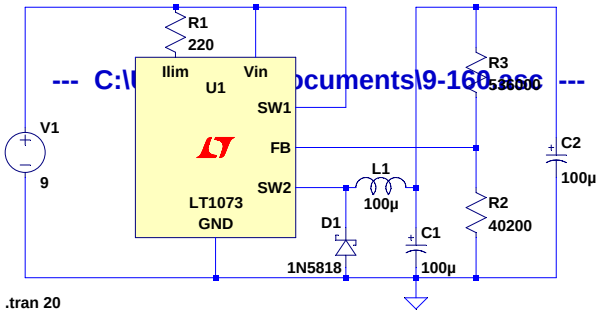

(c) 9 V to 3 V converter.

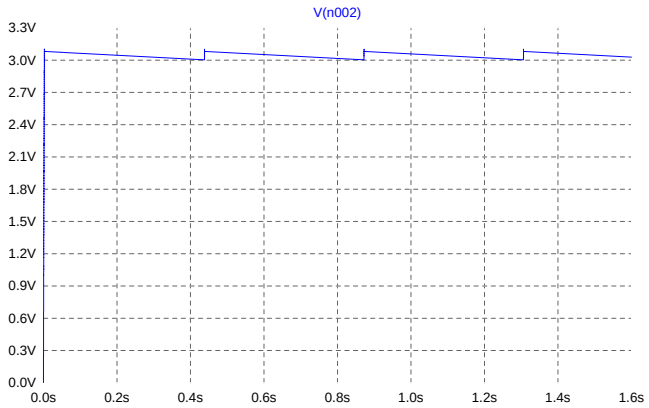

(d) Simulated output of the 9 V to 3 V converter.

Figure 4.21: 4.21a-4.21d show how the LT1073 is configured for step-up and step-down conversion.

4.8 Summary

In this chapter, several hardware options for the various sub-systems of the instrument were reviewed. The proposed architecture was shown to include two pulse generators, which are made up of a PRF generator, a pulse driver and a pulse shaper. Vernier time-stretching is achieved by a cross-correlation procedure, which consists of a mixer and an integrator followed by an amplifier.

4.8.1 PRF Generator

Relaxation oscillators and timing IC's do not meet the acceptance criteria for the design as they are not sufficiently stable and require tuning to operate at the correct frequency. Crystals are the favoured choice for the PRF generator as they are very stable and can operate with low power CMOS circuitry. A silicon oscillator is also favoured for initial prototyping as they have a much larger frequency tuning range. The stability of the silicon oscillator, however, is not as good as the crystal oscillator.

4.8.2 Pulse Driver

Step recovery diodes did not meet the acceptance criteria as they demand a high bias current and are more suited to operating at PRF's over 10 MHz. This approaches the maximum unambiguous range of the instrument. A pulse driver from a MIR was also presented, which showed good promise. Short pulses at high PRF's could be generated but their amplitude was very low. The avalanche pulse driver, on the other hand, produced much higher amplitude pulses but suffered from long recovery times, which limited the maximum PRF. Some circuitry was, however, suggested to overcome this limitation. The effects of stray reactance in the pulse driver circuitry was also examined and it was shown that poor circuit layout can easily result in broad pulses with low amplitude.

4.8.3 Pulse Shaper

Passive filters were favoured for this sub-system as any active CW oscillator would impact negatively on the power budget. Two different filters were examined. A dielectric resonator (DR) filter was constructed and it was observed that only a very narrow bandwidth could be achieved. It was noticed, however, that careful manipulation of the resonator improved the operating bandwidth, which warranted further research. A hairpin filter was also proposed and it was shown that a very good response could be achieved with careful optimisation. Both these filters also had the advantages of small size and low cost.

4.8.4 Directional Coupler

A passive microstrip branch-line coupler was the favoured circuit for this sub-system. A simulation showed that the coupler was able to perform the function of a duplexer but the operating bandwidth was not sufficient for a UWB signal. The disadvantage of high loss in the coupler was also noted. A ferrite circulator could be used as an alternative, but was not considered because of the complicated fabrication and high cost associated with the device. A drop-in COTS circulator would be the best option to use as a substitute.

4.8.5 Cross-correlator

A COTS mixer can be selected to perform the multiplication while a simple RC integrator and amplifier can carry out integration. The design for a common-emitter amplifier is presented and simulated, in which good gain, low noise and low power consumption are achieved.

Chapter 5

Hardware Construction & Testing

This chapter focuses on the PCB design, construction and testing of the various subsystems discussed in Chapter 4. The schematics were captured using *EagleCAD* and the boards were laid out using the built-in board editor. The Gerber files were generated by Samuel Ginsberg and the boards fabricated and tested in the Department of Electrical Engineering at UCT. The waveforms captured by the measurement instruments such as the oscilloscope and network analyser have been exported to Microsoft Excel.

5.1 Hardware Suppliers

The components for the project were selected by an extensive search of several company's websites and by consulting application notes and books. Components were selected based on cost and the user requirements. The silicon oscillator, the LTC6907, used in the reference clock circuit was sourced form *Linear Technology.* The dielectric resonators at 5.8 GHz were supplied, with the author's gratitude, by *Zhejiang Jiakang Electronics Co.Ltd.* Most of the components were given as samples by the various manufacturers, free of charge. The switching regulator for the step-up high voltage supply was constructed using a LT1073 IC from *Linear Technology*. Various inductors used in the switching power supply were supplied from *Gowanda* and *NIC Components Corp.* Additional COTS components came from local distributors, *RS Components* and *Communica*.

5.2 Choice of substrate and Board Layout

Firstly, the substrate on which the circuit will be laid out was considered. FR4 was used to construct most of the circuits, but when used at higher frequencies the losses and dispersion became too high and an alternative substrate was investigated. It was discovered that the FR4's poor performance was due to the fact that at high frequencies

its dielectric loss dominates over its conductor loss [51, Chapter 7]. This is because it has a relatively high dielectric constant which varies between 4.2 and 4.7, which causes a large amount of flux to be absorbed. Signals propagate slower and the transmission lines become dispersive. This can cause problems with broadband signals. *Rogers 4003C* substrate was selected as a replacement for FR4. The dielectric constant of the *Rogers* boards was given as 3.38 and loss was quoted as being only 25% of the losses experienced when using FR4 [12].

Although stripline transmission lines are less dispersive, microstrip transmission lines were still chosen for the design because they are not buried between the substrate and are easily accessible. To avoid the dispersive effects of the microstrip, the transmission lines were made as short as possible. Adhesive copper foil tape was purchased for a quick method of laying down microstrip lines and to reduce the need for making several prototype printed circuit boards.

5.3 PRF Generator

Both the crystal and silicon oscillator circuits that were described in the previous chapter were fabricated. The construction of both circuits was very straight forward. The crystal oscillator, shown in Figure 5.1a, was constructed on double-sided Rogers 4003C according to the schematic in Figure 4.3a. A crystal at 3.579 MHz is used to generate the output as shown in Figure 5.1b. Unfortunately there were no crystals available in small quantities at frequencies below 1 MHz, which made the silicon oscillator necessary for testing the avalanche pulse driver.

The silicon oscillator shown in Figure 5.2, was constructed on double-sided FR4 according to the schematic in Figure 5.2a. R2 and C3 were added to the initial silicon oscillator circuit, as recommended by the manufacturer, to form a 100 Hz low pass filter so that periodic noise generated by the switching power supply would not interfere with the oscillator. The voltage drop across R2 is negligible because of the low supply current. The measured outputs for PRF frequencies of 250 kHz and 3.58 MHz are shown in Figure 5.3. Table 5.1 summarises the performance of both circuits. As expected the crystal was more stable and had a better rise-time.

Table 5.1: Table showing the measured rise-time (t_r) of the oscillators.

Type	Measured t_r [ns]	Predicted t_r [ns]	Predicted stability
Crystal	6.6	7	50 ppm
Silicon	9.5	10	0.28 %

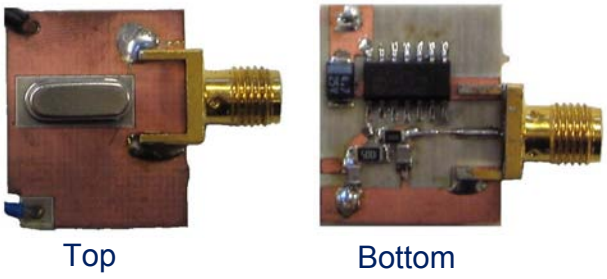

(a) Photo of constructed crystal oscillator.

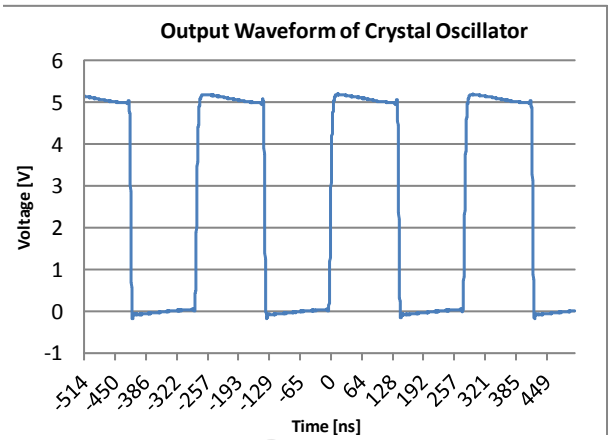

(b) Measured output at 3.58 MHz of Crystal Oscillator.

Figure 5.1: Photo of the crystal oscillator and corresponding output waveform at 3.58 MHz.

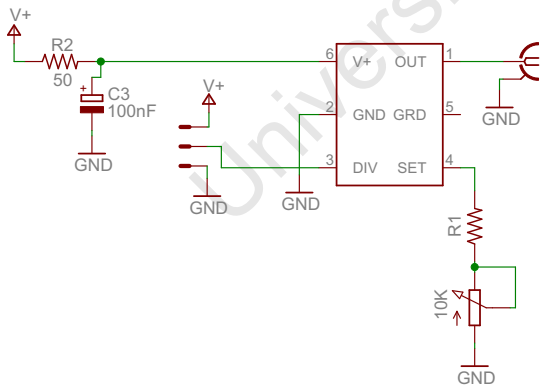

(a) Schematic of the PRF generator.

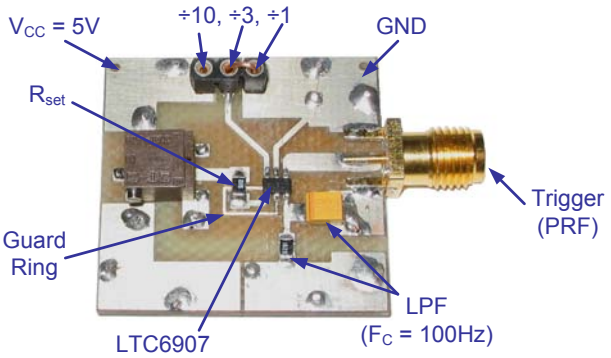

(b) Photo of the constructed PRF generator.

Figure 5.2: 5.2a) The schematic of the silicon PRF generator. 5.2b) The finished construction. A 10 kΩ potentiometer was added in series with R1 so that the frequency could be fine-tuned. Jumpers were added at pin 3 so that the full output frequency range could be used without having to rebuild the board.

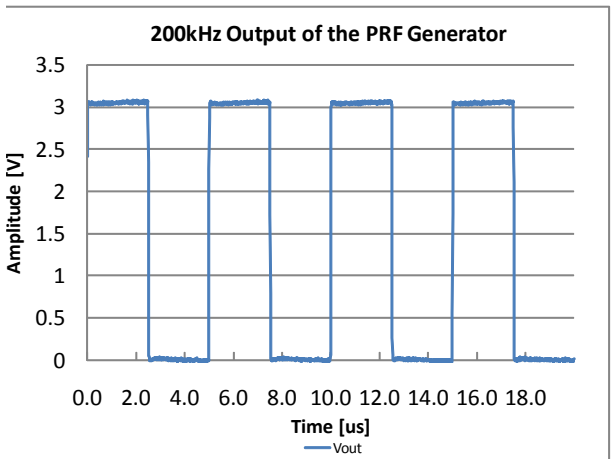

(a) Measured 200 kHz output.

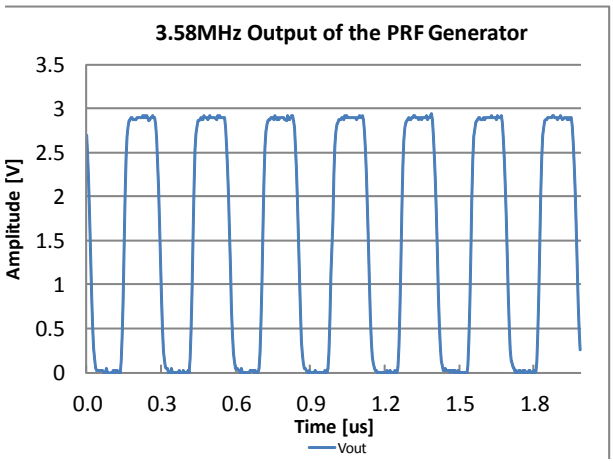

(b) Measured 3.58 MHz output.

Figure 5.3: 5.3a) The measured output waveform with a 200 kHz PRF, which closely resembles the simulated waveform in Figure 4.5a. 5.3b) The measured output waveform at 3.58 MHz, which resembles the simulation in Figure 4.5b.

5.4 Pulse Driver

Both the MIR and the avalanche pulse driver circuits presented in Chapter 4 showed good promise in simulation and it was decided that both should initially be fabricated and tested. The PCB's were made on high frequency Rogers 4003C substrate.

5.4.1 MIR Pulse Driver

The construction of the MIR is well documented by Staderini [77] and in a previous UWB project at the University of Cape Town by Chang [8]. A two-channel version of the original MIR circuit, shown in Figure 5.4, was designed and constructed with surface mount components for this application. The resulting pulse train, illustrated in Figure 5.5, was able to meet the requirements in terms of PRF and pulse-width, however, the amplitude of the pulses was low and could not be improved any further. It must be noted that the oscilloscope that was used was limited to a bandwidth of 1 GHz, so the actual pulse is likely to have better rise-times.

Since a resonant circuit was being used as the pulse shaper, it was decided to focus on the avalanche pulse driver as the amplitude of the pulses was much higher, which would lead to higher amplitude shaped pulses. This presented quite a challenge, which is documented in the subsequent sections.

5.4.2 Which Transistors Give the Best Avalanche Behaviour?

Not all transistors are suitable for avalanche circuits. It must also be noted that transistors of the same type may not avalanche similarly. Transistors that have been de-

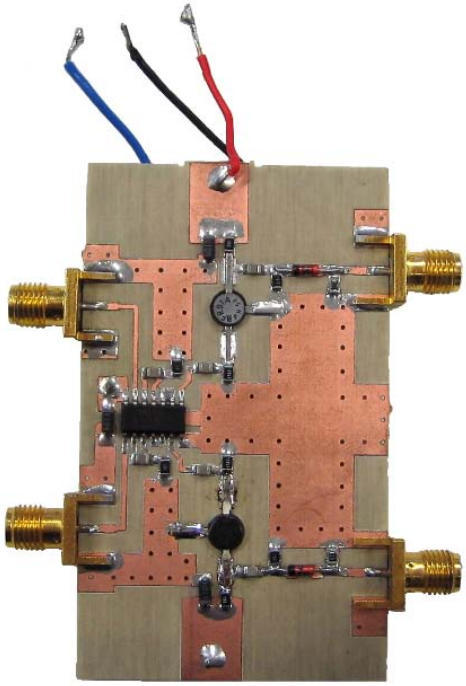

Figure 5.4: A two-channel MIR transmitter. The input from the PRF generators is via the SMA connectors on the left side of the circuit board and the output pulse is measured from the SMA connectors on the right side of the board. A 5 V power supply (blue) for the logic and a 15 V power supply (red) is required.

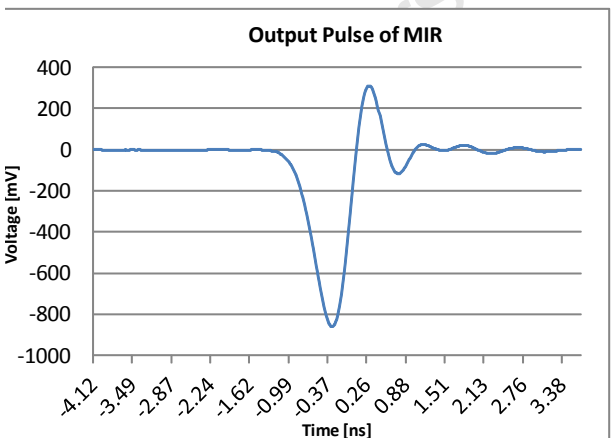

(a) A single output pulse of the MIR.

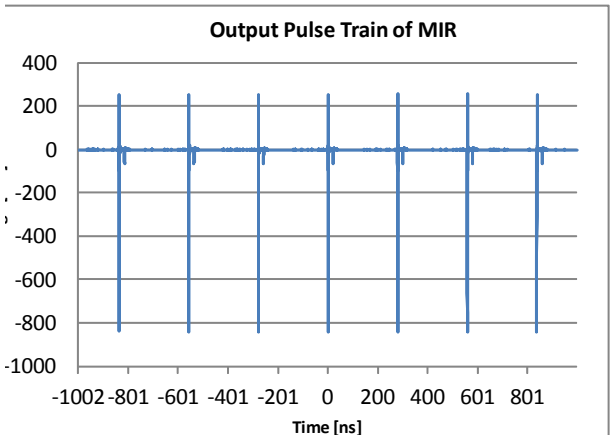

(b) Pulse train output of the MIR.

Figure 5.5: 5.5a) A view of a single, negative pulse output from the MIR circuit. The pulse width is measured to be 650 ps while the rise-time and fall-time are measured to be 260 ps and 565 ps respectively. It is noted that the amplitude of the negative pulse is around 850 mV and that there is an overshoot of 300 mV on the rising edge. 5.5b) The repetition of the MIR pulse train is at 3.58 MHz. An artifact can also be observed 21 ns from each pulse, which is caused by the falling edge of the trigger pulse.

signed for fast switching circuits are usually the most promising [51]. Nevertheless some hand selection is usually necessary. Transistors that come in the metal-can package usually work the best and are able to dissipate heat faster. Some transistors also come in surface mount packages and this can be favourable due to the shorter lead lengths and the lower inductance of the package compared to the metal-can package. There are also transistors which are specifically sold for their avalanche function such as the Zetex 413-417 series but they are significantly more expensive than regular switching transistors. A test circuit was built to test the avalanche behaviour of a handful of products.

Equipment Used

- Sampling oscilloscope (TSD5052B)
- 20dB attenuator
- Camera charger
- Pulse driver test circuit

Method

In order to test the avalanche transistors, the charging circuit for the flash was taken out of a disposable camera. The circuit was able to charge up to nearly 330 V, which was suitable for avalanching almost any transistor. Figures 5.6a and 5.6b show the schematic and the test setup with the constructed circuit. The camera flash charger was connected to the supply V+. The charge button was held down, increasing the supply voltage with time, while the output at X2 was monitored on the oscilloscope. A 20 dB attenuator was placed on the input channel so that the maximum input voltage of the oscilloscope was not exceeded and the input impedance was set to $50\,\Omega$. This means that the recorded voltage had to be multiplied by 10 to obtain the actual voltage. When the transistor avalanched, a pulse triggered the oscilloscope and the supply voltage was recorded. The results are tabled below. All transistors are NPN.

Results

The results show that it is possible to achieve the required pulse-width and very fast rise-time with low cost, switching transistors operating in avalanche mode. As can be seen in Table 5.2 and Figure 5.7, the high cost, avalanche transistor (FMMT413) did not stand out in this experiment. The 2N3904 was chosen as the best candidate because it produced the highest pulse amplitude when compared with supply voltage.

One limitation of this test procedure is that the pulses were captured using a Tektronix TDS5052B sampling oscilloscope, since a better scope was not available at the time.

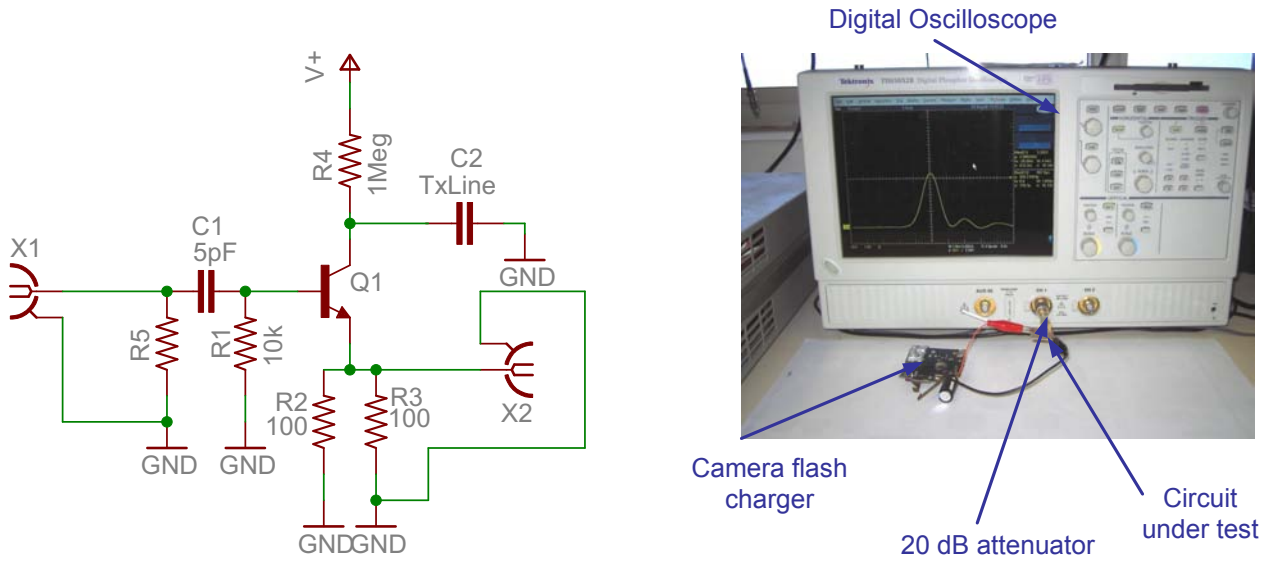

(a) Circuit schematic.

(b) Photo of the test setup.

Figure 5.6: 5.6a) The circuit that was used for the avalanche test. Each different transistor is placed in the same circuit. 5.6b) shows how the equipment has been setup and shows one of the transistors under test.

The Tektronix scope only has 500 MHz single-shot bandwidth and a maximum effective sampling rate of 5 GSa/s. Since the signals are band-limited to 500 MHz, the actual pulse should have better rise and fall times than the measured pulse.

Table 5.2: The parameters of pulses produced by various avalanching transistors. Pulse-width and rise-times are very similar due to the identical charge storage element and circuit layout. Note-worthy parameters are the pulse amplitude and the required supply voltage to achieve avalanche breakdown.

Part No.	Supply Required [V]	FWHM [ns]	Rise Time [ps]	Amplitude [V]
2N2369A	≈108	1.3	930	11
2N3904	≈110	1.15	915	33
2N2219A	≈165	1.2	900	36
MMBT2222	≈160	1.1	812	35
FMMT413	≈180	1.2	930	33
2N3019	≈260	1.2	980	50

5.4.3 Charge storage elements

It was decided that an open circuit transmission line, which behaves like a capacitor, would be used as the charge storage element. The amount of charge stored is, therefore, dependent on the length of the line. The line could then be trimmed until a suitable pulse shape had been achieved. Discrete capacitors could also be used, but in practise yielded poor results.

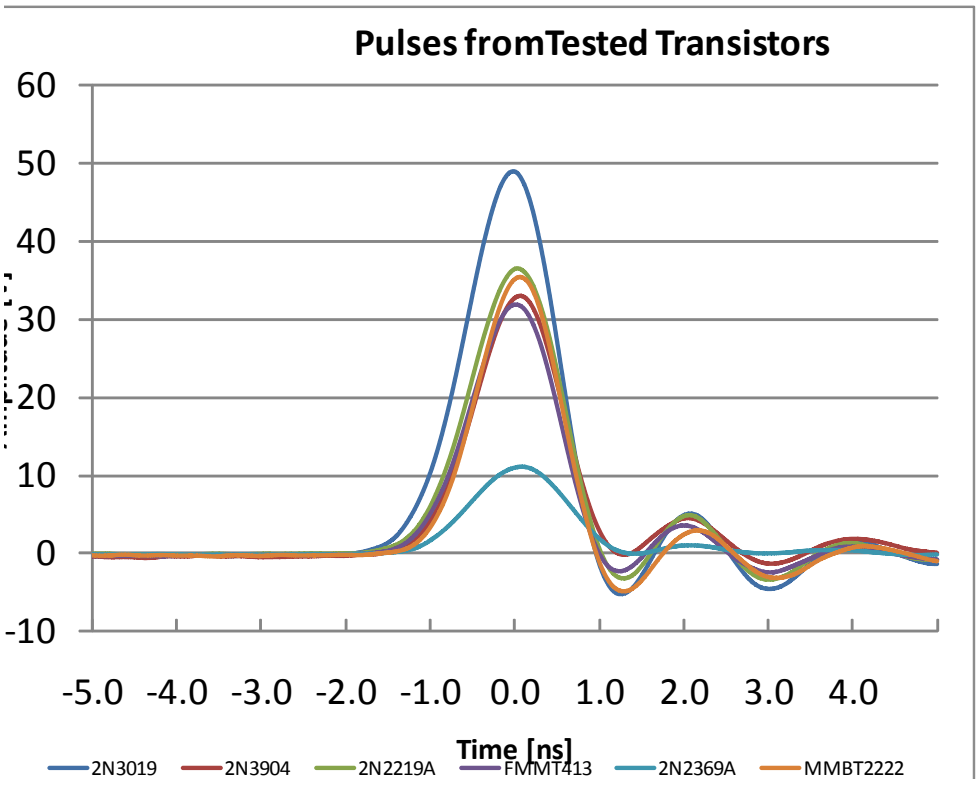

Figure 5.7: Graph of the output pulses generated by each transistor under test.

5.4.4 Layout

As mentioned in Section 4.3.3, inductance's have a big effect on the output pulse. When laying out the circuit, the best results were achieved when the leads were kept as short as possible, since even short conductors act like transmission lines when high frequencies or fast pulses are propagating which results in reduced bandwidth, signal attenuation and slower rise and fall times [44]. Surface mount resistors are also recommended for their small size and mounting the transistor on the other side of the board then allows the connecting lead lengths to be kept to a minimum.

Figures 5.8 and 5.10 show the evolution of the avalanche pulse driver circuits. Earlier versions were built on FR4 substrate and the more recent versions are on the Rogers 4003C.

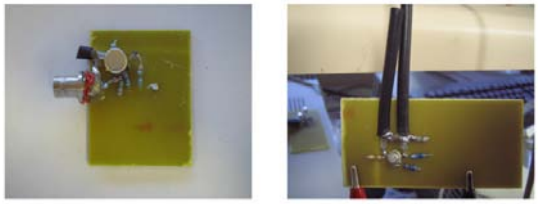

Figure 5.8: Earlier test versions of the avalanche pulser built on single-sided FR4 with leaded components yielded inferior results because of the extra inductance.

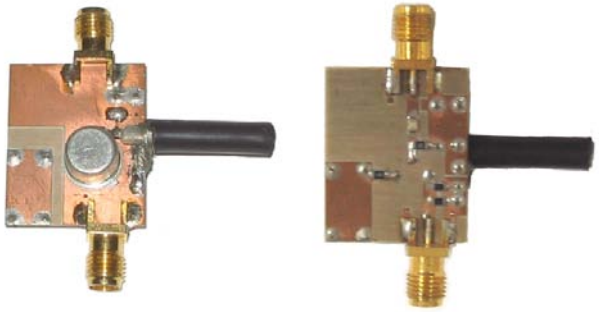

Figure 5.9: Careful layout with surface mount components was able to improve the pulse amplitude.

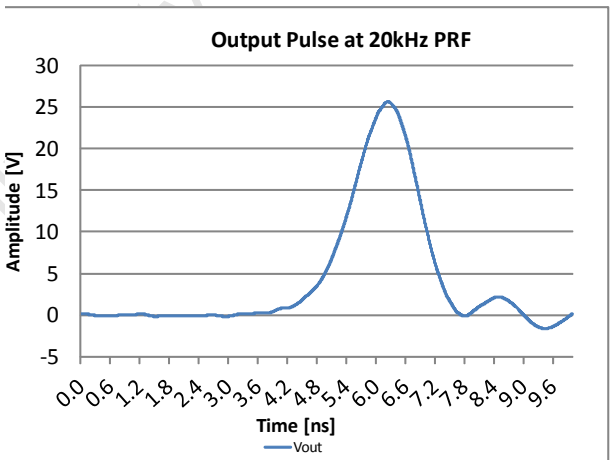

Figure 5.10: Output pulse of the pulse driver when PRF = 20 kHz. Increasing the PRF leads to a drop in pulse amplitude, as predicted in the simulations. The pulse generator stops working when the frequency is increased to 50 kHz. Ripple on the trailing edge of the pulse can be seen, which is due to the mismatch between the $50\,\Omega$ charge storage element and the load resistor plus the internal resistance of the transistor.

In an attempt to improve the PRF of the avalanche pulse driver, a charging network, which was described in Section 4.3.3, was added. In practise, the PRF could only be improved to a maximum of 400 kHz, which was well below the 3.58 MHz predicted, a shortcoming of the simulation. Figure 5.13b shows that the poor repetition frequency is caused by a delay in the re-charging of the storage element. The power supply requirements were also a severe limitation, which meant that a PRF of only 250 kHz, shown in Figure 5.13a could be obtained.

It must be noted the the amplitude of the pulses is lower than in the simulations. In addition to the losses caused by additional stray inductance, the voltage drop across the load resistor is, in practise, limited to approximately $V_{CBO(BR)} - V_{CEO(BR)}$, which is a property of the individual transistor according to Herden [35].

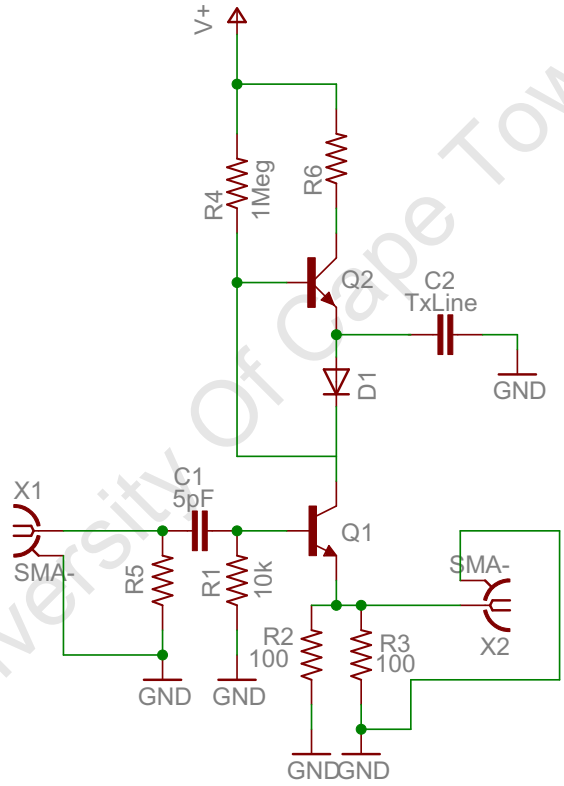

Figure 5.11: Schematic of the pulse driver with the charging network.

5.5 RF Pulse Shaper

5.5.1 DR Filter

In order to improve on the earlier DR filter design and achieve a wider bandwidth, the Q-factor of the resonator has to be reduced. It was found that this could be done by closing the gap between the transmission lines and by having the resonator sitting on

er_charge.sch (Sheet: 1/1)

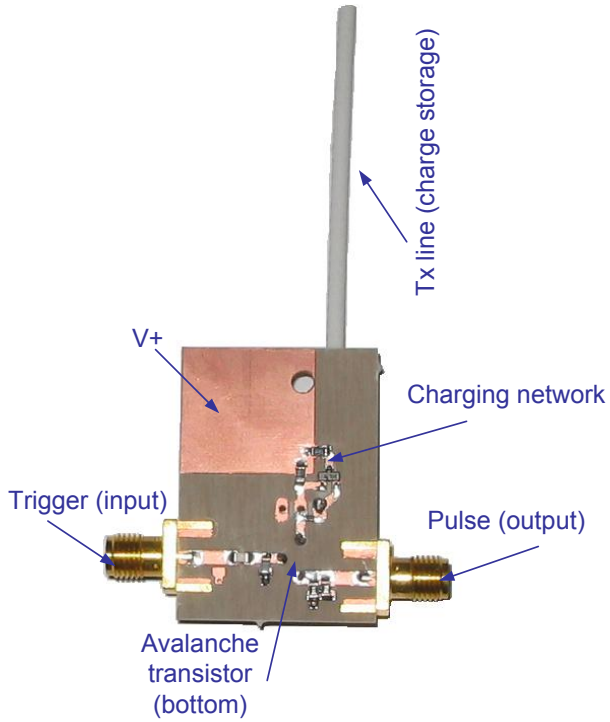

(a) Photo of the pulse driver with a charging network.

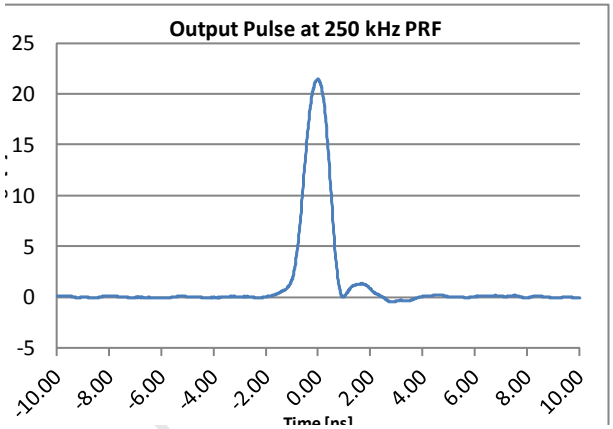

(b) Measured output pulse.

Figure 5.12: 5.12a) A photo of the fabricated pulse driver with the charging network. 5.12b) A single output pulse which shows a pulse-width of 1.05 ns, rise and fall times of 700 ps and 535 ps respectively and an amplitude of 21 V.

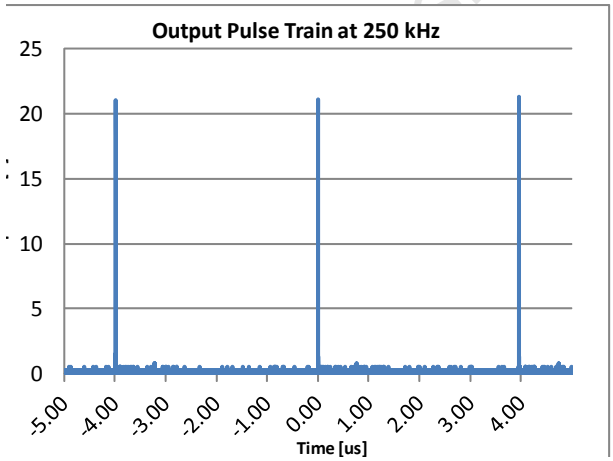

(a) Output pulse of the pulse driver with a charging network and PRF = 250 kHz.

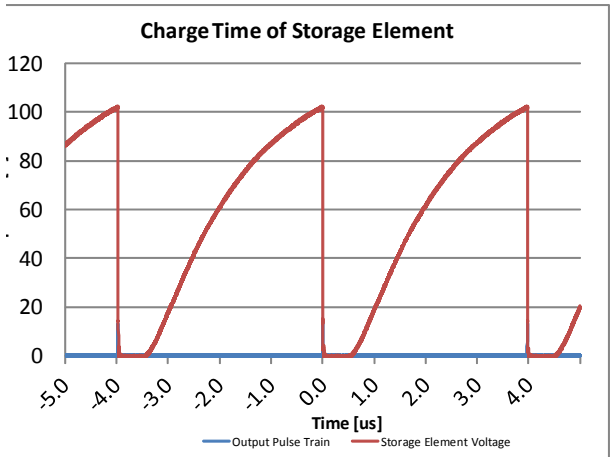

(b) Re-charging of the storage element in between pulses.

Figure 5.13: The results of adding a charging network show an increase in the achievable PRF from 20 kHz to 400 kHz without sacrificing pulse amplitude. Power constraints, however, prevent the circuit from being used at over 250 kHz. One possible limitation of PRF is the recovery time of 0.5μs before the storage element begins to charge, most likely linked to the recovery of the diode D1.

top of the transmission lines so that it became saturated with flux. This would also improved the coupling and result in a better insertion loss.

Equipment Used

- Vector Network Analyser (Agilent E5071B)
- Dielectric Resonator Filters

Method

The six filters shown in Figure 5.14 were constructed to test which one would give the best response. Three different widths between the transmission lines were set to determine how much the Q-factor of the filter was reduced and whether it would allow a pulse with a bandwidth of around 1 GHz to pass. The lengths of the transmission lines were also decreased to determine if the insertion loss could be improved.

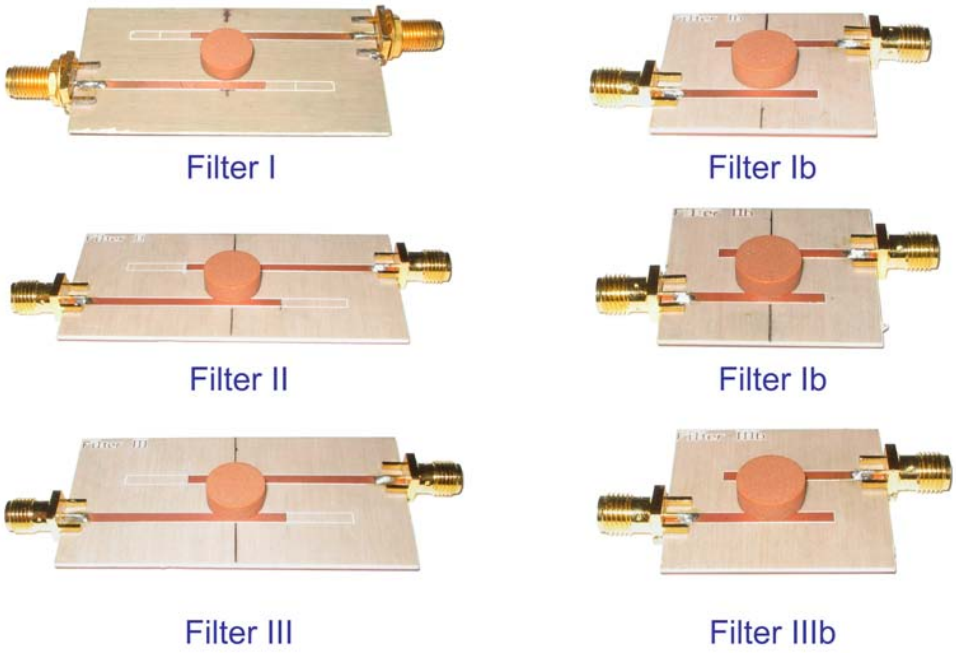

Figure 5.14: Photo of the filters to be tested.

The resonator was carefully placed at the centre of the PCB, one-quarter wavelengths of the centre frequency away from the ends of the transmission lines. The S_{11} and S_{21} parameters were measured on the network analyser and the results of each filter were compared.

Results

Figures 5.16a and 5.16b show the S_{21} plots of each of the six filters. The filters are labelled I to III, I being the largest gap between the transmission lines and III being

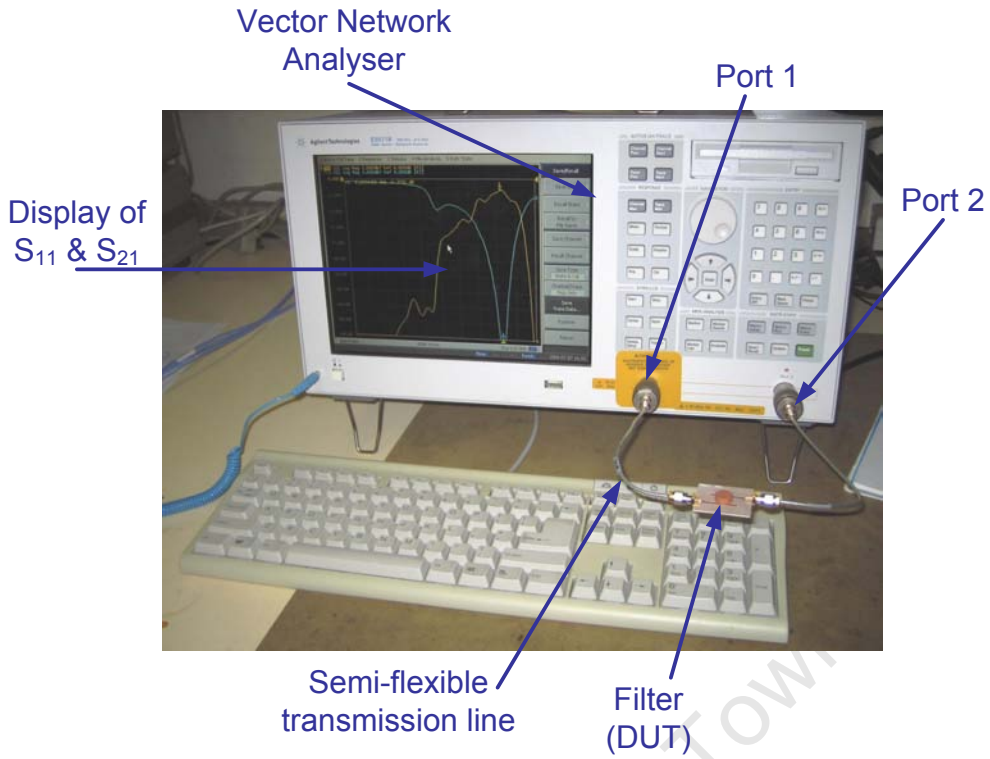

Figure 5.15: Photo of the filter test setup.

the shortest gap. Versions of these filters with shorter transmission line lengths are then labelled Ib to $IIIb$.

Ultimately it was found that, although the bandwidth could be increased by careful placement of the DR and adjustment of the gap in the transmission lines, the out of band rejection of the filter became worse. A significant amount of energy at lower frequencies was able to pass through the filter which would lead to distortion of the 5.8 GHz signal because of the high level of low frequency components in the baseband signal. For this reason, the DR filter failed to meet the acceptance criteria. The hairpin filter then became the best option.

5.5.2 Transmission line filter

In order to overcome the limitations of a simulation performed with linear models, it was necessary to design a planar layout of the hairpin filter and apply an EM analysis and optimisation to the problem. The EM analysis is the best way to predict the response of the filters before fabrication and allows one to make small adjustments in the parameters to achieve the best possible end result.

Method

This evolution is illustrated in Figure 5.18 after the optimiser was allowed to run for 72 hours. Each iteration of the optimiser takes approximately 5 minutes. As can be

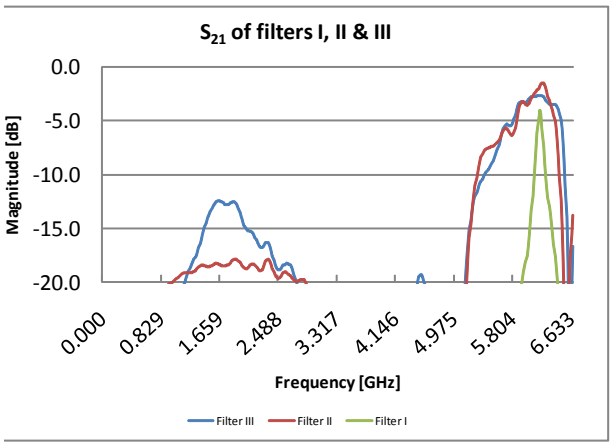

(a) S_{21} parameters of filters I to III.

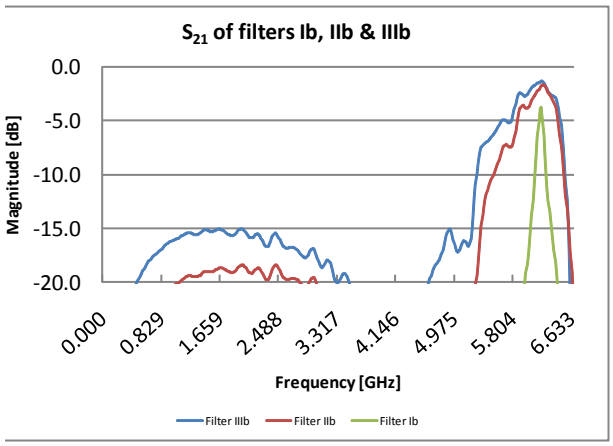

(b) S_{21} parameters of filters Ib to $IIIb$.

Figure 5.16: Filters II and III, show that the bandwidth of the filter has increased. The shorter the gap, the wider the bandwidth becomes. The shorter microstrip lines also have a small effect on the insertion loss. It was also noted that the centre frequency of the filter was not 5.8 GHz, as expected, but rather 6.17 GHz. One explanation could be the mismatch in the dielectric mediums of the resonator and substrate leading to a different resonant frequency.

seen in Figure 5.17, which shows a diagram of the first 2 poles of the seven-pole hairin filter that was designed, there are several variables that control the response of the filter. The optimiser tracks the value of each variable and changes these variables by a small amount each iteration. It then compares each result with that of the previous iteration and with the desired optimum filter response. If the new iteration has a result which is closer to the desired response than that of the previous iteration, the values of the variables are kept. The process continues until the optimiser converges on the desired filter response. To speed up the optimisation process, a range for each variable is entered manually, thus eliminating any invalid values or values that cannot be physically realisable by the fabrication equipment.

Results

Fabrication of the filter was fairly difficult because the gap between some of the lines was very narrow (approximately 5 mil). This approached the limitations of the PCB milling machine and as can be seen in Figure 5.19, which shows the narrow gap under a microscope, the drill leaves rough edges which, in such a small gap, cause a slight deviation from the desired outcome in filter response.

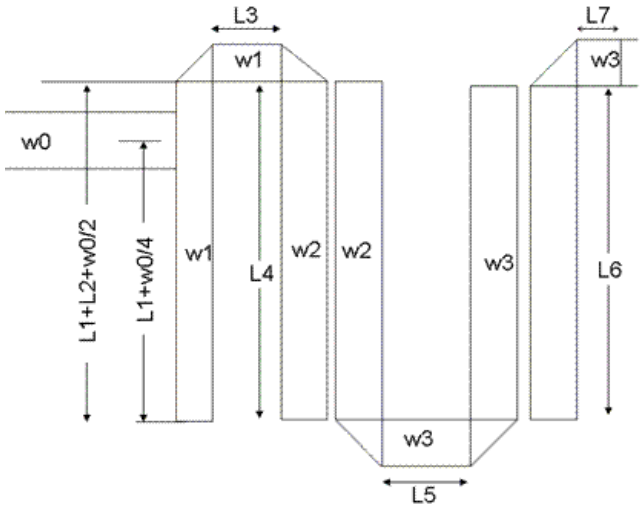

Figure 5.17: A diagram showing the large number of varibles that need to be optimised. This large number of variables can only be optimised using sophisticated computer algorithms available in Genesys and would be impossible to do manually.

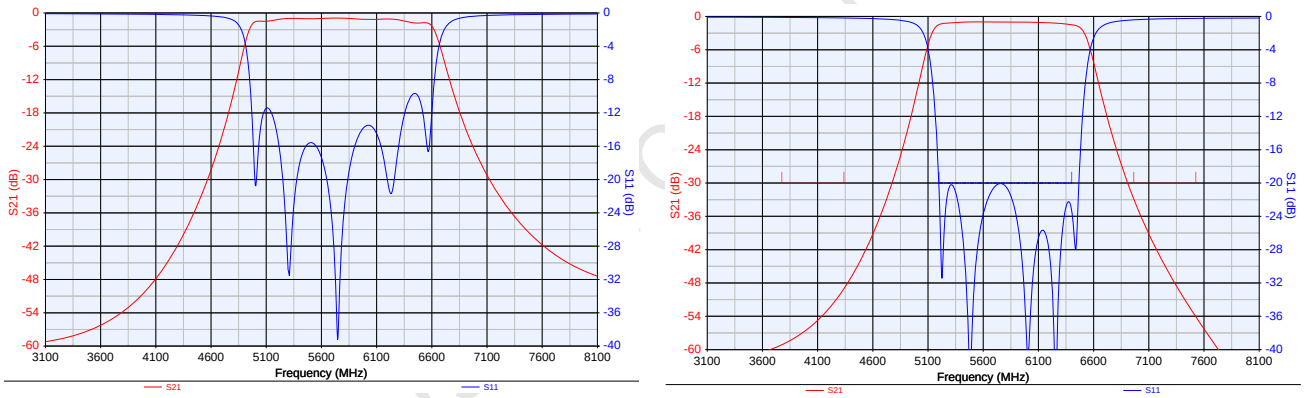

(a) EM response.

(b) Optimised response.

Figure 5.18: 5.18a and 5.18b illustrate how the hairpin filter design evolves from a theoretical linear model to an EM optimised circuit. Note the reduction in bandwidth and shift in centre frequency between that of Figure 4.15b and Figure 5.18a, which is why the initial bandwidth is made much higher than actually needed. After optimisation, the correct passband, $5.8\,\mathrm{GHz} \pm 500\,\mathrm{MHz}$, and good matching, $\leq 20\,dB$, is achieved.

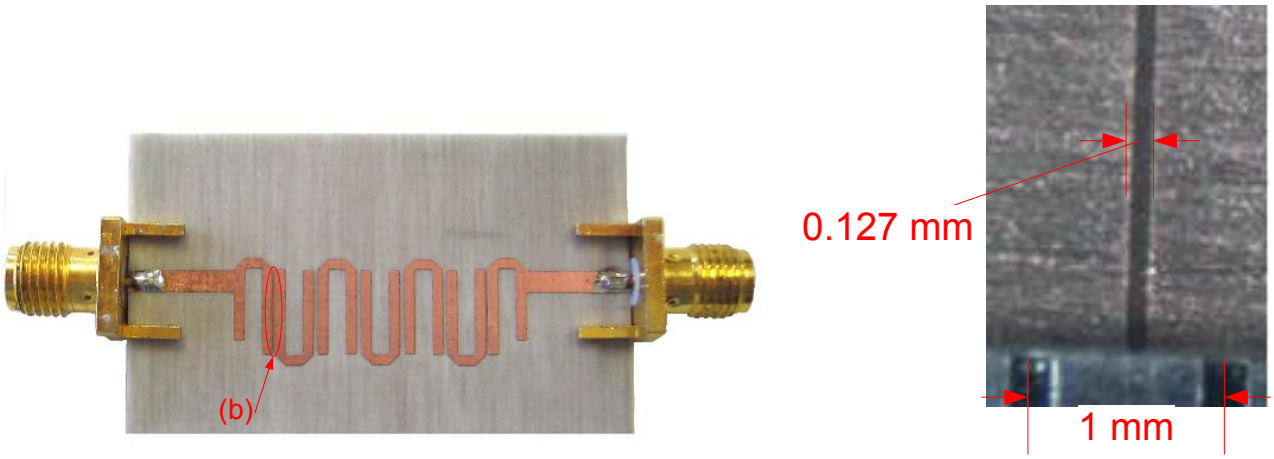

(a) Fabricated hairpin filter.

(b) Microscope view.

Figure 5.19: 5.19a shows the fabricated hairpin filter. The area surrounded in red is a microscope view of the very narrow gap which separates two microstrip lines and shown in 5.19b.

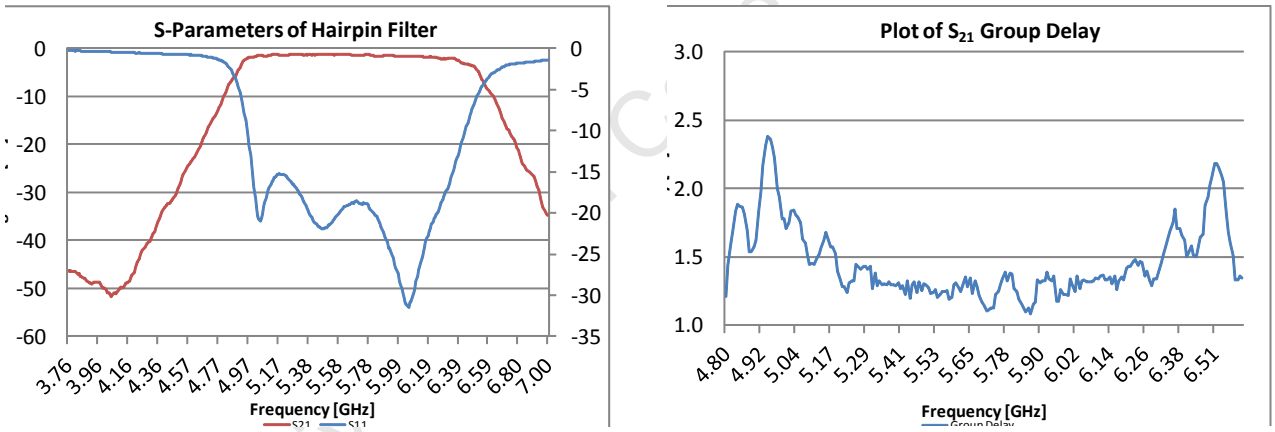

(a) S11 and S21 Parameters.

(b) S21 Group Delay.

Figure 5.20: 5.20a shows the S_{11} and S_{21} parameters of the hairpin filter. When compared to the simulated design, it can be seen that the passband is centred on 5.8 GHz with 1 GHz bandwidth. Matching is also good with a return loss of less than 15 dB over the passband. 5.20b shows a group delay plot of S_{21} which indicates that there some concern for dispersion around the 3 dB cut-off points of the filter.

5.6 Branch-Line Coupler

As discussed in Section 4.5, the branch-line coupler is a suitable device to be used as a duplexer but the standard "two-branch" coupler described and simulated in Section 4.5.2 has the disadvantage of being very narrowband and not useful for such wideband signals. This disadvantage can be overcome by adding supplementary sections to the structure to increase the usable bandwidth [53, 52, 50, 51, pg 226].

In practise, however, it can be very difficult to implement more sections in microstrip because the outside branches usually require very high impedance's, which can exceed the limits of ones fabrication capabilities. In addition, the line-widths required by the lower impedance lines create an undesirable aspect ratio, which affects the lengths of the quarter-wavelength sections [64]. CAD software is ideal for solving this issue because the impedance range can be specified before synthesis and optimisation to ensure that the circuit can be physically constructed.

Method

Using the properties of the dielectric material such as the substrate thickness and the minimum line-width that could be fabricated on the PCB machine, it was determined that the usable microstrip impedance range on Rogers 4003C was $35\Omega - 120\Omega$. *Genesys* does not have a synthesis tool for multi-branchline couplers so a three-branch Chebyshev coupler from [64] was used as a starting point. An EM simulation was run on the microstrip layout shown in Figure 5.21. The optimiser was run without any restrictions on the line impedance's but the results exceeded the upper frequency limit of 120Ω on the outer-most branches. The impedance of the outer branches was then held constant at 120Ω and the optimiser was run again. The final results of the optimisation are shown in Figure 5.22.

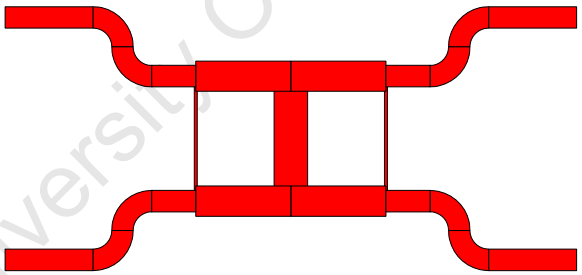

Figure 5.21: Layout of multi-branchline coupler.

Results

After being satisfied with the simulation results, the coupler was fabricated, as shown in Figure 5.23. The results of the measurements are shown in Figure 5.24, which show that the bandwidth of the coupler was able to be increased to allow a signal with 1 GHz of bandwidth centred on 5.8 GHz to pass. A small amplitude imbalance is noted between the two output ports due the limitation in achievable line impedance's and fabrication tolerance. It is, however, within acceptable limits.

Figure 5.20: Layout of multi-branch-line coupler

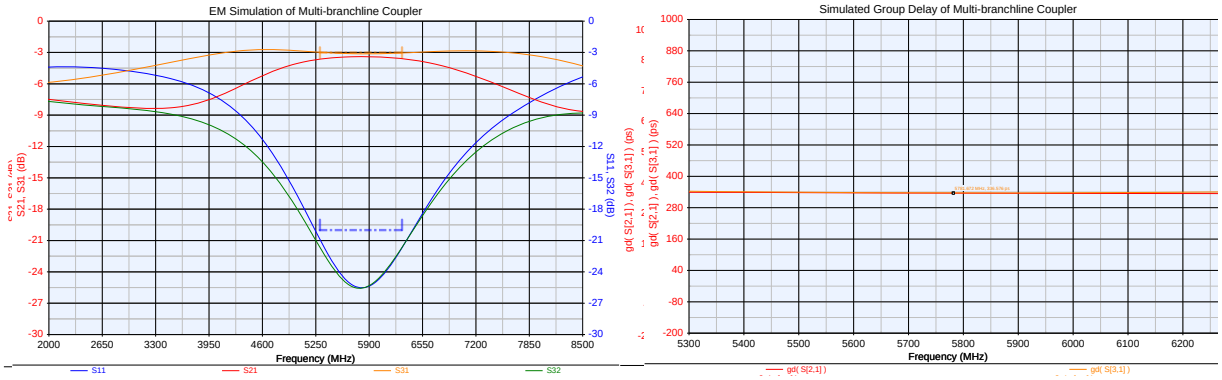

(a) EM simulation S-parameter results.

(b) EM simulation of Group Delay.

Figure 5.21: The results of the EM simulation after final optimisation. S-parameter data shows good constancy to the requirements. It is desired that the group delay is constant within the passband, as shown in Figure 5.22b, to minimise dispersion.

Results

After being satisfied, fabricated as shown in Figure 5.22. The results, which show that the bandwidth, now a signal with 1 GHz of bandwidth centred at 5.8 GHz, imbalance is noted between the two output, impedance's and fabrication tolerance.

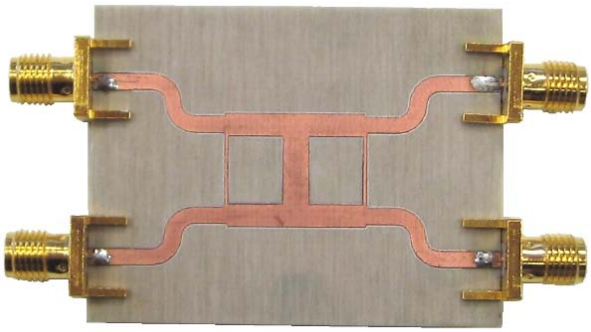

Figure 5.23: Photo of the fabricated multi-branchline coupler. SMA connectors are added to the ports for measurement equipment.

5.7 Integrator and Amplifier

Figure 5.24 shows the circuit for the receiver voltage amplifier. Three stages of the

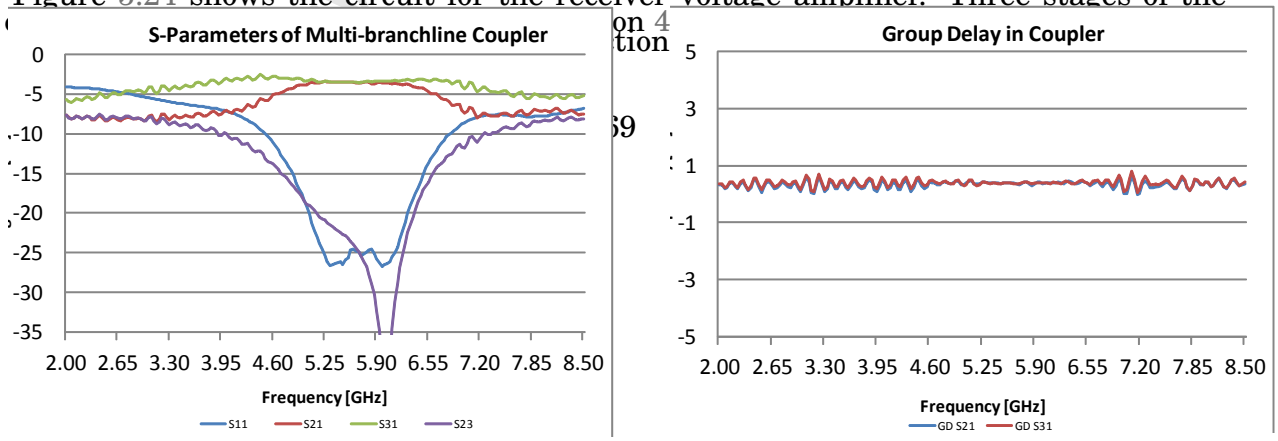

(a) S-parameter measurement results.

(b) Group delay measurement results.

Figure 5.24: Results of measurements taken on the Agilent E5071B VNA. The S-parameters, in Figure 5.24a, show a vast improvement in usable bandwidth centred on 5.8 GHz. The group delay, shown in 5.24b, is is also relatively consistent at 400 ps, which means that there would be little dispersion in the signal while it is propagating through the coupler. Isolation is more than 20 dB over most of the desired bandwidth.

5.7 Integrator and Amplifier

Figure 5.25 shows the circuit for the receiver voltage amplifier. Three stages of the common-emitter amplifier discussed in Section 4.6.2 have been cascaded. The transistor used was the 2N5109, an RF transistor with a gain bandwidth product of 1 GHz and a noise figure of 3dB. The gain of each stage is 28 (14.5 dB), which gives a total gain of around 43 dB. Quiescent current is chosen at 100 μA for each stage. Ultimately the total gain, measured with a continuous sinusoidal signal at 70 kHz, was 40.5 dB. In order to bias the output DC level for maximum AC signal swing, potentiometers were added to the biasing networks for fine tuning. Very little modification was necessary as the circuit performed as predicted by the Spice simulations. Figure shows the response of the intergrator together with the amplifier up to 1 MHz. Since the integrator circuit behaves like a low-pass filter at 32 kHz, the test signal at 70 kHz is attenuated to 31 dB.

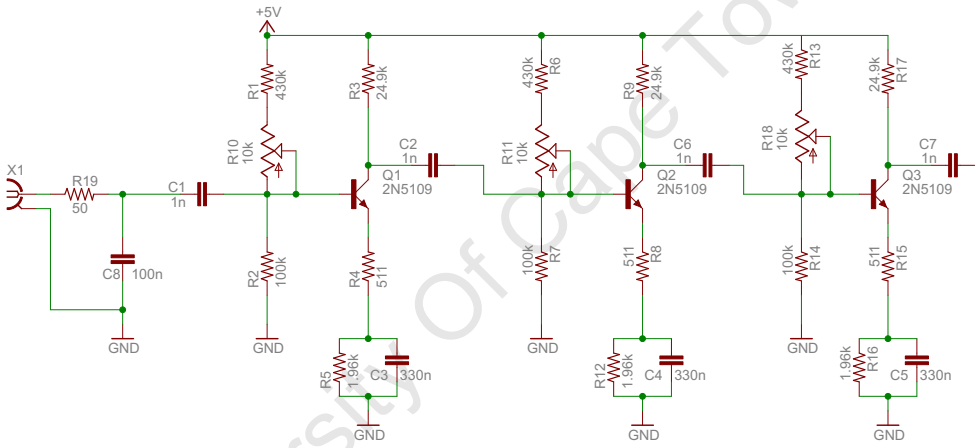

Figure 5.25: Schematic of the integrator and voltage amplifier.

5.8 Additional Power Supply

The schematic of the step-up DC-DC converter is shown in Figures 4.21a. R1 is selected to limit the switching current of the device. C1, C2 and C3 form voltage doublers with the diodes, MUR120 fast switching, to keep the voltage at pin SW1 below its maximum of 50 V. The input is the regulated 9 V from the original ultrasonic instrument.

Figure 5.28 shows the constructed circuit built on double sided FR4. The output waveform is shown in Figure 5.29 and compares well with Figure 4.21b. Low ESR (Equivalent Series Resistance) capacitors were used, which improved the output ripple to that shown in the initial simulation. The circuit can easily be modified to output a voltage of 15 V for use in the MIR pulse driver.

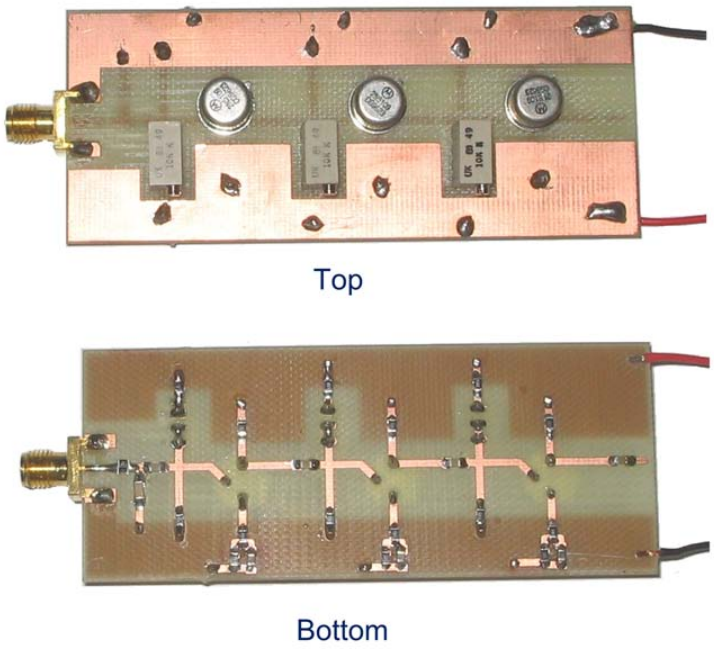

Figure 5.26: Photo of the constructed integrator and amplifier circuits.

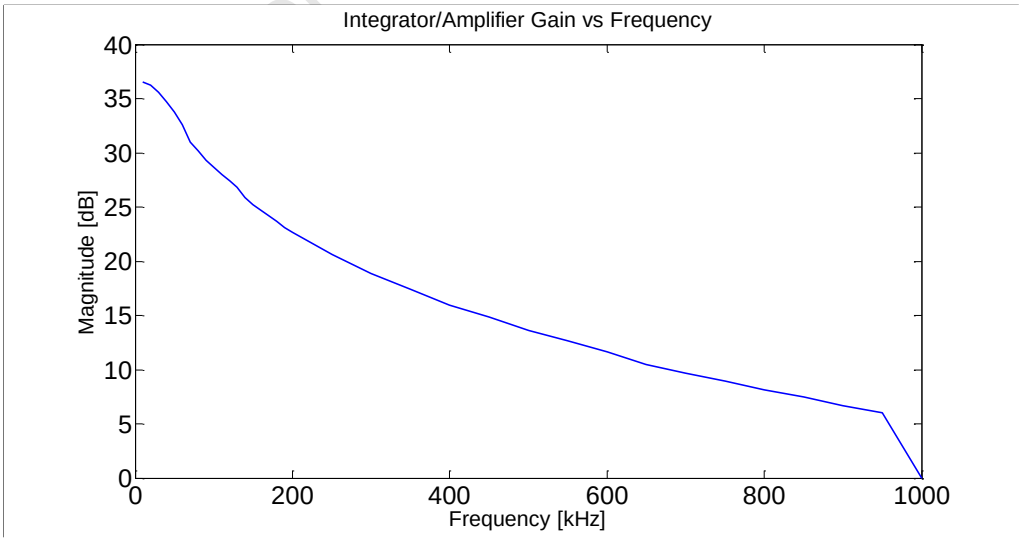

Figure 5.27: Plot of the gain versus frequency for the intergrator/amplifier circuit. The gain is very good at low frequency below 30 kHz at 36.5 dB.

A step-down converter was not required since all the low voltage circuitry could use the regulated 5 V already available on the instrument.

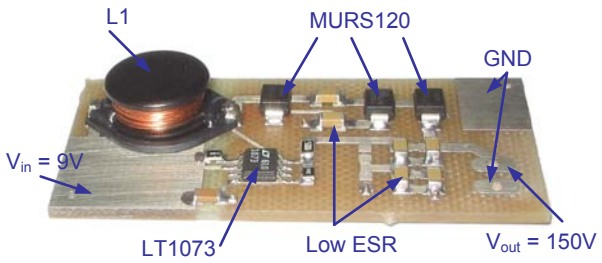

Figure 5.28: Photo of the constructed step-up DC-DC converter.

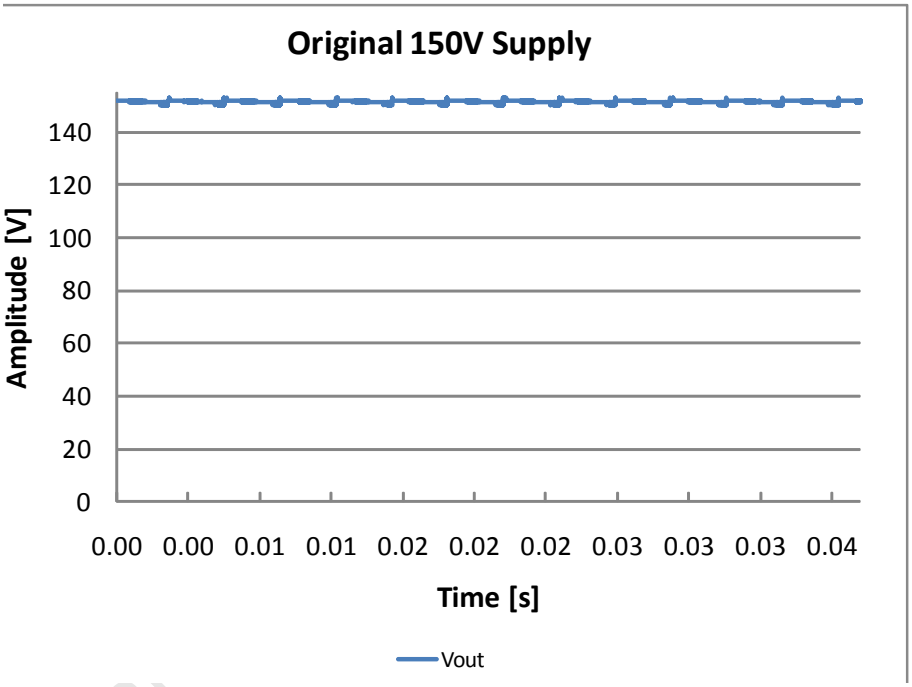

Figure 5.29: Measured output of the step-up converter with low ESR capacitors. Voltage ripple is less than 2 V.

5.9 Summary

The various sub-systems have been constructed and the measured waveforms have been compared to the predicted waveforms and instrument specifications.

5.9.1 PRF Generator

It was determined that crystal based oscillators would be the best option for generating the trigger signals for the pulse drivers due to their superior stability. A simple, low cost, low power circuit utilising CMOS logic was constructed to produce a 3.58 MHz

square-wave with a rise-time of less then 7 ns. Better, more expensive crystals can be used to further improve the stability of the output. This met the acceptance criteria for the sub-system.

In order to simplify the prototyping of the pulse driver, a silicon oscillator was also constructed that could provide a tunable square-wave with a rise-time of less than 10 ns. Although it was useful in the design process, it was determined that the stability of the silicon oscillator would not be sufficient to implement the Vernier time stretching in the final system integration as maintaining a constant TSF relies on low trigger period jitter.

5.9.2 Pulse Driver

Both the MIR and the avalanche transistor circuits were seen as good candidates for the pulse driver. From the simulations, it was seen that both circuits were able to produce pulses with a pulse-width of 1 ns and fast rise-times less than 800 ps. The MIR had the advantage of a high PRF but the disadvantage of a low output pulse amplitude. The avalanche transistor had the advantage of a high pulse amplitude but a low PRF. Both circuits were initially constructed but it was ultimately decided, due to time constraints, that the focus would be on the avalanche transistor pulse driver.

Various transistors were tested for good avalanche behaviour. It was determined that the best option was the 2N3904. The FMMT413, a transistor made specifically for avalanche use, did not show any clear advantages over the regular transistors that were tested. It was decided that a transmission line should be used to store the charge for the avalanche transistor as most small packaged capacitors were not able to withstand the high supply voltage required to bias the transistors. Layout also proved to be a significant challenge. Earlier constructions used ordinary leaded components, however, the stray inductance and capacitance proved to be too high and small surface mount versions had to be constructed.

Measurement of the pulse-width and rise-time was limited by the one-shot bandwidth the oscilloscope. An oscilloscope with a better one-shot bandwidth would likely indicate narrower pulse-width and faster rise-times. Ultimately the pulse driver was able to produce short, 1 ns pulses with amplitudes of 21 V. The PRF was increased, with the addition of a charging network, to a maximum of 400 kHz. A PRF of 250 kHz was deemed more appropriate because the higher PRF exceeded the supply current limit.

5.9.3 Pulse Shaper

The dielectric resonator filter was initially the favoured choice for the pulse shaper. Careful placement of the resonator and readjusting the microstrip lines enabled prototype filters to be constructed onto PCB with improved bandwidth and insertion loss

over initial designs. Several dielectric resonator filters were fabricated but in the end it was found that by increasing the bandwidth, the out of band rejection of the filter decreased such that low frequencies were able to pass through the filter. Due to the high energy of the low frequency spectral components of the base-band signal, it was determined that there was insufficient isolation in the filter and that the desired signal at 5.8 GHz would become severely distorted.

The DR filter was abandoned in favour of a microstrip hairpin filter. The use of EM simulation and optimisation software was crucial in the design. A filter was fabricated that had a bandwidth of over 1 GHz at a centre frequency of 5.8 GHz. There was good matching with return losses less than 15 dB the passband. This met the requirements for the sub-system.

5.9.4 Branch-line Coupler

It was determined that the bandwidth of a regular, two-stage branchline coupler could be improved by adding more stages. A three-stage branchline coupler was designed by utilising EM simulation and optimisation software. The practical range of microstrip impedance's that could be fabricated was limited by the substrate material and the capabilities of the PCB milling machine, making a CAD approach very useful. After fabrication, it was seen that the bandwidth was indeed improved to around 1 GHz, centred at 5.8 GHz and that the isolation was more than 20 dB over most of the desired bandwidth. It is likely that the response could be improved if the board is professionally fabricated as outside manufacturers are able to achieve better tolerances. The sub-system, therefore, did meet the acceptance criteria.

5.9.5 Cross-correlator

A connectorised double-balanced mixer was used for the multiplication. The integrator circuitry and the voltage amplifier were then constructed together on one PCB. Three common-emitter amplifiers were cascaded to achieve a voltage gain of at least 40 dB. This corresponded very closely with the simulations and met the acceptance criteria.

5.9.6 Power Supply

It was determined that a single power supply was required to step-up the regulated 9 V on the instrument to a suitable high voltage to bias the avalanche transistor pulse driver or the MIR. The LT1073 was chosen because the output voltage could easily be set by changing two resistors and the switching current could also be limited for compatibility with the power supply constraints. Low ESR capacitors were used to reduce the high output voltage ripple that was seen in the simulations.

Chapter 6

System Testing

Chapter 5 focused on the fabrication and evaluation of the various individual sub-systems. In this chapter, these sub-systems are brought together and tested for their combined performance. Firstly the TSF is derived from measurements on the PRF generators. The three sub-systems of the transmitter are then connected to evaluate the shaped RF output pulses in the frequency and time domain. Tests are then performed on the entire system to evaluate the time stretching technique and achievable accuracy. The compliance of the system to the rest of the desired specifications is then also discussed.

6.1 Testing of PRF Generator

Equipment Used

- Universal counter (HP 53131A)
- 2 x PRF generators

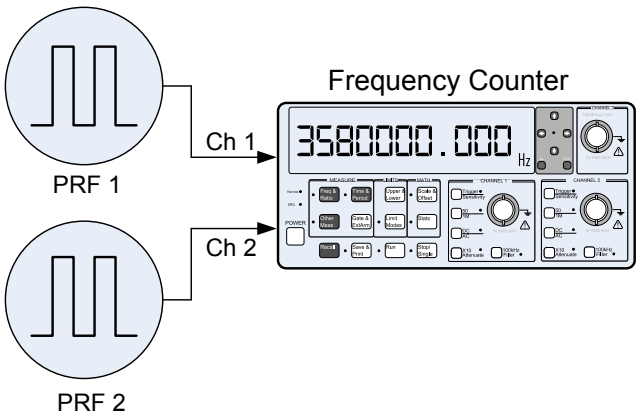

Figure 6.1: Diagram of the equipment setup for testing the PRF generators.

Method

Two PRF generators from Figure 5.1 were constructed. A small tuning capacitor was added to one of the PRF generators to pull the frequency by a small amount. The output frequencies of both PRF generators were then measured and compared on a Universal Frequency Counter as shown in Figure 6.1. The tuning capacitor was turned until the difference between the PRF's was approximately 43.7 Hz as per the requirement. Unfortunately, adding a tunable element degraded the stability of the output signal so the tunable capacitor was replaced with the closest fixed capacitor value. The resulting measured frequencies and estimated TSF is shown in Table 6.1.

The procedure was repeated with the output of the crystal connected to a 74HC4040 ripple counter, in order to divide the frequency by 16. This would allow for the crystal PRF generator to be used as the trigger to the avalanche pulse driver, which only has a maximum achievable PRF of 250 kHz. These results are shown in Table 6.2.

Results

Table 6.1: Table showing the measured PRF and calculated time stretched repetition rate of the crystal PRF generators. The calculated TSF is 92820.

	Frequency [Hz]	Period [s]
1	3580111.75	$279.3208899 \times 10^{-9}$
2	3580073.28	$279.3238992 \times 10^{-9}$
T_{rep}	38.57	2.59269×10^{-2}

Table 6.2: Table showing the measured PRF and calculated time stretched repetition rate of the crystal PRF generators with frequency division. The calculated TSF is 9965.

	Frequency [Hz]	Period [s]
1	223808.52	4.4681051×10^{-6}
2	223786.06	4.468554×10^{-6}
T_{rep}	22.46	4.45236×10^{-2}

Table 6.3: Table showing the calculated TSF and effective sampling rate, $f_{s,eff}$, for the avalanche pulse driver and the MIR based on the measured PRF's.

	$TSF = \frac{T_1}{T_2 - T_1}$	$f_{s,eff} = \frac{1}{T_2 - T_1}$
MIR (3.58 MHz)	92820	332.3 GSa/s
Avalanche (223 kHz)	9965	2.2303 GSa/s

As can be seen, the closest difference between the PRF's was 38.57 and 22.46 for the 3.58 MHz and the 223.8 kHz signals respectively. This corresponded to a TSF of 92820 for the MIR and 9965 for the avalanche pulse generator. The effective, real-time, sampling rate after time expansion was calculated to be 2.23 GSa/s for the avalanche and 332.3 GSa/s for the MIR.

These results indicate a problem with the PRF of the avalanche pulse driver method. The Nyquist sampling rate for a 5.8 GHz signal is at 11.6 GSa/s, which is much higher than the achieved 2.23 GSa/s. The difference between the transmit and reference PRF's at 223 kHz would have to be in the order of 2 Hz to achieve a more suitable effective sampling rate but attempts to do this were unsuccessful. This failure was most likely due to the period jitter of the avalanche pulse driver, which will be discussed further later.

6.2 Testing of Power Spectrum

Equipment Used

- Spectrum analyser (Agilent E4407B)
- PRF generator + avalanche pulse driver
- PRF generator + MIR pulse driver
- RF pulse shaper (5.8 GHz)

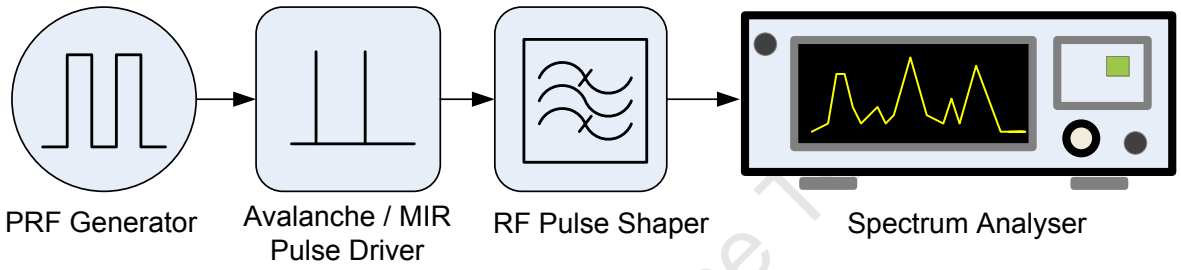

Figure 6.2: Diagram of the equipment setup for testing the power spectrum of the transmitted pulse train.

Method

The power spectrum of the transmitter was tested using a spectrum analyser as shown in Figure 6.2. Firstly, the power spectrum of the baseband pulses was measured, which requires a DC block to be placed on the input of the spectrum analyser for protection. Secondly, the DC block was removed and replaced with the 5.8 GHz hairpin filter shown in Section 5.5.2. Since there is no direct dc path through the filter, the DC block is unnecessary. The test was initially run with the avalanche pulse driver and then with the MIR pulse driver. The resulting spectra are illustrated in Figure 6.3

Results

It was seen that the spectrum of the baseband pulses is indeed very wide as expected. Unfortunately, it was also observed that there was no measurable power in the 5.8 GHz band. The signal levels in the band of interest are likely very weak and possibly well below the noise floor. This means that the chosen method of pulse shaping using a filter is too inefficient to demonstrate a shaped RF pulse. However, it was noted that there was sufficient energy at lower frequencies in the spectrum to produce a measurable result.

The likely reasons for the failure of these waveforms to exhibit sufficient power in the band of interest are discussed below:

- *Insufficient pulse width and rise-time* - the bandwidth of the waveform is determined by the rise-time and pulse width. As discussed earlier, faster rise-times and narrower pulse widths give increased bandwidth. Consequently, the rise-time and pulse width of these pulse generators need to be improved to obtain a wider bandwidth signal. Likely causes of the limited rise-time are the sharpness of the base trigger and the characteristics of the switching transistor itself, such as feedback capacitance, and the characteristics of the charge storage element, such as stray inductance.

- *Pulse shape* - The pulse shape resembles that of a Gaussian-like function, which has a very large portion of its spectral content close to DC, as can be seen in Figure 6.3. Unfortunately, due to time constraints, suitable alternative pulse shapes, such as first-derivative Gaussian monopulses and Gaussian doublets, could not be investigated. Monopulse and doublet waveforms exhibit a shifted spectrum centred at high frequency with much lower power at and around DC [27]. This means that more energy should be available at the desired band after filtering .

- *Dispersion effects* - The dispersion in the microstrip transmission lines as well as the planar microwave components could also result in distortion and the widening of the pulses, leading to a decrease in achievable bandwidth.

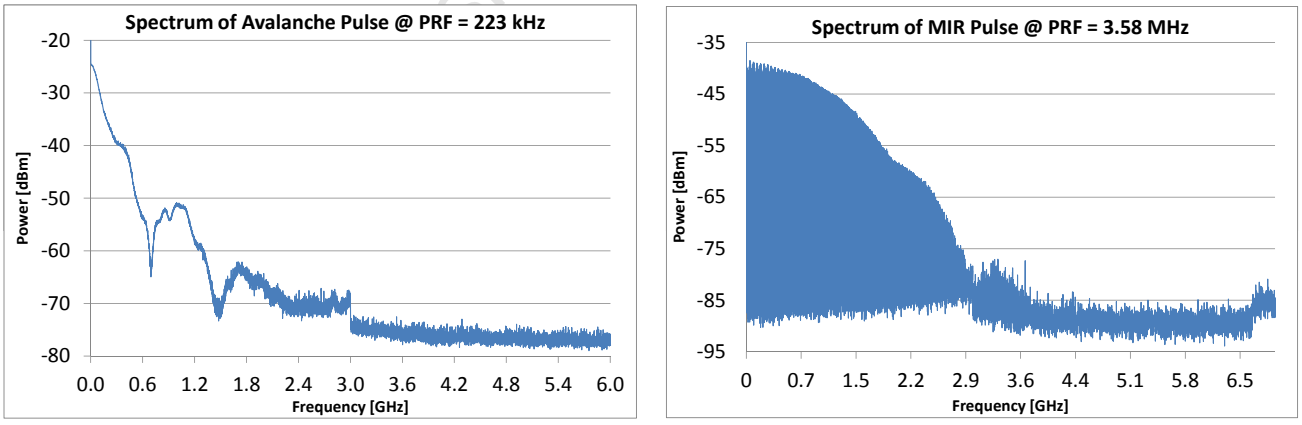

(a) Power spectrum of the avalanche pulses.

(b) Power Spectrum of the MIR pulses.

Figure 6.3: 6.3a) Shows the spectrum of the baseband avalanche pulses. There are measurable spectral components up to 2 GHz. The spectral lines cannot been seen due to the limited number discrete frequency points that can be displayed (max. 8192). The shape of the spectrum is also not Gaussian as expected, so there is concern that the pulse train is not coherent. 6.3b) Shows the spectrum of the baseband MIR pulses. Measurable spectral components up to 3 GHz are observed due to the faster rise-time of the MIR pulses. The spectral lines spaced at the PRF are also seen as well as a close to Gaussian shape.

Another filter was designed and fabricated in the same fashion as the previous filter to demonstrate a shaped output pulse. The centre frequency was chosen at 580 MHz with a bandwidth of 100 MHz, i.e. the same fractional bandwidth as the original 5.8 GHz filter. The response of this filter is illustrated in Figure 6.4.

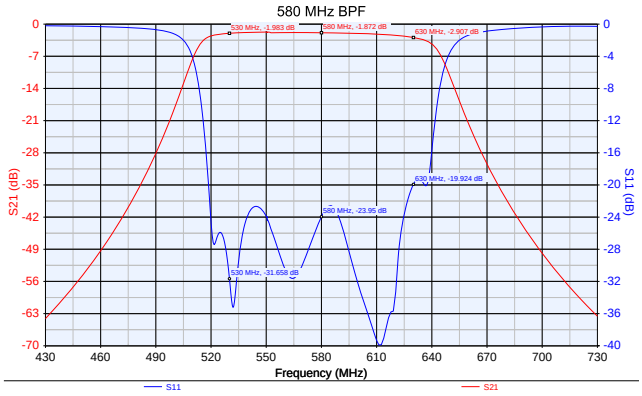

(a) S-parameters of the filter.

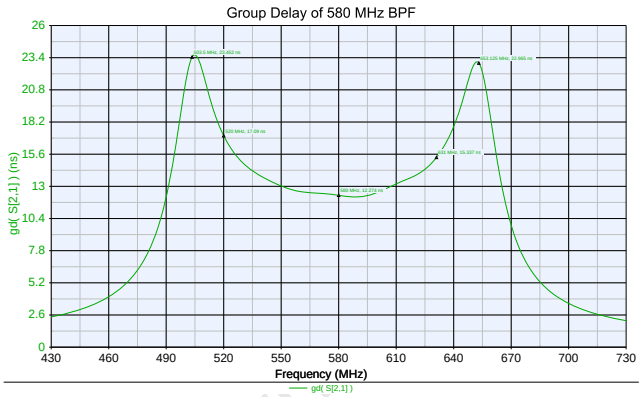

(b) Group delay of the filter.

Figure 6.4: 6.4a) Shows the S-parameters of the filter. The centre frequency is observed at 580 MHz and the 3 dB bandwidth is slightly over 100 MHz. Insertion loss is around 1.8 dB. 6.4b) Shows the group delay of the filter. It is observed that the delay at the 3dB points is nearly twice the delay over the rest of the pass-band.

Once the RF pulse shaper had been replaced, the output spectrum was measured with both the avalanche pulse driver and the MIR pulse driver. As shown in Figure 6.5, there was sufficient energy in this frequency band to produce a measurable output. A low pass filter with a cut-off frequency of 900 MHz was added to reject spectral components in higher frequency pass-bands caused by the periodic nature of the distributed circuit elements of the hairpin filter. The mean output power over the band was also measured to be -29 dBm or 1.26 uW.

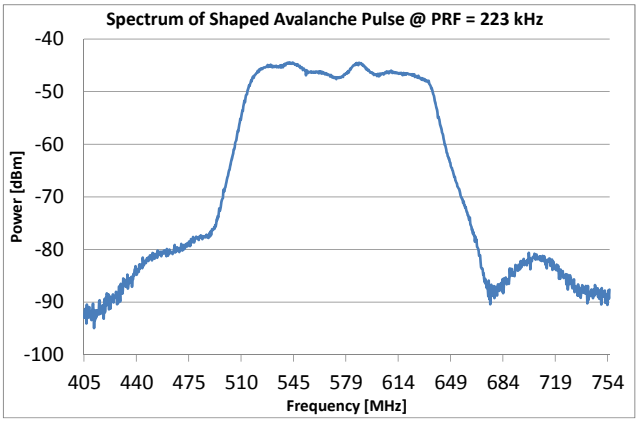

(a) Shaped avalanche pulse spectrum.

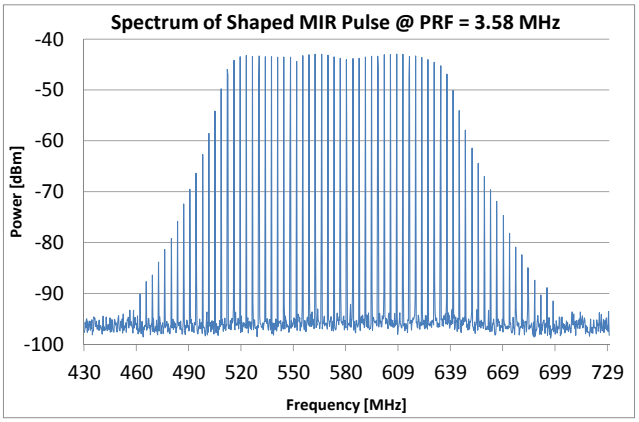

(b) Shaped MIR pulse spectrum.

Figure 6.5: 6.5a & 6.5b) Show the spectra of the shaped pulses from the avalanche and MIR circuits respectively. The total band power of the shaped output signal is very similar for both circuits. This can be explained by the fact that although the MIR has lower amplitude pulses, its higher PRF allows it to contribute the same amount of total energy over the band.

6.3 Time Domain Testing of RF Pulse Shaper

Equipment Used

- Sampling oscilloscope (Agilent 54833A)
- PRF generator + avalanche pulse driver + pulse shaper (580 MHz BPF & 900 MHz LPF)
- PRF generator + MIR pulse driver + pulse shaper (580 MHz BPF & 900 MHz LPF)

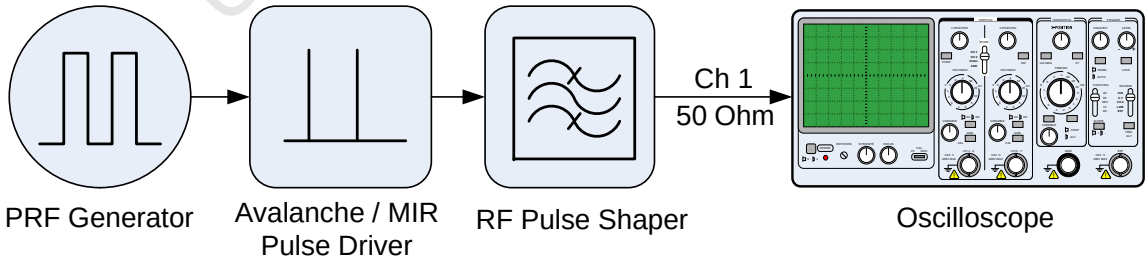

Figure 6.6: Diagram of the equipment setup for testing the output of the transmitter in the time domain.

6.3.1 Shaped Output Pulse Train

Method

The transmitter was connected directly to the input port of the sampling oscilloscope, as shown in Figure 6.6, for a time-domain analysis of the shaped output pulses. The input impedance of the scope was set to 50Ω. The 580 MHz RF pulse shaper, discussed in the previous section, was once again used in place of the 5.8 GHz shaper. The resulting time-domain waveforms are shown in Figure 6.7.

Results

It was seen that the pulse width had broadened from 1 ns at the input to around 12 ns at the output. This was expected because the 580 MHz filter only had a bandwidth of 100 MHz, while the input pulse had a bandwidth of 1 GHz. It was also noted that there were several delayed pulses trailing the main pulse. This can be explained by Figure 6.4b, in which it was shown that the frequencies at the 3 dB cut-off points of the filter took nearly twice as long to propagate, a phenomenon known as dispersion.

In order to remove the dispersive effects of the filter, a dispersion equaliser would have to be added to the design. Figure 6.8 shows a somewhat ideal dispersion equaliser, designed in *Genesys* using the *Equaliser Tool*. Unfortunately, due to time constraints, the design could not be fabricated but is nevertheless shown for illustrative purposes.

The peak power of the pulse, P_t, into 50Ω can also be calculated from the time domain voltage plots:

$$P_{t,av} = \frac{V_{peak}^2}{R} = \frac{(600 \times 10^{-3})^2}{50} = 7.2\,\text{mW} \tag{6.1}$$

$$P_{t,MIR} = \frac{(75 \times 10^{-3})^2}{50} = 112.5\,\mu\text{W} \tag{6.2}$$

6.3.2 Period Jitter

Method

The transmitter circuit is connected directly to the sampling oscilloscope with the input impedance set to 50Ω. The display persistence of the oscilloscope is then set to *infinite*. This means that every time the scope is triggered the resulting pulse is held on the screen, allowing one to observe if there is any period jitter. The results are shown in Figure 6.9 below.

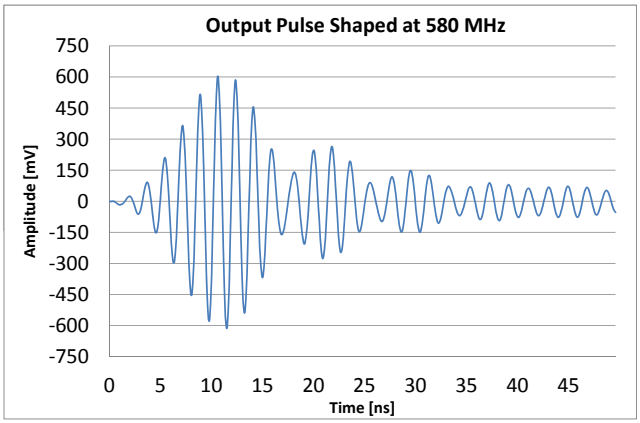

(a) shaped output pulse of avalanche pulse driver.

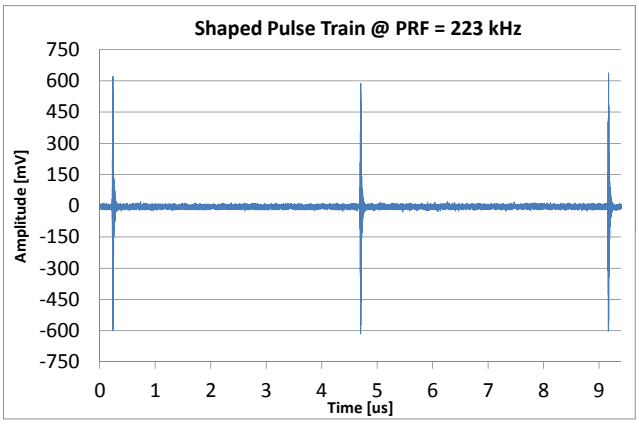

(b) Shaped avalanche pulse train.

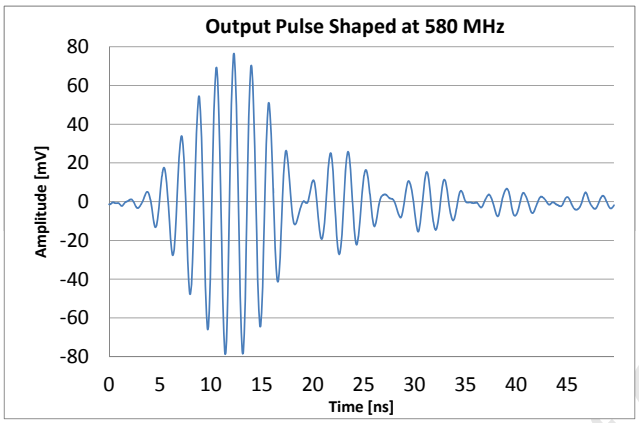

(c) Shaped output pulse of MIR.

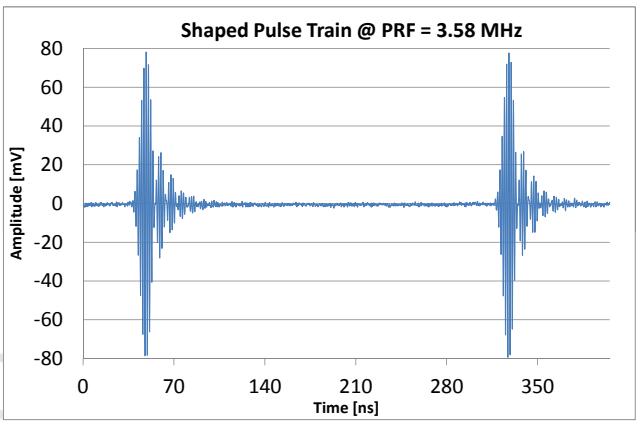

(d) Shaped output pulse train of MIR.

Figure 6.7: The time domain plot of 6.7a) a shaped pulse from the avalanche driver, the MIR ıe ampli- e pulses.

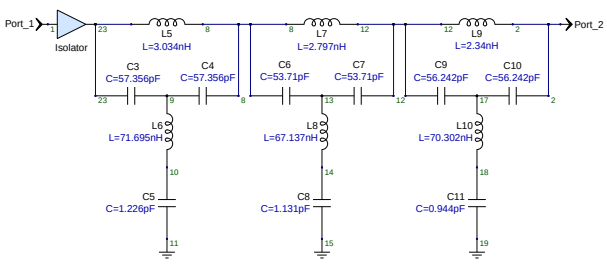

(a) schematic of ideal equaliser.

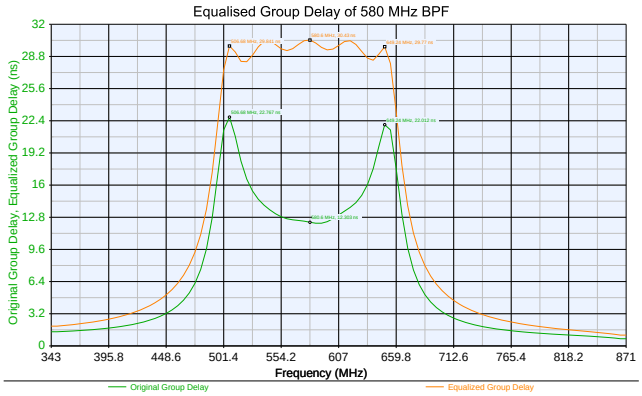

(b) Equalised group delay.

Figure 6.8: Shows how an equaliser is able to be synthesised to allow constant group delay and minimise dispersive effects. 6.8a) Shows a circuit for a suitable three-section equaliser. 6.8b) Shows the delay as a function of frequency both before and after equalisation.

Results

The avalanche pulse driver has a peak-to-peak jitter of about 300 ps while the MIR has a peak-to-peak jitter of less 100 ps. Although it is likely that the scope does introduce some jitter due to its own noise, one can clearly see that the avalanche circuit produces significantly more period jitter than the MIR circuit even though they both use the same crystal source in their PRF generator. This is likely the consequence of noise being fed-back into the collector bias of the avalanche circuit during the switching action, which results in inconsistencies in the point of breakdown between pulses.

This does not pose as much of a problem in this demonstration at 580 MHz because the period of the signal is at 1.72 ns and much greater than the period jitter. However, the period of the target carrier frequency of 5.8 GHz, is at 172 ps, which means that the phase of the avalanche pulse could vary by over 360 degrees from one pulse to the next. This will give rise to severe distortion in the output waveform and lead to a decrease in accuracy, since the cross-correlation sampling technique in the time stretching process requires strong stability. A better crystal source would likely allow for the MIR pulse driver to meet the required 50 ps specification.

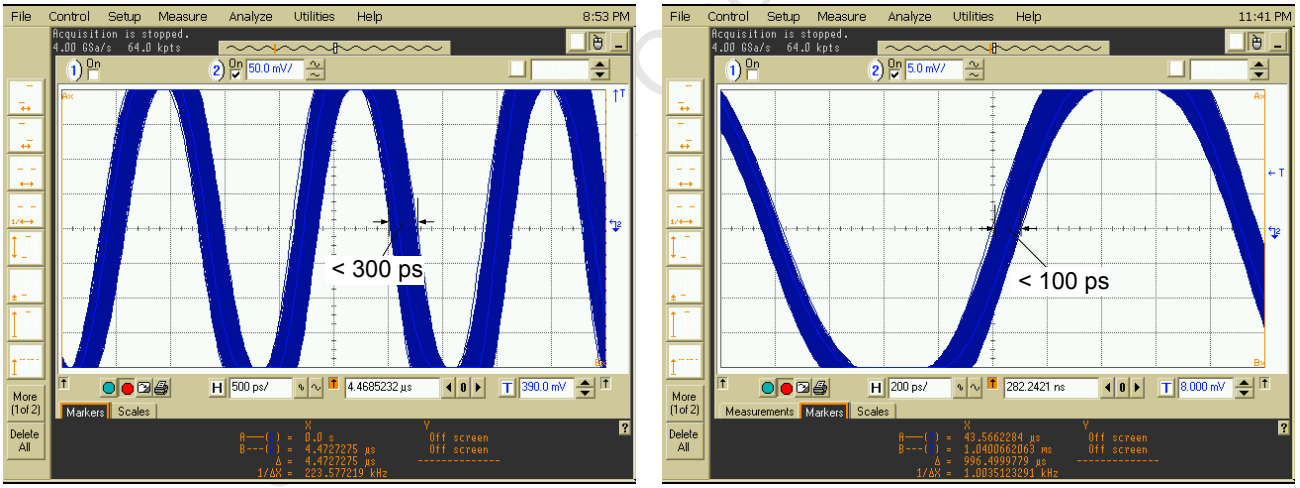

(a) Avalanche pulse driver period jitter.

(b) MIR pulse period jitter.

Figure 6.9: Screen shots of the pulse period jitter captured over a 5 s interval for the avalanche and MIR pulse drivers.

6.3.3 Time to Failure of Avalanche Transistor

Transistors operating in avalanche mode are prone to failure. The circuit was left to run continuously for 150 hours while the output pulses were monitored to determine if and when failure occurred. The primary reason for the failure of transistors operating in avalanche mode is overheating. If the PRF is too high then the heating caused by the avalanche current may exceed the maximum heat dissipation of the transistor.

It was noted that the circuit was able to run without failure for the entire duration of the test. Therefore, it can be assumed that the maximum heat dissipation of the package is not being exceeded. The effects of longer operation times are still unknown.

6.4 Testing of Time Stretched Output

Equipment Used

- Sampling oscilloscope (Agilent 54833A)
- All transceiver sub-systems

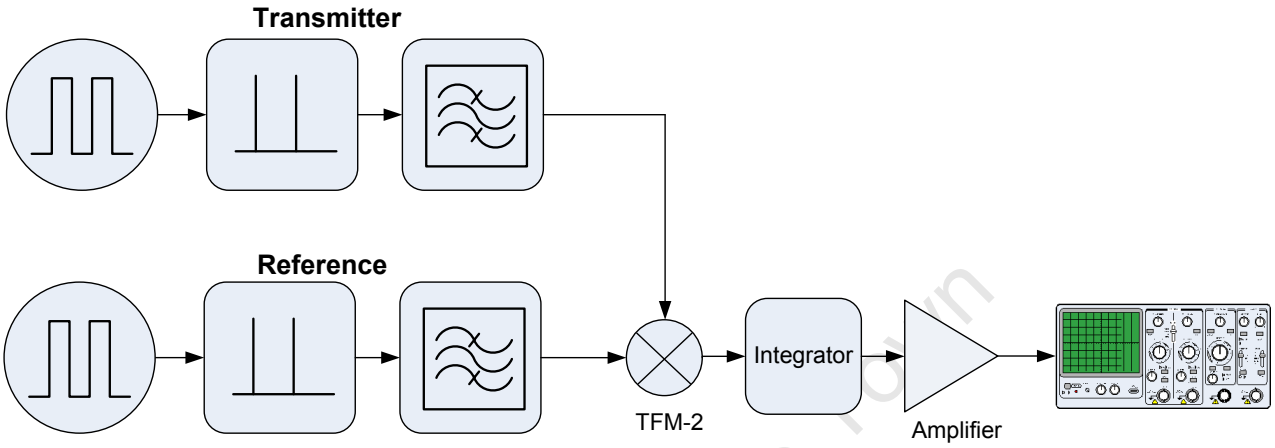

Figure 6.10: Diagram of the equipment setup for testing the time stretched output. The mixer that was used is the TFM-2 from Minicircuits.

Method

The sub-systems of the instrument are connected as shown in Figure 6.10 to demonstrate the time stretching. As mentioned in section 6.1 above, the predicted time stretching factors are 92820 for the MIR and 9965 for the avalanche pulse generator. The new PRF for the time stretched output should, according to calculation be at 38.57 Hz for the MIR and 22.46 Hz for the avalanche pulse. First, the real time waveform is captured on the oscilloscope. Next, the time stretched output is captured. The data is then compared with the theoretical results.

Results

It was observed on the oscilloscope, as shown in Figure 6.11, that the PRF of the avalanche transmit pulse train was 223 kHz but that the PRF of the time expanded pulse train was 22.65 Hz, which was slightly off from the predicted 22.46 Hz. On closer examination it was noticed that the TSF was not very stable and that the PRF in fact drifted between 20.8 Hz and 23.4 Hz over a relatively short period of time. This was confirmation that the low effective sampling rate and high period jitter, discussed in Sections 6.1 and 6.3.2, had a very negative effect on the TSF stability. At this point it was decided that the avalanche pulse driver method should be abandoned as it would not be able to meet the acceptance criteria for the instrument hardware.

The MIR, however, yielded much better results. It was observed on the oscilloscope, as shown in Figure 6.12, that the PRF of the transmit pulse train was 3.58 MHz and that the PRF of the time expanded pulse train was 38.57 Hz as predicted by the calculated TSF. The time expanded PRF was also very stable over the short term with no noticeable drift or instability.

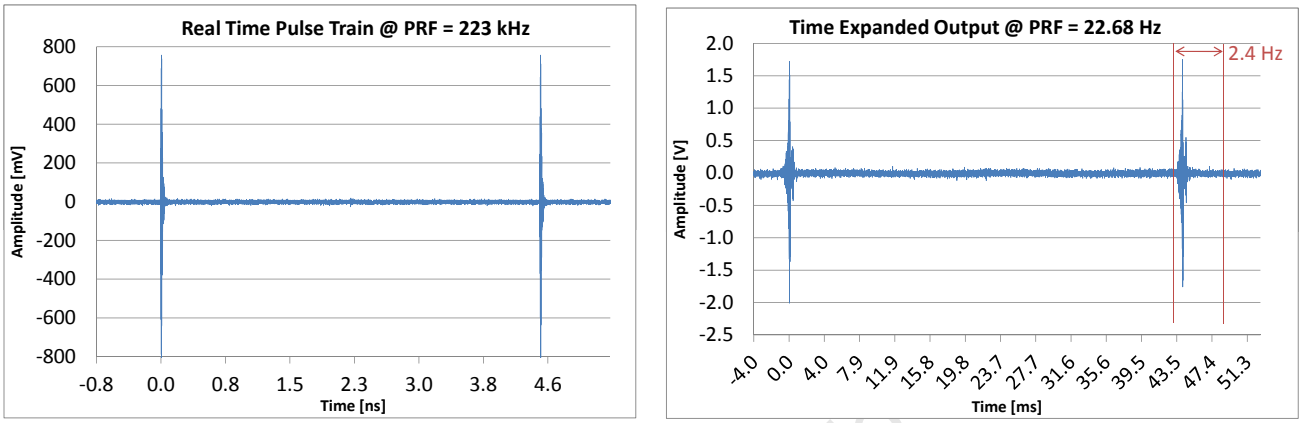

(a) Output pulse train of the transmit pulse generator. (b) Time stretched PRF output with TSF = 9665.

Figure 6.11: A comparison between 6.11a) the real-time pulse train and 6.11b) the time stretched pulse train generated with the avalanche pulse driver. The time expanded PRF showed a drift of approximately 2.4 Hz, which indicates TSF instability.

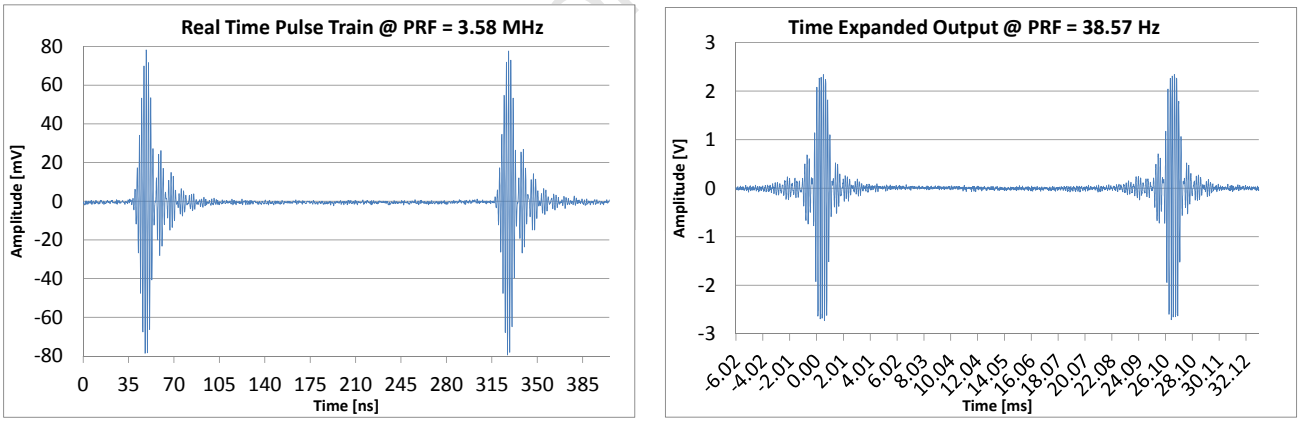

(a) Output pulse train of the transmit pulse generator. (b) Time stretched PRF output with TSF = 92820.

Figure 6.12: A comparison between 6.12a) the real-time pulse train and 6.12b) the time stretched pulse train generated with the MIR pulse driver.

6.5 Testing the Time Interval Measurement on an Echo Pulse

Equipment Used

- Sampling oscilloscope (Agilent 54833A)
- All transceiver sub-systems
- Splitter
- Various lengths of transmission line

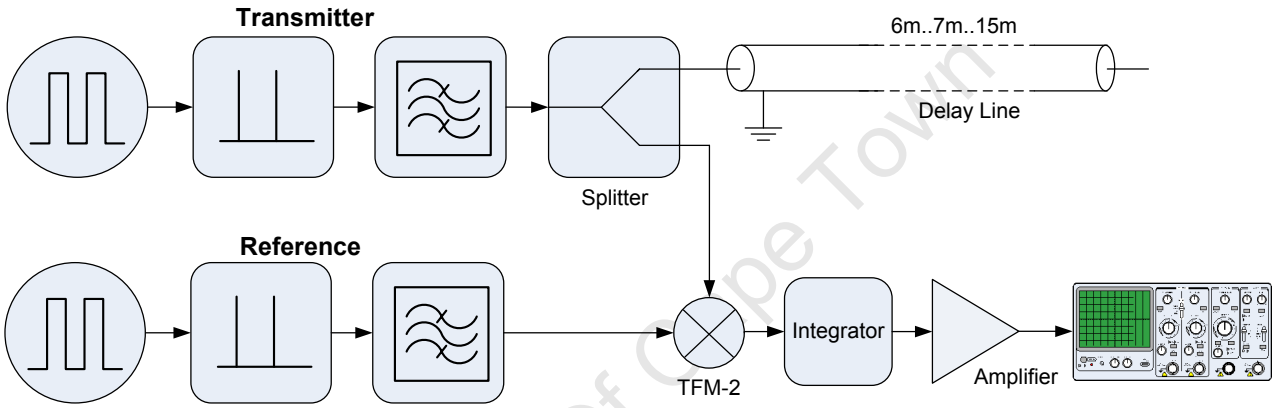

Figure 6.13: Diagram of the equipment setup for testing the time interval measurement between a transmitted pulse and a received echo using a time stretching technique.

Method

Unfortunately, there was no suitable antenna available at the time of the testing, since a lower frequency at 580 MHz was used. The branch-line coupler and 5.8 GHz horn antenna could, therefore, not be integrated into the final demonstration. The setup from Section 6.4 was modified to include a splitter and delay line, as shown in Figure 6.13, to simulate an echo pulse from a surface at different distances from the transmitter. One output port of the splitter is connected to the mixer and the other output is connected to one side of the transmission line. The other side of the transmission line is left open-circuit so that the portion of the signal that travels down will reflect back towards the mixer.

Known lengths of transmission line that represented delays of 6 m up to 15 m in steps of 1 m were cut. Distances at less than 6 m could not be effectively tested as these echos could not be differentiated from the long, 12 ns transmit pulse plus the dispersion from the filter, which was causing a large unwanted blind zone. The real-time pulse-echo time interval for each distance was measured on the scope and recorded as the

actual time interval. The time expanded interval was then measured and recorded as the *expanded time interval*. The expanded time interval was then divided by the TSF calculated in Section 6.1 and this result, recorded as the *calculated time interval*, was then compared to the actual measurement to calculate the *distance error*. Table 6.4 shows a summary of the results and Figure 6.14 shows an example of a measurement with an echo at a range of 10 m.

Results

The results for the MIR show that each measurement is within 1 cm of the actual value except for at 14 m. This is because there was an error in the initial measurement and it had to be re-done at a later stage. It is likely that the TSF had drifted to a slightly different value in the several hours between which the measurements occurred. Since the measured distances are within 2 cm of the actual value for a wide range of measurements, it can be assumed that the measurement process is accurate to the required 2 cm.

There is also sufficient time to capture up to 25 individual time-expanded distance measurements between the measurement update rate of 1 Hz. Averaging several measurements will result in a further improvement in the achievable accuracy.

Table 6.4: Table showing the results of the time interval measurements of distances 6 m to 15m using the MIR. TSF = 92820.

Dist. [m]	Actual TI [ns]	Exp. TI [ms]	Calc.TI [ns]	Dist. Error [cm]
6	41.2721	3.836405	41.33166	**-0.89**
7	47.2722	4.381865	47.2082	**0.96**
8	53.2721	4.945508	53.28063	**-0.13**
9	61.6345	5.727334	61.70367	**-1.04**
10	67.2725	6.236429	67.18842	**1.26**
11	73.0905	6.781891	73.06498	**0.38**
12	79.3616	7.372807	79.43123	**-1.04**
13	87.6263	8.12736	87.56044	**0.99**
14	93.0918	8.657547	93.27243	**-2.71**
15	99.3221	9.213373	99.26064	**0.92**

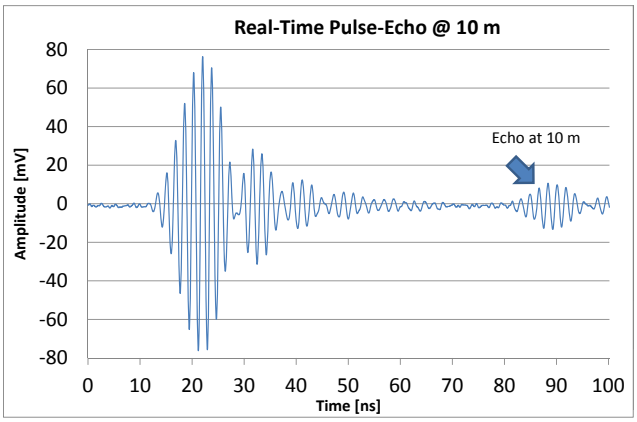

(a) Pulse and received echo signal at 10 m.

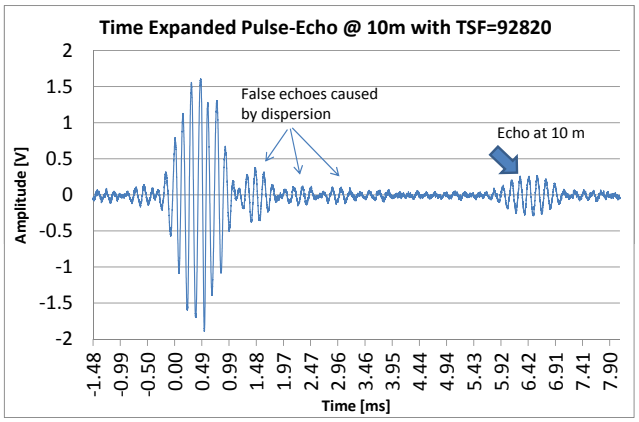

(b) Time expanded transmitted pulse and corresponding echo signal at 10 m, TSF=92820

Figure 6.14: An example of a time expanded output with an echo signal at a range of 10 m. This output range profile resembles that of an acoustic system and can can be processed using the same techniques as those on board an ultrasonic level measurement instrument.

6.6 Current Consumption

Table 6.15 shows a breakdown of the average current consumption of the active components in the radar transceiver. In most cases the supply current has been over-stated to ensure that the system is compatible with the existing power supply limitations. As can be seen, the total average current is at 2.8 mA. The remaining current is for use by the existing microprocessor and power supply hardware on the original ultrasonic instrument.

Figure 6.15: Table showing the current consumption of the various transceiver components.

Sub-system	Avg supply current
2 x Crystal PRF generator	2 x 400 uA
2 x MIR Pulse driver	2 x 850 uA
Amplifier (3-stage)	3 x 100 uA
Total	2.8 mA

6.7 Cost of Components

Table 6.5 shows a breakdown of the costs of the components. As can be seen, the design is very economical with the total cost coming in at about R450, which is below the user requirement of R1000. This does not include the costs of the RF antenna, which is likely to be a major contributor to the overall cost. It is likely that the component costs will come down further if ordered in larger quantities. These prices were quoted for the minimum order quantity.

Table 6.5: Table showing the cost of the components for the radar transceiver.

Component	Cost
Rogers substrate	R234
74HC04	R4
BRF91A	R7
Crystals	R12
TFM-2 Mixer	R120
BAT81	R2
2N5109	R42
Passives	R25
Total	R446

6.8 Specifications Achieved

Table 6.6 compares the desired instrument specifications, developed in Chapter 3, with the actual specifications obtained in the final demonstration hardware. As can be seen, the instrument was able to meet most of the desired specifications. As mentioned before, one of the shortcomings of the design was its inability to demonstrate at the operating frequency and bandwidth specifications due to the lack of spectral energy in the region of 5.8 GHz produced by the short baseband pulses. This meant that the constructed filter could not be used and had to be replaced by a filter at a lower centre frequency.

In addition to the instrument specifications it was also shown that the instrument could meet the following user requirements:

- Accuracy of 2 cm - It was demonstrated that the measured range was within 2 cm of the actual range over 10 different ranges. There is also sufficient time in the time expansion procedure to average several measurements to further improve the overall accuracy.
- Low cost - An audit of the component costs for the demonstration hardware showed that total cost was well below R1000, although the cost of the antenna was not included.
- Compliance with 4-20 mA loop power supply - An audit of the current consumption showed that the instrument required an average current of 2.8 mA and could indeed be loop powered.

Table 6.6: Consistency with the desired instrument specifications.

Specification	Desired Value	Obtained Value
Type	Pulsed radar	$\surd$
Operating frequency	5.8 GHz	580 MHz
SNR	$\geq 13\,\mathrm{dB}$	$\surd$, with integration gain
P_t	$\geq 165\mu W$	$113\mu W$
T_e	$\leq 1000\,K$	$\surd$
Rise-time	$\leq 800\,ps$	$\surd$
Bandwidth	$\geq 1\,GHz$	100 MHz
Pulse width	$\leq 1\,ns$	$\surd$
PRF Tx	3.58 MHz	$\surd$
PRF ref	3.58 MHz - 43.7 Hz	3.58 MHz - 38.57 Hz
PRF jitter	$\leq 43\,ps$	$\leq 100\,ps$ peak to peak
TSF	82000	92820
Antenna	Beam-limited	n/a
Antenna Beam-width	$\leq 20°$	n/a
Power supply	24 V @ < 4 mA	$\surd$

6.9 Summary

Final testing of the complete transceiver revealed some shortcomings of the avalanche pulse driver. Firstly, it was seen that the low PRF resulted in a poor effective sampling rate and TSF, which meant that the time stretching technique could not be applied satisfactorily. It was observed that the resulting TSF was unstable and varied considerably over time and from pulse to pulse.

Secondly, it was noticed that there was a much higher period jitter associated with the avalanche pulse driver when compared to the MIR pulse driver, both of which utilised the same crystal PRF generator circuit. This high period jitter combined with the low effective sample rate also resulted in severe distortion of the time expanded output signal.

It was ultimately decided that the MIR pulse driver would be the best choice to use in the final design. The high PRF resulted in a very favourable TSF and a very high effective sampling rate. In addition, the low period jitter resulted in a very stable TSF and a reliable time expanded output, although for a 5.8 GHz carrier this would have to be slightly improved with a better crystal source.

Final integration of the sub-systems also revealed that using a filter to separate the desired frequency components at 5.8 GHz was far too inefficient to produce any kind of measurable result. It was seen that the frequency spectrum of the baseband pulses lacked sufficient energy at frequencies higher than 3 GHz. Insufficient rise-times of the pulses, pulse shape choice and dispersion were highlighted as the likely reasons for the waveform to have failed to exhibit sufficient power at 5.8 GHz.

It was, however, shown that the time expansion could indeed be demonstrated at a

lower frequency of 580 MHz and bandwidth of 100 MHz. Tests were performed with echo pulses from 10 different ranges using a delay line. The results showed that the range error in all of the measurements was within 1 cm of the actual range, which means that the overall accuracy of the technique is within the required 2 cm.

Time domain analysis of the RF pulses also revealed the presence of dispersion which caused unwanted signals close to the transmitted pulse. These signals were also transferred to the output in the time expansion process which resulted in an increased blind-zone in which close targets could not be detected. A dispersion equaliser was recommended to correct the group delay of the filter to minimise the dispersion.

Ultimately it was shown that the demonstration hardware showed good compliance to the desired specifications as well as the power and cost user requirements. Although not all the specifications were met, a good platform for further development has been created. Some recommendations for future design revisions will be discussed in the next chapter.

Chapter 7

Conclusions and Recommendations for Future Work

This chapter highlights the important findings presented in this dissertation. Recommendations are then given for possible future work.

7.1 Conclusions

7.1.1 Instrument Specifications

- A pulsed radar should be used in the transceiver because it is the most compatible with the pulsed TOF technique utilised in the existing ultrasonic instrument. In addition, the pulsed radar has the advantage of lower power operation, a lower component cost and less prone to interference between the transmitter and receiver circuitry.
- The operating temperature and pressure ranges can be achieved by using radar because electromagnetic wave propagation velocity is barely effected by changes in these parameters. A maximum error of only 0.134% is expected, which can be calibrated into the distance measurement.
- An operating frequency of 5.8 GHz would be used because it complies with the industry regulations and will be easier and cheaper to implement in first generation hardware than 24 GHz. It was, however, noted that there are many technical advantages of using an operating frequency of 24 GHz.
- The timing hardware on the existing acoustic sensor is not compatible with the requirements for TIM on radar signals. A Vernier time expansion technique should be used to expand the output time domain profile to a suitable scale so that the existing ultrasonic instrument can be used to calculate the level measurement as per the requirement. A time stretching factor of at least 82000 is required to

expand a frequency of 5.8 GHz to a frequency in the same order as an acoustic signal.

- To achieve the accuracy requirements the instrument should be designed according to the specifications in Table 3.4.

7.1.2 Demonstration Hardware

- The architecture of the instrument should follow the design in Figure 4.1, which requires two pulse train generators consisting of a PRF generator; a pulse driver; an RF frequency shaper; a frequency mixer along with an integrator and amplifier.

- Although silicon square-wave oscillators were useful in the prototyping stages, a crystal, CMOS based, square-wave oscillator should be used in the PRF generator because crystals present the best overall stability. Better, more expensive crystals can ultimately be used to further improve the stability of the PRF generator output.

- The MIR and the avalanche transistor were seen as the two best candidates for the instruments pulse driver. Both circuits were able to produce pulses with a pulse-width of 1 ns and fast rise-times less than 800 ps. The MIR had the advantage of a high PRF but the disadvantage of a low output pulse amplitude. The avalanche transistor had the advantage of a high pulse amplitude but a low PRF. While both circuits were constructed, it was decided that the focus should be put on the avalanche pulse driver to try and improve its PRF as previous work on the MIR had already been documented. Unfortunately these attempts were unsuccessful, which resulted in the avalanche method failing to meet the acceptance criteria.

- The MIR pulse driver should be used because the avalanche pulse driver was unable to meet the PRF specifications and exhibited increased period jitter together which resulted in an unsatisfactory time expansion. The MIR, however, was able to meet all of the pulse specifications. A PRF of 3.58 MHz was achieved and resulted in a TSF of 92820 when combined with a reference pulse train. An effective sample rate of 332 GSa/s was also achieved which meets the Nquist criteria for 5.8 GHz and above.

- Using a filter to separate the desired frequency components at 5.8 GHz was far too inefficient to produce any kind of measurable result. It was seen that the frequency spectrum of the baseband pulses lacked sufficient energy at frequencies higher than 3 GHz. Time domain analysis of the RF pulses at a lower frequency of 580 MHz also revealed the presence of dispersion caused by the non-constant

group delay of the bandpass filter, especially around the 3 dB points. Either the rise-time of the pulses has to be improved, to increase higher frequency spectral energy, along with the implementation of a dispersion equaliser, to correct the group delay, or a different method of generating the RF carrier should be considered.

- The branch-line coupler could not be integrated into the final system due to the fact that the system could not be tested at the designed operating frequency.
- The mixer, integrator and amplifier performed well as predicted.
- Testing performed on the complete system with a carrier frequency of 580 MHz and 100 MHz of bandwidth showed that an accuracy of 2 cm could be achieved along with sufficient time to perform averaging to further improve the accuracy if necessary.
- Average current consumption was 2.8 mA, which was below the user requirement of 4 mA. The instrument will be able to meet the requirement to operate off a 4-20 mA current loop.
- The cost of the components was kept very low. The total cost excluding an antenna was well below the required R1000.
- The design is considered very compact but it exceeded the size requirements due to its modular design. A new, single board layout should be done to reduce the circuit size.

7.2 Recommendations for Future Work

- A better quality crystal should be used to improve the trigger period jitter.
- A circuit to lock the PRF generators to a fixed difference frequency should be implemented. This will ensure that any medium to long term drift between the two output frequencies can be corrected so that the TSF remains stable. One technique, used by McEwan [58], is illustrated in Figure 7.1. The system consists of two crystal controlled square-wave generators. The Tx generator is a stand-alone free-running XO (crystal oscillator) and the Ref Generator is a VCXO (voltage controlled crystal oscillator). The system maintains the TSF by comparing the period of the time stretched output, Δ, with that of a preset reference period, Δ_{ref}, which is set to the desired TSF. The controller generates a voltage proportional to the error between the measured time stretched period and the reference period and adjusts the voltage to the VCXO to compensate for any change. A constant time stretched period at Δ_{ref} is , therefore, maintained. The advantage

of this setup is that there is no interference between the two oscillators as they are completely separated.

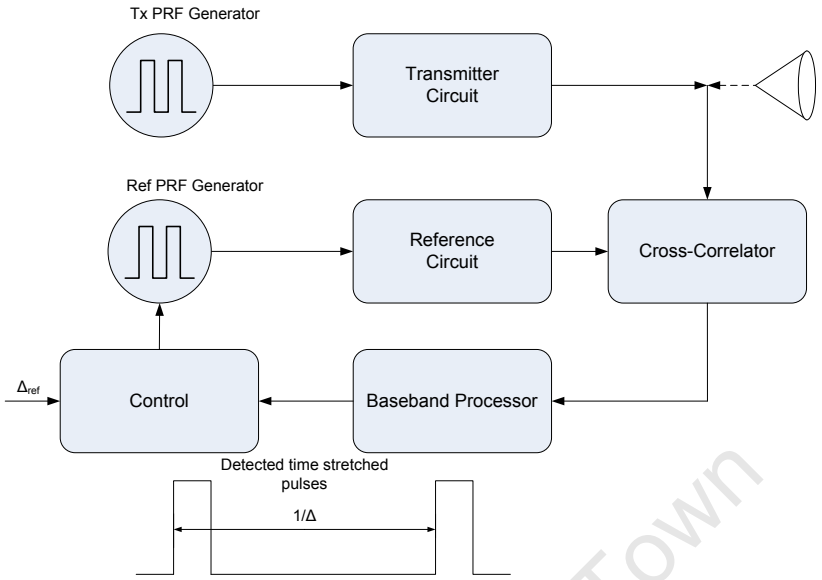

Figure 7.1: Block diagram of a dual clock locking system. The baseband processor detects the time stretched transmitted pulses. The period between the time stretched pulses is then compared to the reference period and the frequency of the VCXO is adjusted to compensate for any drift between the two oscillators.

- The technique of generating the RF pulse should be reconsidered. It is recommended that an active up-conversion stage is added since it is unlikely that sufficient energy can be filtered from wideband baseband pulses, especially if one wants to go to 24 GHz in future designs. McEwan [59] and Fehrenbach [22] show circuits for the implementation of a low-Q oscillator. The oscillator is also powered completely by the driving pulse from the pulse generator on its input terminal. Due to the low Q-factor the oscillations start and die very quickly and the envelope of RF output pulse resembles that of the driving pulse.

- Integration of the transceiver with the existing ultrasonic platform should be performed.

- A suitable wide-band antenna should be designed according to the specifications in Table 3.4.

Bibliography

[1] *Dispersion and UWB antennas*, may 2004. doi: 10.1109/UWBST.2004.1320956.

[2] ACAM-USA. Tdc-gpx - ultra-high performance 8 channel time-to-digital converter. TDC-GPX Datasheet.

[3] Johannes Auret and Willem Herholdt. Applied intrinsic safty part 1 and part 2. *Elektron*, 10:22–24 and 13–15, September and November 2005.

[4] BAPI. Understanding 4-20 ma current loops. Application Note, 2006. http://www.bapihvac.com/CatalogPDFs/I App Notes/Current Loop Configs.pdf (Last Accessed August 2010).

[5] R G Baron. The vernier time-measuring technique. *Proceedings of the IRE*, pp: 21–30, 1957.

[6] H Bosma. On stripline y-circulation at uhf. *IEEE Transactions on Microwave Theory and Techniques*, MTT-12:61–72, January 1964.

[7] Neil Chadderton. The ztx415 avalanche mode transistor: An introduction to characteristics, performance and applications. Technical report, ZETEX, January 1996. Application Note 8.

[8] A. Chang. A micropower uwb transmitter. Master's thesis, University of Cape Town, 2006.

[9] Dudley B. Chelton, Edward J. Walsh, and John L. MacArthur. Pulse compression and sea level tracking in satellite altimetry. *Journal of Atmospheric and Oceanic Technology*, 6:407–438, 1989.

[10] G D Cormack and A P Sabharwal. Picosecond pulse generator using delay lines. *IEEE Transactions on Instrumentation and Measurement*, 42:947–948, 1993.

[11] Dataforth Corporation. 4-20ma transmitters. Application Note AN104, . http://www.dataforth.com/catalog/pdf/an104.pdf (Last Accessed August 2010).

[12] Rogers Corporation. High frequnecy laminates - product selection guide, .

[13] Datel. 4-20ma current loop primer. Datel DMS Application Note 20, 2005. http://www.datelmeters.com/data/meters/dms-an20.pdf (Last Accessed August 2010).

[14] Datel. 4-20ma current loop configurations and faq. Datel DMS Application Note 21, 2005. http://www.datelmeters.com/data/meters/dms-an21.pdf (Last Accessed August 2010).

[15] Walter Day. Dielectric resonators as microstrip-circuit elements. *IEEE Transactions on Microwave Theory and Techniques*, 18:1175–1176, 1970.

[16] Analog Devices. Loop-powered 4-20ma sensor transmitter. AD693 Datasheet.

[17] Peter Devine. *Radar Level Measurement - The Users guide*. Vega Controls Ltd., 2000.

[18] Charles Elachi. *Introduction to the Physics and Techniques of Remote Sensing*. John Wiley & Sons, 1987.

[19] Charles Elachi. *Spacebourne Radar Remote Sensing: Applications and Techniques*. IEEE Press, 1987.

[20] B L Elphick. A method of applying an avalanche transistor generated 70 ns gating pulse to a focused photomultiplier. *Journal of Scientific Instruments*, 2:953–955, 1969.

[21] C. Fay and R. Comstock. Operation of the ferrite junction circulator. *IEEE Transactions on Microwave Theory and Techniques*, MTT-13:15–27, January 1965.

[22] Josef Fehrenbach. Microwave pulse generator. US Patent 6,380,815, April 2002.

[23] E S Fulkerson, D C Norman, and R Booth. Driving pocket cells using avalanche transistor pulsers. Technical report, Lawrence Livremore National Laboratory University of California, 1996.

[24] Larry W. Fullerton. Time domain radio transmission system. US Patent 4,979,186, December 1990.

[25] Ellen Fussel. A level playing field - radar scores points in industry. Instrument Society of America Website: http://www.isa.org/link/Level2003 (Last Accessed August 2010), October 2003.

[26] M Gerding, T Musch, and B Schiek. A noval approach for a high-precision multitarget-level measurement system based on time domain reflectometry. *IEEE Transactions on Microwave Theory and Techniques*, 54:2768–2773, 2006.

[27] M. Ghavami, L. B. Michael, and R. Kohno. *Ultra Wideband Signals and Systems in Communication Engineering*. John Wiley & Sons, Ltd, 2004.

[28] ARC Advisory Group. Radar level device worldwide outlook - five year market analysis and technology forecast through 2007. Technical report, ARC, 2003.

[29] P Guillon, B Byzery, and M Chaubet. Coupling parameters between a dielectric resonator and a microstrip line. *IEEE Transactions on Microwave Theory and Techniques*, 33:222–226, 1985.

[30] D J Hamilton, J F Gibbons, and W Shockley. Physical principles of avalanche transistor pulse circuits. *Proceedings of the IRE*, 47:1102–1108, 1959.

[31] Jeongwoo Han and Cam Nguyen. A new ultra-wideband, ultra-short monocylcle pulse generator with reduced ringing. *IEEE Microwave and Wireless Component Letters*, 12:206–208, June 2002.

[32] J P Hansen and W A Schmidt. A fast risetime avalanche transistor pulse generator for driving injection lasers. *Proceedings of the IEEE*, 55:216–217, 1966.

[33] M J Heim. Pulsed radar for mm-precision in tank gauging. *Electricity + Control*, October:72 – 74, October 2005.

[34] W M Henebry. Avalanche transistor circuits. *Review of Scientific Instruments*, 32: 1198–1203, 1961.

[35] W B Herden. Application of avalanche transistors to circuits with a long mean time to failure. *IEEE Transactions on Instrumentation and Measurement*, 25: 152–160, 1976.

[36] *Pulse and Waveform Generation with Step Recovery Diodes*. Hewlett Packard. Application Note 918.

[37] Gerhard A. Hofbauer. Advanced system techniques for precision fmcw radar systems.

[38] Paul Horowitz and Winfield Hill. *the Art of Electronics 2nd Ed.* Cambridge University Press, 1995 (low price ed.).

[39] Nathan Ida. *Engineering Electromagnetics*. Springer, 2004.

[40] National Instruments. Fundamentals, system design, and setup for the 4 to 20 ma current loop. Tutorial, April 2008. ftp://ftp.ni.com/pub/devzone/pdf/tut 6940.pdf (Last Accessed August 2010).

[41] ITU-R. Framework for the introduction of devices using ultra-wideband technology. Recommedation ITU-R SM.1756, 2006.

[42] Cam Nguyen Jeong Soo Lee. Novel low-cost ultra-wideband, ultra-short-pulse transmitter with mesfet impulse-shaping circuitry for reduced distortion and improved pulse repetition rate. *IEEE Microwave and Wireless Component Letters*, 5: 208–210, May 2001.

[43] Jozef Kalisz. Review of methods for time interval measurements with picosecond resolution. *Metrologia*, 41:17–32, 2004.

[44] Dr R S Khandpur. *Printed Circuit Boards: Design, Fabrication, Assembly and Testing*. McGraw-Hill, 2006.

[45] Ari Kilpela and Juha Kostamovaara. A laser pulser for tof laser radar. Taken from the Electrical Engineering Website of the University of Oulu, Finland http:www.ee.oulu.fi/ arik/pulse.htm.

[46] David Kirkby. *A Picosecond Optoelectronic Cross Correlator using a Gain Modulated Avalanche Photodiode for Measuring the Impulse Response of Tissue*. PhD thesis, UCL, April 1999.

[47] Yasutoshi Komatsu and Yoshikazu Murakami. Coupling coefficient between microstrip line and dielectric resonator. *IEEE Transactions on Microwave Theory and Techniques*, 31:34–40, 1983.

[48] Chris Lamakul. Advancements in radar level. Instrument Society of America Website: http://www.isa.org/Content/ContentGroups/InTech2/Features/2003/July22/Advancementsin (Last accessed August 2010), July 2003.

[49] J S Lee, C Nguyen, and T Scullion. New uniplanar subnanosecond monocycle pulse generator and transformer for time-domain micorwave applications. *IEEE Transactions on Microwave Theory and Techniques*, 49:1126–1129, 2001.

[50] Kyungwoo Lee, Kunsup Kwon, and Sangseol Lee. Design of a multisection impedance-transforming branch-line hybrid using a genetic algorithm. *Microwave and Optical Technology Letters*, 22:436–439, 1999.

[51] Thomas H. Lee. *Planar Microwave Engineering*. Cambridge University Press, 2004.

[52] R Levy. Directinal couplers. *New York : Academic*, 1:115–209, 1966.

[53] R Levy and L. Lind. Synthesis of symmetrical brach-guide directional couplers. *IEEE Transactions on Microwave Theory and Techniques*, MTT-16:80–89, 1968.

[54] Jin Liu, Xianzhong Chen, and Zheng Zhang. A noval algorithm in the fmcw microwave liquid level measuring sytem. *Institute of Physics Publishing - Measurement Science and Technology*, 17:135–138, December 2005.

[55] A Lundy, J R Parker, J S Lunsford, and A D Martin. Avalanche transistor pulser for fast-gated operation of microchannel plate image-intensifiers. *IEEE Transactions on Nuclear Science*, NS-25:591–597, 1978.

[56] J Mankowski and M Kristiansen. A review of short pulse generator technology. *IEEE Transactions on Plasma Science*, 28:102–108, 2000.

[57] Thomas E. McEwan. Short pulse microwave transceiver. US Patent 6,191,724, February 2001.

[58] Thomas E. McEwan. Self locking dual frequency clock system. US Patent 6,373,428, April 2002.

[59] Thomas E. McEwan. Loop powered radar rangefinder. US Patent 6,535,161, March 2003.

[60] Y Mizushima and Y Okamoto. Properties of avalanche injection and its application to fast pulse generation and switching. *IEEE Transactions on Electron Devices*, ED-14:146–157, 1967.

[61] P V A Mohan and B S Sonde. Sinusoidal oscillators using avalanche transistors. *Proceedings of the IEEE*, 64:565–566, 1976.

[62] Norman Morrison. *Introduction to Fourier Analysis*. Wiley-Interscience, 1994.

[63] Juergen Motzer. A puls radar gauge for level measurement and process control. *Microwave Syposium Digest*, 3:1563–1566, 2000.

[64] Mashahiro Muraguchi, Takeshi Yukitake, and Yoshiyuki Naito. Optimum design of 3-db branch-line couplers using microstrip lines. *IEEE Transactions on Microwave Theory and Techniques*, MTT-31:674–678, 1983.

[65] T Musch. A review of radar tdr techniques for measuring level. *Electricity + Control*, October:75 – 76, 2005.

[66] L L Nagy. High frequency, short pulse, band limited radar pulse generator for ultrashort range radar systems. US Patent 3,940,696, February 1976.

[67] S Panton and B Cherek. Microwave pulse generator and pulse-echo ranging system. US Patent 6,597,309, July 2003.

[68] Abelardo Podcameni and Luiz Fernando Martins Conrado. Design of microwave oscillators and filters using transmission-mode dielectric resonators coupled to microstrip lines. *IEEE Transactions on Microwave Theory and Techniques*, 33: 1329–1332, 1985.

[69] David M Pozar. *Microwave and RF Design of Wireless Systems*. John Wiley & Sons, 2001.

[70] Pavel Protiva, Jan Mrkvica, and Jan Machac. Universal generator of ultra-wideband pulses. *Radioengineering*, 17:74–78, 2008.

[71] Gareth Rees. *Physical Principals of Remote Sensing*. Cambridge University Press, 2001.

[72] Pawel Rulikowski and John Barret. Truly balanced step recovery diode pulse generator with single power supply. In *IEEE Radio and Wireless Conference*, pages 347–350, 2004.

[73] SiversIMA. Fmcw transceiver. RS3400S/00 Datasheet. http://www.siversima.com.

[74] Merrill I. Skolnik. *Introduction to Radar Systems, 3rd Edition*. Irwin/McGraw-Hill, 2001.

[75] P Spirito. Static and dynamic behaviour of transistors in the avalanche region. *IEEE Journal of Solid State Circuits*, 6:83–87, 1971.

[76] P Spirito and G F Vitale. An analysis of the dynamic behaviour of switching circuits using avalanche transistors. *IEEE Journal of Solid State Circuits*, 7:315–320, 1972.

[77] Enrico M. Staderini. *Everything you always wanted to know about UWB radar...: a practical introduction to the ultra wideband technology*. Tor Vergata University of Rome, 2001.

[78] George W. Stimson. *Introduction to Airborne Radar, 2nd Edition*. SciTech Publishing, 1998.

[79] Ferrel G. Stremler. *Introduction to Communication Systems 3rd Ed.* Addison Wesley Longman, 1992.

[80] James D. Talyor. *Introduction to Ultra-WideBand Radar Systems*. CRC Press, 1995.

[81] James D. Taylor. *Ultra-Wideband Radar Technology*. CRC Press, 2001.

[82] James D. Taylor and Thomas E. McEwan. *The Micropower Impulse Radar*, chapter 6, pages 155–164. CRC Press, 2001.

[83] Linear Technology. Micropower dc/dc converter adjustable and fixed 5v, 12v, . LT1073 Datasheet.

[84] Linear Technology. Micropower, 4khz to 4mhz resistor set oscillator in sot-23, . LTC6907 Datasheet.

[85] Jonathan Ward. Design and implementation of a non-contact level measurement instrument. Master's thesis, University of Cape Town, 2010.

[86] Y. Wu and F Rosenbaum. Wide-band operation of microstrip. *IEEE Transactions on Microwave Theory and Techniques*, MTT-22:849–856, October 1974.

[87] Alfred R. Zieger, David W. Hancock, George S. Hayne, and Craig Purdy. Nasa radar altimeter for the topex/poseidon project. *Proceedings of the IEEE*, 79:810–825, 1991.

Appendix A

Matlab Code

```
%*******************************************************************************
%This section shows the matlab code used to generate the figures shown
%in section titled "Time and Frequency Domain Analysis of Pulse Radar
%Signals"
%*******************************************************************************

y1=0;
y2=0;
t = -2e-9:1e-11:2e-9;       %define time axis
sig = 0.5e-9;               %sigma (std.dev)
y1=exp(-(t.^2)/(2*sig^2));  %formula for Gaussian pulse
plot(t,y1,'blue')           % plot Gaussian pulse

figure                      %new figure
sig=0.5e-9;                 %define sigma
C=((sqrt(2*pi))*sig);       %Pieces of the formula for FT of gaussian
A=(sig^2);

w=-((2*pi)*5e9):((2*pi)*1e6):((2*pi)*5e9);
f=-5e9:1e6:5e9;                                 %define freq axes
Fw = C*exp(-((A*(w.^2))/2));                    %formula for FT of Gaussian
plot(f,Fw);                                     %plot FT of Gaussian

figure
Ts=279.32961e-9;                %define PRI
n=5;                            %number of pulses
T=-n*Ts:Ts:n*Ts;
Ys=ones(1,((2*n)+1));
stem(T,Ys);

figure                          %plot diracs
Ws=((2*pi)/Ts);
W=-n*Ws:Ws:n*Ws;
Os=Ws*ones(1,((2*n)+1));
stem(W,Os);

figure
N=500;
SW=-N*Ws:Ws:N*Ws;
Freq=SW/(2*pi);
SFw = Ws*C*exp(-((A*(SW.^2))/2));   %diracs weigted by FT of a Gaussian
stem(Freq,SFw);

figure
T=2.5e-9;
Sfw = (1/T)*(abs(Fw)).^2;       %formula for PSD
plot(f,Sfw);                    %Plot PSD




%*******************************************************************************
%                                   END
%*******************************************************************************
```

```
%*******************************************************************************
%This section shows the matlab code used to generate the figures shown
%in section titled "A Vernier Time Stretching Approach for Time
%Interval Measurement". The first block of code (Part A) uses
%only the mathematical formulae shown in section "A Vernier Time
%Stretching Approach for Time Interval Measurement",while the second
%block of code (Part B) uses the standard multiplication and integration
%function of Matlab. Both blocks of code give the same result which
%verifies that the mathematical formula for the time stretched output
%waveform is correct.
%*******************************************************************************
%*******************************************************************************
%                                  PART A
%*******************************************************************************

y1=0;
y2=0;
t = -15000e-9:1e-11:15000e-9;    %define time axis
sig = 0.5e-9;                    %sigma (std.dev)
T1=279.32961e-9;                 %PRI of first pulse train
T2=279.43302e-9;                 %PRI of second pulse train

for n=-60:1:60;
    y1 = y1 + exp(-(t-n*T1).^2/(2*sig^2));   %build up pulse train
    y2 = y2 + exp(-(t-n*T2).^2/(2*sig^2));
end

i=1;
C=sqrt(pi*(sig^2));
Diff=((T2-T1)^2);
Denom=((2*sig)^2);
for N=-60:1:60;
    vout(i)=C*exp(-((N^2)*Diff)/Denom);  %build up integral
    T(i)=((N*T1)+(N*(T2-T1)/2));         %time axis for intral
    i=i+1;
end
%vout=(vout/max(vout));  %normalise the integral plot (optional)

figure
plot(t,y1,'red')
hold on
plot(t,y2,'blue')

figure

YY=y1.*y2;
plot(t,YY,'blue');       %plot the integral and multiplication on
                         %same axis
hold on
plot(T,vout,'red')
Fac=(T1/(T2-T1)) %output the time stretching factor

%*******************************************************************************
%                              END OF PART A
%*******************************************************************************
```

```
%*******************************************************************************
%                                  PART B
%*******************************************************************************

y1=0;
y2=0;
t = -15000e-9:1e-11:15000e-9;    %define time axis
sig = 0.5e-9;                    %sigma (std.dev)
T1=279.32961e-9;                 %PRI of first pulse train
T2=279.43302e-9;                 %PRI of second pulse train

for n=-40:1:40;

    y1 = y1 + exp(-(t-n*T1).^2/(2*sig^2));   %build up pulse train
    y2 = y2 + exp(-(t-n*T2).^2/(2*sig^2));

end

YY=y1.*y2;

figure
plot(t,YY)

j=1;                      %manual integration
for N=-40:1:40;

    x1 = (1500001-13970) + (N*27940);  %find the integral under each spike
    x2 = (1500001+13970) + (N*27940);
    cx = YY(x1:x2);
    %figure
    %plot(cx)
    I(j) = intdump(cx,27941);
    T(j)=((N*T1)+(N*(T2-T1)/2));
    j=j+1;
end
I=I/max(I);
figure

plot(t,y1,'red')
hold on
plot(t,y2,'blue')

figure

plot(t,YY,'blue');  %plot the integral and multiplication on
                    %same axis
hold on
plot(T,I,'red')

Fac=(T1/(T2-T1))    %shows the stretching factor

%*******************************************************************************
%                                END OF PART B
%*******************************************************************************
```

```
%*******************************************************************************
%This section shows the Matlab code used to generate the figures shown
%in the section titled "Simulation of  Time-stretching Algorithm"
%*******************************************************************************

t = -0.75e-9:2e-11:0.75e-9;              %set up a time axis 1ns long
t2= 0:2e-11:1.5e-9;                      %shift origin keep sample rate
sig=0.18e-9;
ye=exp(-(t.^2)/(2*sig^2));

figure                                   %new figure

plot(t2,ye)
xxyy = [0 2e-9 0 1];                    % set axis
axis(xxyy)

tt = 0:2e-11:160e-6;                    %setup same sample rate but longer time
d1 = [0:1/3.58e6:160e-6]';              %setup PRF = 3.58MHz
y1 = pulstran(tt,d1,ye,50e9);           %generate pulse train of gaussians

figure                                  %new figure

plot(tt,y1)                             %plot pulse train
xxyy2 = [0 160e-6 0 5];                 %set axis
axis(xxyy2)

d2 = [0:1/(3.58e6-87.4):160e-6]';       %setup PRF = 3.58MHz - (small amount)
y2 = pulstran(tt,d2,ye,50e9);           %50e9 = the sample rate

figure

plot(tt,y2)                            %plot pulse train with longer PRF
axis(xxyy2)

figure

yye = cat(2,(zeros(1,100)),(0.75*y1)); %Place transmit pulse and echo
y1e=yye(1:length(y1));
yt=y1e+y1;
YT=cat(2,(zeros(1,50)),yt);
YTe=YT(1:length(y1));
plot(tt,YTe);
axis(xxyy2)

figure

YY = YTe.*y2;                           %Multiply transmit and reference
plot(tt,YY)                             %pulse trains

%*******************************************************************************
```